Technical University of Denmark

DTU

Groundwater recharge and capillary rise in a clayey till catchment

Schrøder, Thomas Morville

Link back to DTU Orbit

DTU Library
Technical Information Center of Denmark

Groundwater Recharge and Capillary Rise in a Clayey Till Catchment

Thomas Morville Schrøder

Groundwater Recharge and Capillary Rise in a Clayey Till Catchment

Ph.D. Thesis

Thomas Morville Schrøder

2003

Groundwater Recharge and Capillary Rise in a Clayey Till Catchment

Preface

The present thesis is the outcome of my research in 1997-2001 towards the Ph.D. degree at the Technical University of Denmark, Environment & Resources DTU. Funding has been granted by the University and supplemented for the experimental part by the Geological Survey of Denmark and Greenland. My advisor and mentor in the final phase was Professor Dan Rosbjerg, who is thanked for fruitful discussions and support to what I believe can be a contribution to hydrology.

I wish to thank Professor Eggert Hansen for emphasizing the pre-drainage regime, Professor Flemming Bo Pedersen for weir design guidelines, and Associate Professor Hans Lund for his model of global radiation. My former colleagues at the Danish Geotechnical Institute tested wells with a long screen, while Ole Larsen at University of Copenhagen provided equipment for electrical sounding and borehole logging. Per Rasmussen, Per Nyegaard, and Frants von Platen at the Survey helped on the first applied pressure gauges and initiated the geological and topographical modeling. Bent Jørgensen, Danish Meteorological Institute, gave me access to archived atmospheric data. Jesper Skovdal Christiansen, formerly at DHI–Water & Environment, assisted me on the MIKE SHE code.

I appreciate that Kurt Jensen and Ivan Boserup accepted the heavy disturbance of their property and took care of my well being, especially when a railway line cut through cables laid out, farm machines torpedoed wells, water voles undermined one weir, and car batteries flattened on dark winter eves. I am indebted to the technicians Jan Larsson and deceased Klaus Fæster Hansen for fabrication of equipment. Klaus was the key person for implementation of the experimental setup, and Per Jensen from the Survey became an immense relief on operating the fragile monitoring network. I must not forget my assistants, the former students Niels–Kristian Terkildsen, Tore Stamp Nielsen, Jacob Gudbjerg, Inge Pedersen, and Haraldur Hannesson who assisted on installation and campaigns of fieldwork.

Thomas Morville Schrøder
27 December 2002

Abstract

Quantification of recharge rates and patterns is essential for sustainable groundwater abstraction. On northern mid- to high latitudes, the common weather is humid and a common geological unit is clay till. Mapping of the tortuous flow through clay till has an unrealistically high cost and models integrating the processes in the surface-groundwater contact have only been developed over the past decade. One traditionally disregarded process is the capillary rise from groundwater in response to surface drying. Diversion via the artificial subsurface drainage can be presented by a linear reservoir, and this contribution dominates the primary calibration target for hydrological models: streamflow. The discharge from deep aquifers to streams is approximately linear and can accordingly be modeled by a number of linear reservoirs. The tempting conclusion is that groundwater recharge is equally linear, so the capillary rise should not be present at all. Moreover, many have speculated whether removal of the artificial subsurface drainage would enhance the aquifer replenishment and thereby the level of sustainable groundwater abstraction.

A literature survey of methods for determination of groundwater recharge clarified that usually only the percolation at some level above the watertable is considered, and the subsequent capillary rise is neglected. Monitoring the very watertable by a number of wells captures the lag phase of recharge, its spatial distribution, and allows for model interpretation of also the capillary rise. Though the number of wells was limited to eleven, they covered two-third of the 16 km^2 study catchment in terms of terrain level. Adopting the variable source concept, they sufficed for a monthly distinction between the dry and wet state in six terrain intervals. From the wet stat area, the uniformly distributed subsurface drainage diverts recharge to the stream. A sequential parameterization of existing modeling tools was unfolded with the assistance of electrical sounding, a minor equilibrium model for determination of the proper boundary condition between the unsaturated zone and groundwater, and tools for mathematical inversion.

This study finds that watertable monitoring render calibration of a groundwater model's surface contact superfluous apart from drain time; vertical conductivity of weathered soil, and snow storage. We have found a first guess of the drain time in 1D by streamflow separation, and calibrated in 3D by MIKE SHE modeling. Preferential conduits are merged into the soil by 2D modeling, and snow storage parameterised by comparison of an automatic and a manual precipitation gauge. The capillary rise accounts for an uphill increase in the long-term net recharge from 200 to 260 mm/y, implying that local topography is mirrored into the aquifer circulation faster than found by regional modeling without this feedback process. Perhaps the capillary rise ties annual evapotranspiration to the North Atlantic Oscillation better than thought of for Denmark, implying that hydrological modeling of clayey catchments can establish area integrated values, which may contribute to the debate on the oscillation's spatial coverage. Moreover, subsurface drainage reduces evaporation from waterlogged areas by an increase in streamflow that is one magnitude larger than the 2 mm/y decrease in aquifer replenishment.

Sammendrag

Bestemmelse af grundvandsdannelsens hastighed og arealmæssige fordeling er essentiel for den bæredygtige oppumpning af grundvand. Det fremherskende vejr på den nordlige halvkugles midt- til høje breddegrader har et overskud af nedbør i forhold til fordampning. Samtidigt er moræneler en almindelig geologisk forekomst, også i det østlige Danmark. Men kortlægning af det stærkt uens moræneler er urealistisk dyr, og hydrologiske modeller som inkluderer processerne mellem jordoverfladen og grundvandet er kun blevet færdige i løbet af halvfemserne. En normalt udeladt proces er grundvandets tilbagekobling til fordampning, kaldet den kapillære stigning. Den almindelige underjordiske afledning via drænrør kan beskrives som et lineært magasin, og dette bidrag dominerer det primære mål for model kalibrering: vandløbsafstrømningen. Grundvandets udstrømning til vandløb fra dybe magasiner er tilstrækkelig lineær til at den kan beskrives med det tilsvarende antal lineære magasiner. Man kunne forledes til at tro, at grundvandsdannelsen også er lineær og der derfor ikke er nogen kapillær stigning. Med henblik på at øge indstrømningen til de pumpede magasiner under moræneleret har det været foreslået at fjerne noget af dræn-lægningen.

Et litteraturstudium af metoder til bestemmelse af grundvandsdannelsen gjorde det klart, at som regel undersøges kun nedsivningen i et bestemt niveau, mens kapillær stigning ikke opgøres særskilt. Derimod vil måling af det frie vandspejl i et antal boringer vise forsinkelsen mellem infiltration og grundvandsdannelse, dens arealmæssige fordeling, og muliggøre model tolkning af den kapillære stignings størrelse. Elleve boringer dækkede to tredjedele af tærren niveauet i det undersøgte opland på 16 km^2. Et koncept for stormafstrømning til vandløb gav mulighed for en månedlig skelnen i seks højdeintervaller mellem tilhør til den tørre kontra den våde del af oplandet, hvor grundvandsdannelsen gav anledning til drænudstrømning. En sekventiel parametrisering af eksisterende modeller er udfoldet med assistance af en kortlægning af jordens elektriske ledningsevne, en ligevægtsmodel til at bestemme randbetingelsen mellem umættet zone og grundvand, samt værktøjer til matematisk inversion.

Dette studium finder at vandspejlsmåling gør kalibrering af en grundvandsmodels overfladekontakt overflødig på nær dræn tid, lodret hydraulisk ledningsevne i den forvitrede zone, og sne magasinering. Vi finder et første gæt på dræn tiden i 1D ved separation af vandløbsafstrømningen, og kalibrerer i 3D ved MIKE SHE modellering. Makroporer er indsat i den forvitrede jord ved 2D modellering, og sne magasinering er parametriseret ved at sammenligne en automatisk og en manuel nedbørsmåler. Kapillær stigning forklarer øgningen i gennemsnitlig grundvandsdannelse op gennem terrænet, fra 200 til 260 mm/år. Topografien vil altså afspejles stærkere i trykniveauet for de pumpede magasiner end modellering uden tilbagekoblingen lader ane. Tilbagekoblingen ser ud til at binde den årlige fordampning stærkere til den nordatlantiske oscillation end man normalt tror for Danmark. Derfor må det antages at hydrologisk modellering af lerede oplande kan bidrage til debatten om oscillationens udbredelse. Drænlægning reducerer fordampningen fra vandlidende arealer og øger vandløbsafstrømningen en størrelsesorden over faldet på 2 mm/år i indstrømning til det pumpede magasin.

Table of Contents

Chapter 1

Introduction

1.1. Background and Objectives

The polar jet equips the northern hemisphere between the mid-latitudes and the polar region, apart from the North American prairies and Siberia, with a humid climate characterized by a surplus of precipitation compared to potential evapotranspiration. Glaciers advanced during the ice ages, most noticeable at these latitudes, and left extensively mixed geological units. The mixing of these glacial till units implies that even a small clay content turns them low-permeable, though preferential conduits has developed - especially in their weathered top. Such clayey till overburdens can reach a thickness of hundreds of meters in the sedimentary basins in front of bedrock areas. In areas with smaller thickness, yet not the scraped overburden in bedrock areas, a well may encounter a sufficiently shallow underlying layer with a large conductivity and pore volume that makes the drilling and operation of such a well for water supply economically attractive. Pumping of these high-permeable "aquifers" has been preferred due to a belief in their protection against manmade pollution on the surface.

Quantification of recharge rates and patterns is essential for sustainable groundwater abstraction. Since mapping of the tortuous flow through the clayey till overburdens has an unrealistically high cost and integrated modeling tools only have been developed over the past decade, not all hydrological processes are considered for examination of the exploitation of regional groundwater resources or the locally increased vulnerability to pollution. Soils and plants dry in response to solar heating and wind. These surface processes are treated together as the one termed evapotranspiration. The drying demand progresses downward in absence of precipitation. Once soil moisture depletion reaches the unconfined groundwater a process of upward flow, termed "capillary rise", is triggered. Though field studies undertaken in semiarid areas indicate that this groundwater feedback to atmospheric forcing potentially exceeds the percolation, tradition has restricted it in humid areas to woods and wetlands. One should bear in mind that clay soil extends the drying demand to large depth because of its relatively straight retention curve, and upward flow also occurs in cultivated fields. Thus, the capillary rise may be a more common process than thought of.

Most studies, especially those outside the scientific community, have only the area integral discharge to streams to calibrate the processes embodied in the water circulation. Many have sought to eliminate the complicating capillary rise that increases the, in a mathematical sense, level of ambiguity. In rainfall-runoff models, the capillary rise can be suppressed by cutting return flow from the uppermost groundwater reservoir to the soil moisture budget of the root zone. In integrated models, some suppress it by adjusting the

characteristics of the unsaturated soil domain: either by a smaller pore volume while downward percolation is facilitated through preferential conduits, or a larger conductivity decrease with moisture content. Others suppress it by replacing the groundwater domain with either "linear reservoirs" or "drainage levels", which divert the recharge passively.

Extensive drainage works were carried out in the clayey agricultural areas of Northern Europe and North America during the past century to prevent waterlogging and thereby secure a timely sowing and harvest, and aeration of the crop roots. Since the diversion via subsurface drainage to streams can be presented by a linear reservoir and the contribution dominates this primary calibration target, it is tempting to believe that the capillary rise is a seldom process. In Denmark, the water act of 1987 served to counteract the evident nitrate leaching. One of the instruments for achieving this goal was restoration of meadows. It has been speculated whether removal of the subsurface drainage would help not just this purpose, but also enhance the aquifer replenishment and thereby the sustainable level of consumption.

The purpose of this study is to investigate the magnitude of the capillary rise in clay till under a humid climate, and how it helps to adjust groundwater to topography and annual weather. Historical records of streamflow, precipitation, temperature, and cloud cover enable a spin-off study of the impact of subsurface drainage on the aquifer replenishment.

1.2. Outline of Thesis

Chapter 2 gives a literature overview on methods for measuring groundwater recharge in a humid climate, and devotes attention to their ability to capture the capillary rise. Chapter 3 is the heart of the thesis. The capillary rise is parameterized and its magnitude derived from an experimental study of a suitable catchment that comprised distributed monitoring of the watertable by a dozen of wells. Chapter 4 establishes an integrated model of the study catchment on the background of the performed parameterization, and explores how the capillary rise ties net groundwater recharge to terrain, and evapotranspiration to weather patterns. Chapter 5 conditions the integrated model to the historical subsurface drainage, and examines its impact on the balance between surface runoff and aquifer replenishment. Chapter 6 condenses the conclusions and brings some suggestions for future work. The appendices sketch the kernel of the experimental work: Appendix A streamflow monitoring with design and validation of rating curves, Appendix B watertable monitoring with the time series reproduced.

Chapter 2

Groundwater Recharge

Groundwater constitutes by far the largest part of the water resource stored on or in Earth's land phase, with the exception of glaciers. It exceeds the sum of lakes, rivers, vadose soil, plants, and the atmosphere by two orders [*Sharma*, 1989]. The replenishing flux that renews this resource is called recharge. Unfortunately, the recharge is one of the more difficult quantities to estimate in groundwater systems, and normally subject to a large error [*Lerner et al.*, 1990]. Most estimation methods were developed for semiarid or arid areas, where the water supply encountered an unsustainable demand early [*Gee and Hillel*, 1988; *Allison et al.*, 1994]. Sporadic overexploitation has also come up in industrialized countries with a humid climate, though they pay more attention to the threat from pollution. Quantification of the recharge rate is a basic precondition for management of both issues. This chapter defines recharge and summarizes the range of experimental approaches that are relevant for investigation in a humid climate.

2.1. Definition and Variability

The humid climate is characterized by a surplus of precipitation over soil evaporation and plant transpiration, and no distinct monsoon. Precipitation becomes the primary source of recharge, whereas seepage from watercourses, other surface bodies, terrain depressions, fractures, and diversion from denser soil or paved areas contribute indirectly with a trivial volume [*Lerner et al.*, 1990]. Once infiltrated and reduced by evapotranspiration, the rest of the moisture percolates down through the vadose zone to the watertable, which, when it is shallow, allows for some to be driven back by a capillary rise in response to the evapotranspiration demand.

Recharge is conventionally conceived as the percolation that crosses the uppermost watertable, whether this is a perched lens or an unconfined aquifer [*Stephens*, 1996]. Early works equated recharge with the net vertical flux, because they were unable to detect the capillary rise [*Sharma*, 1989]. Groundwater is normally extracted from a high-permeable geological layer with a sufficient influx. When the layer is confined under a low-permeable overburden, its influx constitutes just a fraction of the recharge denoted "aquifer replenishment". Getting hold on the flux is hard, but its variation can be read from the changeable state of some dependent variables.

Precipitation, cropping, moisture deficit, and watertable depth govern the temporal variability. Spatial variability conforms to the precipitation distribution via an adjustment of the moisture deficit and the watertable depth according to terrain, geology, and soil. Vegetation displays a significantly smaller correlation length than the watertable depth [*Seyfried and Wilcox*, 1995]; therefore, most studies seek to forecast groundwater recharge

in time before the easier mapping in space [*Lerner et al.*, 1990]. The following outlines the determination of temporal development of groundwater recharge over uniform areas, and mentions mapping when it is an integral part of such a determination.

2.2. Methods of Measurement

Direct measurement of groundwater recharge is expensive and difficult to carry out without disturbance in strong contrast to indirect measurement from the accessible watertable or tension. Comparison of a variety of methods gains confidence, particularly when they rely on complementary observations and calculation procedures. *Lerner et al.* [1990] have proposed five requirements for a good method: 1) accounts for flow that does not recharge, 2) includes relevant processes, 3) limited uncertainty, 4) ease of use, and 5) possible to extrapolate from readily available datasets. Most reviews divide the methods in five categories: A) direct, B) empirical, C) water balance, D) Darcian, and E) tracer. The indirect, B-E, are listed towards a potentially larger degree of success in terms of 1-3 to which we would like to add temperature as an alternative tracer. Table 2.1 summarizes what time scale each method works best at.

Table 2.1. Recommended estimation methods for precipitation recharge, modified from *Lerner et al.* [1990].

Method	Time scale					
	Instant	Event	Season	Year	Historic	Geologic
Direct	3	3	2	2	4	4
Empirical	4	3	2	3	4	4
Water balance	3	1	2	2	2	4
Darcian	2	2	2	2	2	4
Tracer, environmental	4	4	3	3	2	3
" , applied	3	3	1	3	4	4

[1] Optimum, [2] summation over shorter time scales, [3] feasible, [4] infeasible.

2.2.1. Direct Methods

Direct methods for determination of groundwater recharge collect the moisture flux out of an undisturbed soil column and take this intercepted percolation for recharge. A lysimeter setup is made by digging trenches around a monolith, and backfill after the sides have been lined. The bottom must either be lined or the walls driven into an impervious base, if such a base can be reached, but generally it should be deep enough to include the soil volume that plants extract water from to preclude violation of the capillary rise. Furthermore, it should be wide enough to preclude the impact of side lining and soil heterogeneity, and surrounded by similar vegetation to avoid an oasis effect. Lysimeters up to 1000 m^3 have been made [*Kitching and Shearer*, 1982]. Figure 2.1 shows how suitable constructions can

be grouped into four types according to watertable depth and replication of its dynamics. The dynamic setups, given in the top panel, replicate the ambient watertable to avoid an erroneous lag between their outflow and natural recharge. Their watertable can be forced to follow a reference by pumping between inside and outside wells. If the watertable remains below the bottom, the bottom tension can be adjusted from either an assumed hydrostatic equilibrium or the tension of the surrounding soil. The disengaged static setups, given in the bottom panel, apply when watertable dynamics are insignificant or difficult to replicate as in a dense heterogeneous soil. Their lower boundary is established as either a shallow watertable above the lined bottom or gravity drainage corresponding to a deep watertable.

Among the other direct methods, the vacuum extraction with a porous ceramic suction cup must represent the variable soil tension across its surface. Too much suction would attract too much moisture and thus exaggerate recharge [*Brandi-Dohrn et al.*, 1996], especially when the surface intersects preferential conduits. Moreover, the number of cups must constitute a surface that represents the soil heterogeneity. For a deep watertable, the temporal resolution of the reasonably steady recharge could be obtained by a series of snapshots of the vadose profile, though soil coring demands a large number of samples in each depth interval [*Cambardella et al.*, 1994].

Passive capillary samplers apply for a reasonably static watertable. A tolerably undisturbed soil is obtained by excavating a tunnel for the samplers in the side of a trench. They can be made with a large interception area and maintain reliable suction, as their gravity construction is independent of machinery due to the connection of a wetted fiberglass wick that covers the surface with a hanging water column inside the buried box that equals the average undisturbed tension. Recharge reads from regular emptying of the extracted water. Capillary samplers have to be as high as the desired suction depth, so the workload at installation is not necessarily smaller than for lysimeters.
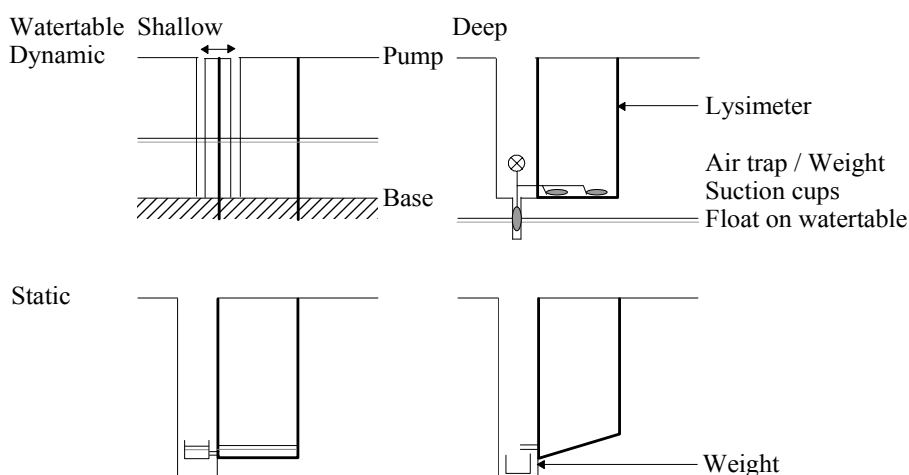
Figure 2.1. Lysimeter types for recharge monitoring: two replicate watertable dynamics; two accumulate percolation, excerpted from *Lerner et al.* [1990] and *Wu et al.* [1996].

Only dynamic lysimeters are able to replicate the watertable and the capillary rise, other direct methods collect percolation at a given depth. In presence of soil heterogeneity, either one large or several instruments should be installed. *Louie et al.* [*2000*] assessed from climate data that eight samplers with a diameter of 0.3 m could overcome heterogeneity at their site. All devices should rest before use for at least one flush of the pore volume, but restoration of reasonably undisturbed conditions may require a waiting for years.

2.2.2. Empirical Methods

Empirical, or black box, methods offer a quick extension in time and reconnaissance into comparable areas in terms of climate, land use, terrain, and geology. Annual recharge has been forecasted from its correlation to another flux in the water balance, *viz.* precipitation, discharge, temperature as a substitute for evapotranspiration, or just the fluctuation of the watertable. A linear correlation with precipitation suffices for a shallow unconfined aquifer, while polynomial and exponential correlation have been reported for other circumstances [*Lerner et al.*, 1990].

Wu et al. [1996] applied techniques from streamflow separation to analyze the outflow record for lysimeters with a fixed watertable and thereby extend the linearity to greater depth. The left side of Figure 2.2 shows the combined recharge of close precipitation events resulting in a tail that perhaps persists until after the onset of the next precipitation cluster. Should recharge arrive before the antecedent has reached the inflexion point on its rising limb, the two events can never be separated. They approximate the percolation lag as time from the last precipitation to the recharge peak (*T1*) less time from the first precipitation to the recharge initiation (*T0*). Below the root zone this lag

Figure 2.2. Recharge correlation to rainfall less evaporation in a lysimeter with a watertable fixed at a depth of 4.5 m. Left: rainfall clustering. Right: correlation for many clusters, from *Wu et al.* [1996].

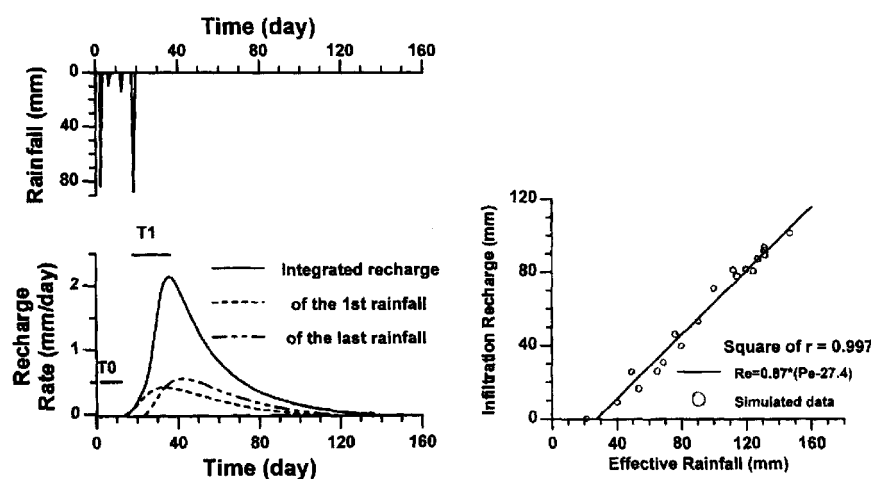proved to be practically independent of the changeable weather, so it was regarded as depth specific and taken as the mean over several clusters. Then, they merge events closer than the percolation lag and subtract evaporation from intermediate drought. Evaporation appeared to decline exponentially over time, in accord with the zero-flux plane method, and so should the recharge tail do. The exponential index could be computed from those recessions that last beyond their inflexion point, which enables estimation by plain extrapolation of recharge remaining after the onset of the succeeding cluster. Unsaturated modeling based on Richards's equation confirmed that also the index could be regarded as depth specific and increases exponentially with depth. After rewriting to effective infiltration versus accumulated recharge, the linearity prevailed to depths greater than 5 m in the soil that comprises alternating strata of fine sand to heavy clay, see the right side of Figure 2.2. Albeit their correlation contains a threshold and some scatter due to the unaccounted transpiration, it encourages an interpolation of recharge, given an insignificant capillary rise, between a few static lysimeters according to the ambient watertable of one well.

The watertable is indeed associated with recharge, but claiming a universal conversion of the watertable fluctuation to recharge is always questionable. Two years may hold the same mean watertable level, but they probably accumulate different summer and winter precipitation and corresponding recharge. Only testing against a proper numerical code can defend an annual correlation, partly because mapping of the spatial variability in a terrain that is not just convex around a single stream requires a countless number of wells [*Salama et al.*, 1993].

The flux out of an area may be measured in discharging surface waters like springs, rivers, or even lakes. Discharge has the appealing advantage compared to precipitation that it accounts for evapotranspiration, though an excessive turnover time of the aquifer would obstruct the recharge correlation. Moreover, catchment delimitation and streamflow separation include empirical judgment [*Rutledge and Daniel*, 1994]. A suitable positioned watertable well can substitute the impractical gauging of springs that trickle from several spots and suddenly burst, and thereby provide an event-based correlation for their small drainage area [*Avery et al.*, 1999]. A lake stage reflecting groundwater seepage through its bed is easy to gauge, but seldom a good indicator due to the fact that its probable seasonal oscillation masks the clustered precipitation events.

2.2.3. Water Balance Methods

Water balance methods derive recharge as a residual from bookkeeping of either the root zone or the watertable zone. *Penman* [1950] instituted the soil moisture, or root zone, budget that divert net infiltration of precipitation P less actual evapotranspiration ET_a into a changed soil moisture storage $d\theta$ and subsequent recharge R,

$$P - ET_a = d\theta + R \tag{2.1}$$

His arrangement works best over a time step similar to the attenuation down to the watertable, since the moisture content is supposed to release recharge mechanically after it has reached a "field capacity". Evapotranspiration continues to deepen the moisture deficit towards a "wilting point", where the immobile moisture will freeze the system until rain sets in again. Operational programs start with a maximum, or potential, evapotranspiration rate corresponding to open water, a pan, or a reference crop with an abundant water supply [*Penman*, 1956; *Makkink*, 1957], and deduce the actual from type and stage of soil and vegetation [*Penman*, 1950; *Kristensen and Jensen*, 1975]. *Finch* [1998] found that recharge estimation based on these empirical curve sets exhibits most sensitivity to rooting depth, field capacity, and wilting point for the soil description, and leaf area for the vegetation description. Because the decrease from the potential is relatively small in a humid climate, he concluded that the important parameters are those of the soil volume.

Attention must be devoted to the actual evapotranspiration rate, particularly for heterogeneous soil. *Penman* [1956] and *Monteith* [1975] established an energy balance at the ground surface that weighs incoming net radiation R_{net} against latent heat λET_a (vapor), in which λ is water's vaporization heat, sensible heat H (temperature), and some heat G vanishing into the ground

$$R_{net} = \lambda ET_a + H + G \tag{2.2}$$

Introducing the Bowen ratio β between sensible and latent heat,

$$\lambda ET_a = \frac{R_{net} - G}{1 + \beta} \tag{2.3}$$

utilizes that humidity and temperature proportionally follow upward diffusivities during evapotranspiration, except above forests. Finding the two quantities at different height can substitute measurement of the turbulent vapor flux by eddy correlation and the mean wind speed as long as their profiles remain undisturbed by other energy fluxes, particularly in the disregarded horizontal dimension [*Dingman*, 1994]. In the presence of a thick low-conductive overburden, the average actual evapotranspiration can be read from the head of the uppermost confined aquifer, resembling the surface load like "a giant lysimeter" [*van der Kamp and Maathuis*, 1991]. This behavior arises because a changed surface load displaces the incompressible pore water before the soil matrix has consolidated. The pressure increment after precipitation reflects net infiltration, plus, to a lesser extent, soil moisture migration to the quasi-steady aquifer replenishment, but annual accumulation should eliminate underground changes.

The root zone budget's uncertainty could also be relieved by rainfall-runoff modeling of the catchment discharge after insertion of some additional reservoirs for surface runoff and groundwater circulation. A model should be designed with the fewest possible free parameters for volume, threshold, and exchange to confine the ambiguity in having extra buttons for fitting the targeted streamflow [*Hendrickson et al.*, 1988]. A popular simplification is the linear reservoir with proportionality between storage and released outflow, a feat performed by a single time constant [*Chow et al.*, 1988]. Figure 2.3 gives an example in which the soil moisture deficit has been monitored for parameterization of the capillary rise. Other works add piezometric head to the target, but this may imply insertion of a 3D groundwater model.

The watertable rise after precipitation should be proportional to recharge via *Todd*'s "specific yield" [1959], defined as the drained volume per unit head decrease per unit surface, but soil heterogeneity and hysteresis complicate matters. Hysteresis lasts from percolating moisture or the rising watertable trap some air until this has degassed. Meanwhile, the fewer interconnected pores would demand a steeper tension gradient to maintain the recharge rate.

If recharge from above does not arrive much faster than the groundwater flow, the watertable rise has to be accounted for groundwater losses like withdrawal by waterworks. Combination of root zone and watertable bookkeeping constrains the recharge uncertainty. *Sophocleous* [1991] calibrated the specific yield from several storms according the soil moisture change over the whole vadose zone and the watertable rise. For the examined sandy till, he observed how a narrow zone for watertable fluctuation against the large field capacity lead to an acceptable small uncertainty, until the recharge season ended and the watertable dropped too deep to uphold correlation with the effective infiltration.
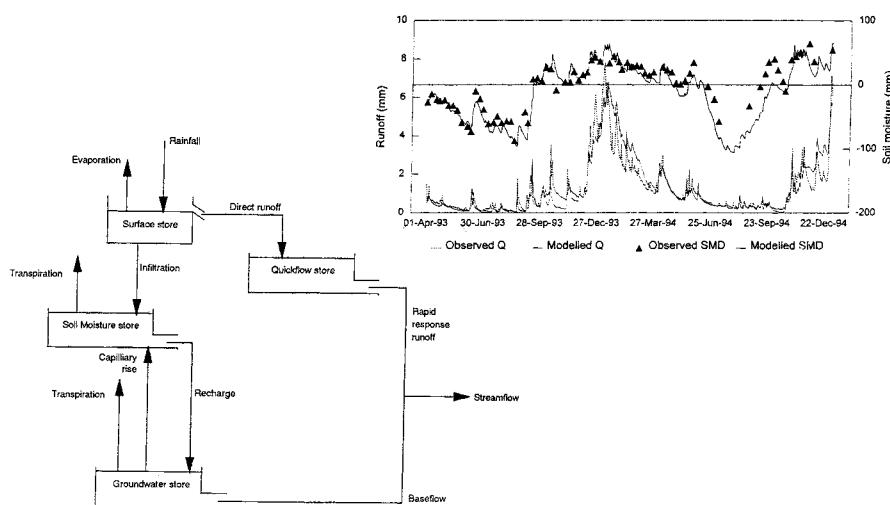

Figure 2.3. *Blackie et al.* [1998] incorporated a soil moisture budget in a rainfall-runoff model to turn recharge and capillary rise into internal figures.

Chu [1996] pointed out that the specific yield also reflects the size of the watertable rise, because recharge passes through the void pore space that the immobile moisture under the non-linear retention curve does not occupy. Clay soil's capillary fringe is seldom compatible with a constant specific yield.

The capillary rise is the primary non-linearity that enters the water balance below the root zone. It cancels out for a sufficiently deep watertable, which enabled *Besbes and de Marsily* [1984] to adopt *Sherman*'s [1932] unit hydrograph from rainfall-runoff modeling. At time *n*, recharge *R* should receive effective infiltration *I* from the *m* preceding time intervals in an unchanging linear combination *u*,

$$R_n = \sum_{i=1}^{m} I_{n-i} u_i \qquad\qquad (2.4)$$

Calver [1997] argued that the linear combination was valid for a monthly resolution of the 70 m deep watertable in a chalk aquifer. The many elements of the unit hydrograph collapse into a few parameters when recharge is thought as a process with little probability for success. The waiting time in such a Poisson process is Gamma distributed with one parameter for intensity and one for the number of apparent reservoirs. *Maas* [1994] Taylor expanded Richard's equation from the average soil moisture content and watertable depth to a convection-dispersion equation that had a solution close to the Pearson type III distribution, generalizing the Gamma distribution with a third parameter for skewness. *Wu et al.* [1997] extended the probabilistic approach by numerical simulation based on Richard's equation of numerous precipitation events, watertable depths, and soil profiles. They succeeded in incorporating a constant capillary rise in the floating number of reservoirs.

2.2.4. Darcian Methods

Adaptation to water's physical flow makes Darcian methods the most versatile of them all. Field observations can be interpreted analytically in just three cases. Pure gravitational drainage equals recharge with the soil conductivity: the unsaturated for a very deep watertable; the saturated for a very shallow. Zero-flux planes evolve according to evapotranspiration and drainage for no infiltration, where the lowermost plane delimits drainage that eventually recharges groundwater. *Sharma et al.* [1991] provide an example for the soil moisture decrease below this plane, but ignore a simultaneous watertable decrease. All other cases are too transient to be examined without a numerical code like Swap [*van Dam et al.*, 1997] or Hydrus1D [*Simunek et al.*, 1998] due to tension development in the root zone and the capillary fringe, and their capillary exchange. Modeling depends crucially on detailed mapping of the heterogeneous soil and its retention characteristics, not to mention plant growth. How to ensure a suitable yet stable solution

for Richard's equation by proper nodal spacing and a conductivity scheme remains a research subject due to the parabolic equation and the imposed abrupt infiltration fronts following precipitation [*van Dam and Feddes*, 2000].

2.2.5. Tracer Methods

The water flow appears from its influence on the distribution of dissolved solutes, dyes, and gasses. We will address the common types for studying percolation and shallow aquifers. *Lerner et al.* [1990] distinguish between two categories for tracers and methods. Tracers, naturally generated or manmade pollution, divide according to their prevalence into environmental tracers covering large areas and applied tracers covering a more limited area. The signature method converts the movement of a labeled parcel to travel time, whereas the throughput method implies equilibrium between the surface influx and the concentration in the vadose zone. Environmental tracers are suitable for the throughput method because of insensitivity to horizontal dispersion, but only the natural remain practicable after a stop for pollution has outdated the manmade.

In the vadose zone, the tracers should be examined, and injected when applied, below the lowermost zero-flux plane to prevent overestimation of recharge due to the loss to evapotranspiration [*Tyler and Walker*, 1994]. The signature method requires measurement of depth profiles for tracer and moisture content. For an environmental tracer, the recharge equals the moisture content that has infiltrated above the labeled parcel, unless a mass loss during evapotranspiration restricts comparison to two sampling times below the lowermost zero-flux plane. Manual interpretation assumes piston flow, in which percolation moves in discrete parcels from its introduction at the surface until later parcels have pushed it to the bottom. Travel time calculation according to the displacement of the center of gravity can be biased by dispersion, in which case a numerical code provides a rigid interpretation frame, either by a sequence of mixing cells or by a full advection-dispersion scheme. A numerical code may likewise account for decay, sorption, soil heterogeneity like preferential conduits, and the root zone. For an applied tracer, the recharge equals the moisture content in the displacement interval of the labeled parcel between its introduction and its sampling.

Conservative tracers do not loose mass during evapotranspiration. Their constant concentration below the lowermost zero-flux plane, as seen from the left side of Figure 2.4, tells what recharge was. Environmental Chloride is widely employed for the throughput method due to its abundance in the precipitation, but its influx history has to be accounted for dry deposition on aerosols from the sea between storms, agricultural fertilizers, harvest, animals, surface runoff, road de-icing, and trends in precipitation or atmospheric concentration [*Phillips*, 1994]. Clay soil's negative matrix surface repels anions and aligns them in the center of the pores, which exaggerates the percolation rate even for equilibrium

between mineral dissolution and adsorption. Provided that these complications are small, the recharge R appears from

$$\overline{P} \cdot \overline{[Cl]}_P = \overline{R} \cdot \overline{[Cl]}_R \qquad\qquad (2.5)$$

where P is precipitation, $[Cl]_P$ and $[Cl]_R$ are Chloride concentration in precipitation and soil moisture, respectively, while the bars denote mean value over time on the left side and over depth on the right side. Chloride and Bromide are common choices for the signature method, both naturally and applied.

Isotopes are atoms of the same element that differ in the number of neutrons. Equilibrium processes enrich the heavier isotopes in compounds with a higher state of oxidation, kinetic processes break the lighter isotopes, and physical diffusion partitions them according to their mass difference [*Alley*, 1993]. Altogether, the stable isotopes approach a temperature dependent equilibrium fractionation in the liquid phase of water, so the precipitation concentration becomes seasonally tagged. *Dansgaard* [1964] found that the turnover is large enough in a humid climate to recognize recharge from successive seasons. How deep this seasonal oscillation can be traced depends on the ratio between piston flow and dispersion.

Oxygene-18's encapsulation in the water molecule makes it a widespread, abundant, and undisturbed environmental tracer, for which *Gehrels et al.* [1998] could uncover the seasonal signature to a depth of 6 m in a sandy soil. Moreover, its observational uncertainty can be controlled from a mass balance utilizing the net concentration of a conservative compound is additive in a mixture of two waters. If two samples contain a pair of covariant stable isotopes, their mixture will fall on a straight line between them in a
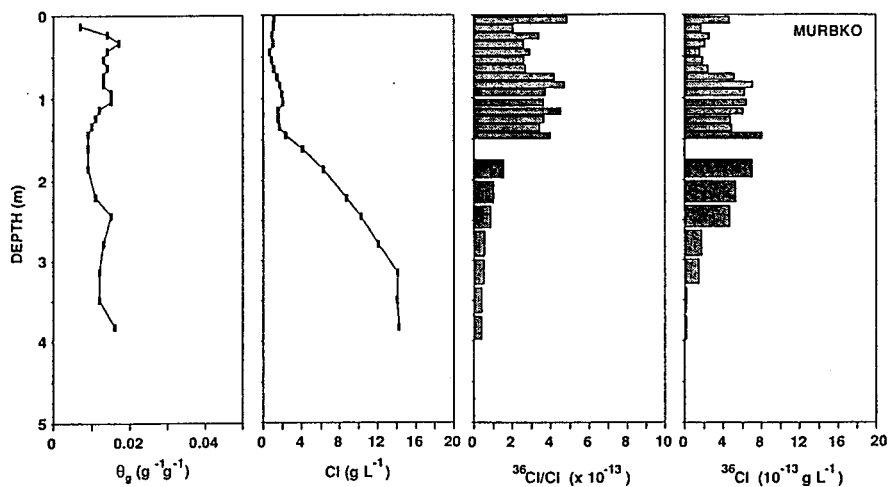

Figure 2.4. *Cook et al.* [1994] compared percolation according to the conservative tracer Chloride's throughput with the moisture content above a bomb signature given by Chloride-36's center of mass.

diagram with the isotopic concentration on the two axes. Oxygene-18 is commonly plotted against the covariant fractionation of deuterium. When precipitation adjusts to the seasonal temperature, it elapses along this line called the local "meteoric" line, and any sample of precipitation, soil moisture, or groundwater should fall on it. The slope of ideally one to eight reflects that two Hydrogen atoms go into the water molecule per Oxygen atom and Hydrogen is sixteen times lighter than Oxygen, but it can be rotated in a semiarid or sub-arctic climate by an increased content of Oxygene-18 due to evaporation or snowmelt, respectively [*Clark and Fritz*, 1997]. The geographically determined intercept reflects an isotopic depletion along the prevailing winds poleward, in over land, and over mountain ranges. Cold winter precipitation that dominates recharge in a humid climate displaces the groundwater content of stable isotopes from the precipitation average. Preferential conduits are present, if the average of the vadose zone fall outside their interval. *Wood et al.* [1997] plugged the unsaturated matrix and groundwater concentration of a conservative tracer into the throughput method for quantification of the bypass, and confirmed it by a stable isotope's end-member equilibrium in the groundwater between the unsaturated matrix and the bypassing precipitation.

Radioactive isotopes are suitable for the signature method, as their extremely low concentration involves virtually no disturbance. Their decay below the watertable pinpoints the groundwater age, defined as time since water was isolated from the atmosphere. An isotope with a half-life similar to the time since atmospheric introduction provides the best documentation of the age [*Lerner et al.*, 1990]. When the trajectory length has been documented from the piezometric head gradient, the recharge rate can be estimated. The larger the number of measurement points, the better the coordination between age and trajectory length. Testing of nuclear bombs in the northern hemisphere during 1952-63 injected Tritium and Chloride-36 into a stratospheric pool, from which their fallout has spread globally as environmental tracers. Mapping of the latitudinal dependence has become less important. Tritium, which vanishes rapidly due to its half-life of twelve years, is uninfluenced by secondary input except for some interaction with Lithium and a seldom production by Uranium/Thorium-series [*Alley*, 1993]. The humid climate's large recharge rate will soon outdate environmental Tritium in the vadose zone, but the established technique remains usable for applied Tritium. Environmental Chloride-36 remains usable in groundwater of a geological age due to its half-life of $300\,000$ years. *Cook et al.* [1994] found that Chloride-36 has traversed the equatorial trade wind barrier into the southern hemisphere, where its signature appears from the right side of Figure 2.4. *Solomon and Sudicky* [1991] called the attention of hydrologists to tritiogenic Helium $^3He^*$, a daughter product of Tritium ^3H. The use for groundwater dating is prolonged for a while by the captured gradual replacement in the closed system, where their concentration ratio relates to age t according to

$$t = \lambda^{-1} \ln\left(\frac{[^3He^*]}{[^3H]} + 1\right)$$

(2.6)

in which λ is Tritium's half-life. Helium-3 must be accounted for a diffusive loss to the vadose zone or dissolved air, and, again, the natural decay in the Uranium/Thorium-series, but the other noble gases provide control for the total loss.

Massive production of Chloroflourocarbons (CFC) 11, 12, and 113 for decades has contributed to the global pool of airborne organic gasses. Reconstruction of the atmospheric concentration is impossible in the vicinity of polluting industry, however, and the temperature sensitive solubility equilibrium with the vadose air makes knowledge of the temperature obligatory for reconstruction of the recharge concentration [*Cook et al.*, 1995]. The groundwater dating must also account for sorption and anaerobic degradation. Radioactive noble gasses are a safer measure. They are inert and their variable solubility cancels out for measurement of the specific activity, *i.e.* the concentration ratio of the isotope to the atom's total. Krypton-85 has a half-life similar to Tritium. It was also introduced by bomb testing, but nuclear fission plants continue to increase the atmospheric content. What overshadows the expensive measurement and the interpolation between the scattered measurement stations probing the atmospheric concentration is that dispersion is less able to bias groundwater dating from this monotonically rising gas than from those that have already peaked [*Smethie et al.*, 1992].

2.2.6. Temperature Methods

The thermal state oscillates seasonally with the precipitation temperature, just like some environmental tracers do. Whether temperature is an equally good measure depends on how homogeneous the exchange between pore water and soil matrix is, but its advantage is the measurement with extremely cheap sensors. The equation of the thermal conductance formulates the influence of water flow q on bulk temperature T as

$$
\begin{aligned}
C_{bulk} \frac{\partial T}{\partial t} &= k_{bulk} \frac{\partial^2 T}{\partial z^2} - q(t) C_w \frac{\partial T}{\partial z} \\
C_{bulk} &= C_s x_s + C_w x_w \\
k_{bulk} &= k_s^{x_s} k_w^{x_w} k_a^{x_a}
\end{aligned}
$$

(2.7)

where z is depth, t time, C thermal capacity [$Jm^{-3}K^{-1}$], k thermal conductivity [$Wm^{-1}K^{-1}$], and x volumetric fraction. Index s, w, and a denote soil, water, and air, respectively. Storage balances diffusion and convection, where storage in air plus convection through air and soil are neglected. Short-time variation in flow and thus temperature has to be interpreted by calibrating a numerical code like Hydrus1D [*Simunek et al.*, 1998].

Analytical solutions exist for comparison of a constant seepage through a homogeneous soil with the seasonal temperature cycle. Its sinusoidal course exhibits a phase lag and dampening with depth that is governed by the seepage rate. A single well should suffice for sampling of seasonal depth profiles, since vertical seepage in the aquifer top does not invoke in-well convectional flow between the measurement screens at different levels [*Taniguchi*, 1993], see the left side of Figure 2.5. The seasonal amplitude becomes significant at larger depth for a large precipitation volume or a large seasonal change in atmospheric temperature. Type-curves have been developed in the sixties for the dimensionless Peclet number that expresses dampening against seasonal phase in a bulk system consisting of soil matrix and saturated pores. The data points of each depth profile fall on one type-curve, and the seepage rate is truly constant, if all profiles taken over the year fall on the same type-curve. These type-curves apply also above the watertable. In a semiarid climate, the water saturation remains small and constant in a sandy soil, for which *Taniguchi and Sharma* [1993] could set the water content to 5 % and derive recharge from the seasonal sine at two depths. A comparative analysis for alternative seasonal courses of the temperature convinced them about the fact that analytical solution works above a depth of 3 m, if the watertable resides at great depth.

Despite the sinusoidal course also is found in a humid climate, see the right side of Figure 2.5, the water content can no longer be taken for being constant. *Tabbagh et al.* [1999] noticed how the thermal capacity and conductivity increase with the water content, but their ratio, the diffusivity, varied only one-third of the capacity in the topsoil above a depth of 1 m. They managed to neglect convection by adopting a constant diffusivity and iterating back and forth between Laplace transformed solutions for the phase lag and the amplitude dampening with depth, though conversion required five seasonal cycles. Albeit
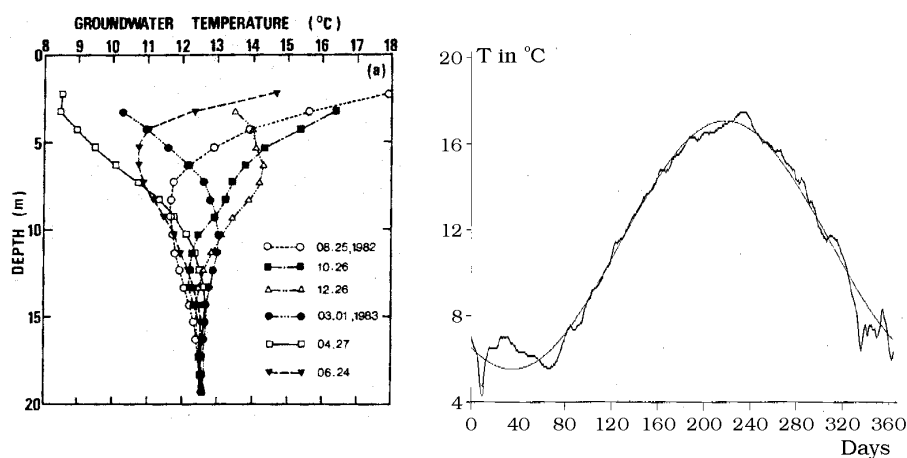

Figure 2.5. Percolation induces a sinusoidal temperature oscillation over the year. Left: groundwater depth profiles [*Taniguchi*, 1993]. Right: vadose zone time series at 1 m depth [*Tabbagh et al.*, 1999].

their approach lacks verification from a complementary method, it opens for a rough estimate based on existing topsoil records from meteorological stations.

2.3. Summary

A literature survey has been performed to identify methods for determination of the changeable groundwater recharge given a humid climate. Most methods only consider the percolation at some level above the watertable and neglect the subsequent upward capillary rise, which leaves an estimate of the naturally occurring net recharge with an incorrect lag phase from the surface and bias due to capillary flow. These errors can be substantial in soils having a deep watertable or comprising clay. The best instrument is a lysimeter with a controlled watertable that resembles the ambient groundwater state, but this would empty the experimental budget before enough instruments were installed for observation of the, probably, spatially variable recharge.

Instead, we pursued an observation network comprising eleven watertable wells, which captures the lag phase of the recharge, its spatial distribution, and allows for interpretation of also the capillary rise with the adoption of a Darcian modeling framework. The mass balance is controlled by bookkeeping of infiltration and groundwater circulation based on observation of precipitation, stream discharge, and data collected by authorities for the evapotranspiration.

References

Alley, W. M. (Ed.), *Regional ground-water quality*, van Nostrand Reinhold, New York, NY, 1993.

Allison, G. B., G. W. Gee, and S. W. Tyler, Vadose-zone techniques for estimating groundwater recharge in arid and semiarid regions, *Soil Sci. Soc. Am. J.*, *58*, 6-14, 1994.

Avery, W. H., J. J. Donovan, and J. N. Ketchum, Recharge estimation by stage-discharge interpolation of springflows from cross-correlated well measurements, *Ground Water*, *37*, 332-337, 1999.

Besbes, M., and G. de Marsily, From infiltration to recharge: use of a parametric transfer function, *J. Hydrol.*, *74*, 271-293, 1984.

Brandi-Dohrn, F. M., R. M. Dick, M. Hess, and J. S. Selker, Suction cup sampler bias in leaching characterization of an undisturbed field soil, *Water Resour. Res.*, *32*, 1.173-1.182, 1996.

Calver, A., Recharge response functions, *Hydrology and Earth System Sciences*, *1*, 47-53, 1997.

Cambardella, C. A., T. B. Moorman, J. M. Novak, T. B. Parkin, D. L. Karlen, R. F. Turco, and A. E. Konopka, Field-scale variability of soil properties in central Iowa soils, *Soil Sci. Soc. Am. J.*, *58*, 1.501-1.511, 1994.

Chow, V. T., D. R. Maidment, and L. W. Mays, *Applied hydrology*, McGraw-Hill Inc., Singapore, 1988.

Chu, S. T., Groundwater recharge and water table rise under equilibrium condition, *Trans. Am. Soc. Agric. Eng.*, *39*, 981-984, 1996.

Clark, I., and Fritz P., *Environmental Isotopes in Hydrogeology*, Lewis publishers Inc., Boca Raton, FL, 1997.

Cook, P. G., I. D. Jolly, F. W. Leaney, G. R. Walker, G. L. Allan, L. K. Fifield, and G. B. Allison, Unsaturated zone tritium and chlorine 36 profiles from southern Australia: Their use as tracers of soil water movement, *Water Resour. Res.*, *30*, 1.709-1.719, 1994.

Cook, P. G., D. K. Solomon, L. N. Plummer, E. Busenberg, and S. L. Schiff, Chloroflourocarbons as tracers of groundwater transport in a shallow, silty sand aquifer, *Water Resour. Res.*, *31*, 425-434, 1995.

Dansgaard, W., Stable isotopes in precipitation, *Tellus*, *16*, 436-468, 1964.

Dingman, S. L., *Physical hydrology*, Prentice-Hall, Upper Saddle River, NJ, 1994.

Finch, J. W., Estimating direct groundwater recharge using a simple water balance model – sensitivity to land surface parameters, *J. Hydrol.*, *211*, 112-125, 1998.

Gee, G. W., and D. Hillel, Groundwater recharge in arid regions - review and critique of estimation methods, *Hydrol. Processes*, *2*, 255-266, 1988.

Gehrels, J. C., J. E. M. Peeters, J. J. de Vries, and M. Dekkers, The mechanism of soil water movement as inferred from O-18 stable isotope studies, *Hydrol. Sci. J.*, *43*, 579-594, 1998.

Hendrickson, J. D., S. Sorooshian, and L. E. Brazil, Comparison of Newton-type and direct search algorithms for calibration of conceptual rainfall-runoff models, *Water Resour. Res.*, *24*, 691-700, 1988.

Kitching, R., and T. R. Shearer, Construction and operation of a large undisturbed lysimeter to measure recharge to the chalk aquifer, England, *J. Hydrol.*, *33*, 217-232, 1982.

Kristensen, K. J., and S. E. Jensen, A model for estimating actual evapotranspiration from potential evapotranspiration, *Nordic Hydrol.*, *6*, 170-188, 1975.

Lerner, D. N., A. S. Issar, and I. Simmers, *Groundwater recharge, a guide to understanding and estimating natural recharge*, Int. Contributions to Hydrogeology, 8, Int. Ass. Hydrogeologists, Verlag Heinz Heise, Hannover, Germany, 1990.

Louie, M. J., P. M. Shelby, J. S. Smesrud, L. O. Gatchell, and J. S. Selker, Field evaluation of passive capillary samplers for estimating groundwater recharge, *Water Resour. Res.*, *36*, 2.407-2.416, 2000.

Maas, C., *On convolutional processes and dispersive groundwater flow*, Ph.D. thesis, Tech. Univ. Delft, Delft, Netherlands, 1994.

Makkink, G. F., Ekzameno de la formulo de Penman, *Repr. Neth. J. Agric. Sci.*, 5, 290-305, 1957.

Monteith, J. L. (Ed.), *Vegetation and the atmosphere*, Vol. 1, Principles, Academic Press, London, UK, 1975.

Penman, H. L., The water balance of the Stour catchment area, *J. Inst. Water Eng.*, *4*, 457-469, 1950.

Penman, H. L., Evaporation: an introductory survey, *Neth. J. Agric. Sci.*, 4, 8-29, 1956.

Phillips, F. M., Environmental tracers for water movement in desert soils of the American southwest, *Soil Sci. Soc. Am. J.*, *58*, 15-24, 1994.

Rutledge, A. T, and C. C. Daniel, Testing an automated method to estimate groundwater recharge from streamflow records, *Ground Water*, *32*, 180-189, 1994.

Salama, R. B., P. Farrington, G. A. Bartle, and G. D. Watson, Distribution of recharge and discharge areas in a first-order catchment as interpreted from water level patterns, *J. Hydrol.*, 143, 259-277, 1993.

Seyfried, M. S., and B. P. Wilcox, Scale and the nature of spatial variability: Field examples having implications for hydrologic modeling, *Water Resour. Res.*, *31*, 173-184, 1995.

Sharma, M. L. (Ed.), *Groundwater recharge*, Proceedings of the symposium on groundwater recharge in Mandurah, Australia, Balkema, Rotterdam, Netherlands, 1989.

Sharma, M. L., M. Bari, and J. Byrne, Dynamics of seasonal recharge beneath a semiarid vegetation on the Gnangara Mound, Western-Australia, *Hydrol. Processes*, *5*, 383-398, 1991.

Sherman, L. K., Stream flow from rainfall by the unit graph method, *Eng. News Rec.*, *108*, 501-505, 1932.

Simunek, J., M. Sejna, and M. T. van Genuchten, *The HYDRUS-1D software package for simulating the one-dimensional movement of water, heat, and multiple solutes in variably-saturated media*, version 2.0, IGWMC-TPS 70, Int. Ground Water Modelling Center, Colorado School of Mines, Golden, CO, 1998.

Smethie, W. M., D. K. Solomon, S. L. Schiff, and G. G. Mathieu, Tracing groundwater flow in the Borden aquifer using krypton-85, *J. Hydrol.*, *130*, 279-297, 1992.

Solomon, D. K., and E. A. Sudicky, Tritium and Helium 3 isotope ratios for direct estimation of spatial

variations in groundwater recharge, *Water Resour. Res.*, *27*, 2.309-2.319, 1991.

Sophocleous, M. A., Combining the soil-water balance and water-level fluctuation to estimate natural groundwater recharge, practical aspects, *J. Hydrol.*, *124*, 229-241, 1991.

Stephens, D. B., *Vadose zone hydrology*, Lewis Publishers Inc., Boca Raton, FL, 1996.

Tabbagh, A., H. Bendjoudi, and Y. Benderitter, Determination of recharge in unsaturated soils using temperature monitoring, *Water Resour. Res.*, *35*, 2.439-2.446, 1999.

Taniguchi, M., Evaluation of vertical groundwater fluxes and thermal properties of aquifers based on transient temperature-depth profiles, *Water Resour. Res.*, *29*, 2.021-2.026, 1993.

Taniguchi, M., and M. L. Sharma, Determination of groundwater recharge using the change in soil temperature, *J. Hydrol.*, *148*, 219-229, 1993.

Todd, D. K., *Groundwater hydrology*, John Wiley & Sons Inc, New York, NY, 1959.

Tyler, S. W., and G. R. Walker, Root-zone effects on tracer migration in arid zones, *Soil Sci. Soc. Am. J.*, *58*, 25-31, 1994.

van Dam, J. C., J. Huygen, J. G. Wesseling, R. A. Feddes, P. Kabat, P. E. V. van Walsum, P. Groenendijk, and C. A. van Diepen, *Theory of SWAP version 2.0: simulation of water flow, solute transport and plant growth in the Soil-Water-Atmosphere-Plant environment*, Rep. 71, Department Water Resources, Wageningen Agricultural Univ., Wageningen, Netherlands, 1997.

van Dam, J. C., and R. A. Feddes, Numerical simulation of infiltration, evaporation and shallow groundwater levels with the Richards equation, *J. Hydrol.*, *233*, 72-85, 2000

van der Kamp, G., and H. Maathuis, Annual fluctuations of groundwater levels as a result of loading by surface moisture, *J. Hydrol.*, *127*, 137-152, 1991.

Wood, W. W., K.A. Rainwater, and D. B. Thompson, Quantifying macropore recharge: Examples from a semi-arid area, *Ground Water*, *35*, 1.097-1.106, 1997.

Wu, J., R. Zhang, and J. Yang, Analysis of rainfall-recharge relationships, *J. Hydrol.*, *177*, 143-160, 1996.

Wu, J., R. Zhang, and J. Yang, Estimating infiltration recharge using a response function model, *J. Hydrol.*, *198*, 124-139, 1997.

Chapter 3

Assessment of Capillary Rise in a Clayey Till Catchment using Streamflow and Watertable Data

Thomas Schrøder
Danish Meteorological Institute

Dan Rosbjerg
Technical University of Denmark

Abstract. We investigate the magnitude of the capillary rise, *i.e.* upward flow from the watertable, in clay till under a humid climate by mapping the monthly value of this and groundwater recharge for six topographical intervals in an underdrained 16 km^2 Danish catchment. The watertable was monitored two years in eleven wells controlled by piezometers, and geology was interpolated by electrical sounding. A precipitation gauge and four discharge stations monitored the catchment drainage. After separation of streamflow contributions from pavement and baseflow, the contribution from the uniformly distributed tile drains corresponded to a variable drainage area in which the watertable was above the drain depth. This revealed the drain time and a loss via vertically oriented preferential conduits in the weathered soil. Watertable increments during storm related bulk conductivity estimated by slug tests to unsaturated characteristics in a USDA soil database. Then, the database and the drain time guided a merger of the preferential conduits into a bulk anisotropy ratio by calibration of a variably saturated 2D model centered on a single drain line. Having found that clay couples the whole vadose zone to the groundwater, a variably saturated 1D model could derive their exchange at wells outside the drainage area. In 1998, the capillary rise stabilized in the valley at 0.7 mm/d for four months, resulting in totally 57 mm against the 334 mm of recharge.

3.1. Introduction

Quantification of recharge rates and patterns is essential for sustainable groundwater abstraction, as overexploitation exhausts the resource and increases its vulnerability to pollution. In Denmark, tap water is almost exclusively taken from groundwater and clay till is usually overlying the pumped aquifers in the densely populated eastern half of the country. Till designates debris which was crushed and left behind by glacial thrusts during the ice ages. Chaotic mixing of this debris implies that tills constitute low-permeable units, even for small clay contents. Little is known about the tortuous flow through them [*Hinton et al.*, 1993; *Gerber and Howard*, 2000].

Catchment modeling was improved through accounting for the linkage between groundwater withdrawal and decreasing streamflow [*e.g. Hansen and Dyhr-Nielsen*, 1982; *Christensen*, 1994]. Plot studies of contaminant transport via preferential conduits such as

fractures, desiccation cracks, burrows, and along plant roots [*e.g. Villholth et al.*, 1998] have contributed to a better understanding of recharge processes. Extensive parameterization has, so far, justified the use of "effective infiltration", *i.e.* precipitation less evapotranspiration, since replenishment of aquifers confined under the clay till grossly is a residual of effective infiltration and lateral diversion via drain schemes to streams.

Solar heating makes plants grow and soils dry out. The drying demand progresses downward in absence of rainfall. Once soil moisture depletion reaches the unconfined groundwater an upward flow is triggered. Field studies undertaken in semiarid areas indicate that the feedback potentially exceeds the percolation [*Prathapar and Meyer*, 1993]. Laboratory studies proved this so-called capillary rise [*Malik et al.*, 1989], which we refer to as the upward water flow from the watertable. Tradition has for humid areas restricted it to woods and wetlands. One should bear in mind that clay soil extends the drying demand to large depth because of its relatively straight retention curve, and upward flow also occurs in cultivated fields.

The capillary rise can be estimated from bookkeeping of the recharge. Recharge depends, in broad terms, on precipitation, temperature, wind exposure, topography, vegetation, land use, and soil. Climatic variability and land use changes govern the spatial and temporal variation of the, in humid areas, almost entirely rainwater-fed recharge [*Lerner et al.*, 1990]. In discharge records, groundwater discharge denoted baseflow has for a century been separated from quickflow, which is characterized by a steeply rising limb and a slowly decreasing recession limb [*Tallaksen*, 1997]. Among others *Troch et al.* [1993] removed some subjectivity by setting baseflow equal to incoming recharge. Baseflow thereby reflects the aquifer properties, albeit unsaturated capillarity remains ignored. *Winter* [1999] reminded about evapotranspiration from areas with a shallow watertable. This breakdown motivates a catchment study in which the capillary rise is distinguished from recharge.

Direct investigation of recharge generation can be carried out with weighing lysimeters at key locations, but true dynamics is only reproduced, if the bottom tension follows the exterior watertable. Indirect investigation may encompass estimation of percolation over time scales longer than seasonal from the concentration of, usually airborne, tracers above the watertable, or assessment of recharge during storm from the watertable rise. Determination from a residual or the pore space on average open for water flow eventually leads to unacceptable errors. Moreover, how should preferential conduits or pumping from waterworks be quantified? *Sophocleous* [1991] recommended a combination of the two water balances. Comparison of complementary methods is a common way to eliminate ambiguity. Tensiometers track the capillary rise indirectly. In clay, the tension gradient changes orientation rapidly, and it jumps abruptly in heterogeneous till. Measurement would require numerous observation points across the

vadose zone of a clayey till, while calibration of a variably saturated model remains a feasible and stable alternative [*Abbaspour et al.*, 1997].

The purpose of this paper is to demonstrate the magnitude of the capillary rise in clay till under a humid climate by mapping the temporal and topographical dependence of this and recharge in a catchment. Section 2 describes the catchment, Section 3 the monitoring, and Section 4 the geology from electrical sounding. Section 5 examines discharge to streams. Wells delimit the drainage area in which the watertable is above the tile drains, and reveal the drain time and how much bypasses the drains via preferential conduits. Section 6 parameterizes the weathered soil. Watertable increments during storm confirm the correlation between slug tests and unsaturated characteristics in a database. Plot modeling guides a merger of preferential conduits into a bulk anisotropy ratio for the soil and describes the topsoil in which no screens are installed. Section 7 outlines unsaturated modeling at each well while it is outside the drainage area. A literature survey and historical records help to determine the proper depth of piezometers and the model underside in the reduced till. Section 8 assembles the mapping, and Section 9 brings our conclusions.

3.2. Study Catchment

Stream valleys traverse gently undulating hills in the rural southwestern Zealand. The backbone of Harrested catchment is a ridge on its western and northern side where the town Slagelse and a forest are located. Topographical delimitation, illustrated in Figure 3.1b, reveals a drainage area of 16.01 km^2 with a relief ranging 14-93 m above mean sea level (m.s.l.) upstream the existing stream gauge *5602*. Pasture and meadows covered the 5 % of the catchment around the open stream and winter wheat dominated the surrounding cultivated cropland. As much as 95-98 % of the soil is classified as clay till. Sandy till in hills, peat and gyttja in hollows, and meltwater and freshwater deposits along the stream constitute the remainder.

Quaternary glacial thrusts eroded drainage channels as tunnel valleys on two flanks of the catchment and one minor inside during the last glaciation. These channels control the course of today's streams. Deposited glaciofluvial sediments, primarily sand and gravel, form a confined regional aquifer which typically is more than 10 m thick and lies 0-15 m below m.s.l. [*Geological Survey of Denmark and Greenland*, 1999]. Dense tertiary clay effectively hinders exchange with the underlying glauconitic sandstone [*Christensen*, 1994]. Uneven channeling and the presence of just one waterworks in the stream valley extracting 70 000 m^3/y imply that the aquifer thickness probably decreases underneath the catchment. The overburden of later deposited glacial till forms an unconfined aquifer. Lodgment till has been dispersed from the valleys over the ridge consisting of terminal till, where flow till has added an irregular surface on its northern part. Because the northern part coincides with a regional water divide the groundwater will mainly cross the

catchment boundary via the confined aquifer. Existing wells suggest an overburden thickness of at least 15-35 m and an aquifer head below a depth of 10-15 m.

Denmark lies in the westerly wind belt, where low pressures carrying frontal rain from the Atlantic occasionally are displaced by high pressures from warming of the landmass that stabilize the air mass until saturation releases convective rain. Humid winters, changeable summers, and a weak monsoon characterize the temperate coastal climate. Precipitation is recorded on a long-term basis at Antvorskov on the northern rim
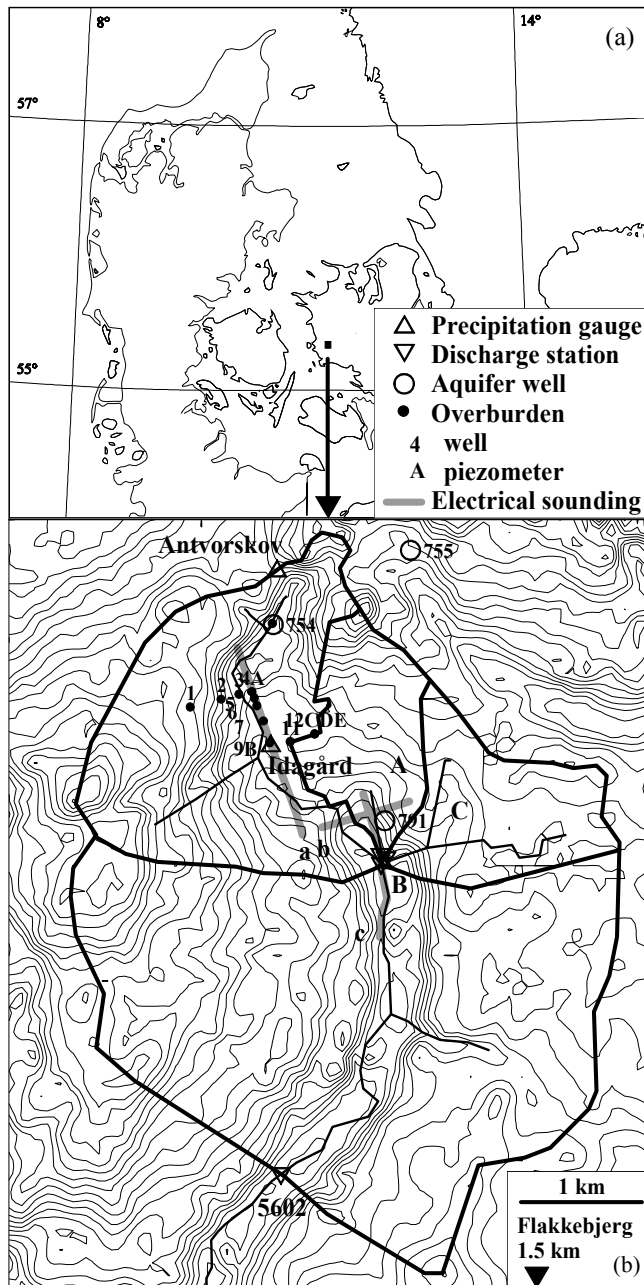

Figure 3.1. (a) Location and (b) instrumentation of study catchment with topographical contours given in 2.5 m intervals. Streams are piped upstream the internal discharge stations.

of the catchment. The catch is corrected for wind and wetting following *Allerup and Madsen* [1980]. Global radiation, temperature, wind, and humidity are recorded at Flakkebjerg south of the catchment. A modified Penman estimate of the potential evapotranspiration has been based on *Mikkelsen and Olesen* [1991]. Annual figures for 1981-99 are 736 and 557 mm, respectively, while average streamflow amounted to 219 mm/y.

3.3. Monitoring Network

Figure 3.1b shows the location of a Hellmann tipping-bucket precipitation gauge at Idagård. The gauge was placed in a lawn pit with its orifice 0.1 m above an anti-splash grid. Insertion of a cross in the funnel during winter impeded snow drifting. Counts of 0.1 mm were accumulated every ten minutes. Precipitation intensities never exceeded the counting ability and a container fed by the gauge has verified its catch. Correction for residual water evaporating from the funnel follows *Allerup and Madsen* [1980].

Three weirs, *A*, *B*, and *C* (see Figure 3.1b), have been installed for discharge measurement. The small energy gradient across the flat meadow around the uppermost open stream restricts the available pond there. Weir *B* with a drainage area of 6.4 km^2 was made broad-crested to ensure critical flow up to 80 % submersion, while terrain steepness allowed fully aerated sharp-crested weirs at the outfall of two tributaries. The two weirs there, *A* and *C*, account for 1.3 and 1.6 km^2 of weir *B*'s drainage area, respectively. Storage between the three control sections 40 m apart is neglected. Triangular design keeps the relative error constant at all stages, except that weir *C* had to be trapezoidal to pass torrents of quickflow. The weirs of steel sheets were driven through the streambed deposits to prevent the escape of lowflow. Excavation of the streambeds formed sediment catches and secured aeration, while pebbles and reinforced plastic counteracted undermining. Propel measurements and bucket filling match the rating curves of *Bos et al.* [1976] for rectangular laboratory flumes, implying that the weir crests remain adequately distant above the frictional streambed.

Wells were drilled into the overburden in the upstream end of the valley around the precipitation gauge and on an adjacent hillslope. Lying 36-61 m above m.s.l. the site spans two-third of the catchment in terms of terrain level. In principle, watertable monitoring requires piezometers covering the zone of fluctuation. A single screen instead of a nest of parallel pipes diminished cost and workload. The 5 m screens of well *1-12* began from a depth of 2 m to avoid erosion. Piezometer *A-E* were drilled into different strata to validate the operational mode of the long screens. Their screens were shortened to 0.5 m to counteract sensitivity to unevenly distributed preferential conduits. Bentonite was back-filled to the surface after the screen interval had been slot in a sand pack. An inner diameter of 25 mm in the 4" auger holes minimizes pressure lag to the formation.

Gillham [1984] noticed that a 0.5 m screen lagged a few seconds behind 0.03 m screens in sandy soil. In clay the lag is smaller when the watertable is above the screen due to a smaller storage capacity, and otherwise larger due to a thicker capillary fringe. Our three well nests *4A*, *9B*, and *12CDE* address that 1) the long screens lagged no more than one minute behind the piezometers. 2) When the watertable resided in the oxidized till the long screens did not form sinks into the reduced bottom layer during precipitation, according to the piezometers. 3) Streamflow separation substantiates that the initial 2 mm of a given day's precipitation bypass the drain schemes, but the specific yield below 15 % implies that the transducers cannot detect this. 4) Upward gradients were not recorded. Placement outside discharge areas qualifies the 1D modeling of the unsaturated flow. Because the watertable rise during storm and its seasonal fluctuation surpass the above listed uncertainties by several magnitudes, the signal recorded in the long screens can be described in a variably saturated model. The aquifer head has been recorded in the main production well of the local waterworks, *791*, and in the observation wells *754* and *755*. Monitoring commenced 1 September 1997 and lasted for two years.

3.4. Hydrogeology

3.4.1. Stratification

Agricultural activity and weathering are the sole structures with consistent correlation length in till [*Hinton et al.*, 1993]. Weathering comprises oxidation, acidification, outwash, and freeze-thaw cycling. Ceiling on piezometric heads in the oxidized till, an indication of efficient terrain-parallel diversion through the highly permeable topsoil, sets the loam underside to the chalk dissolution depth found by *Klint and Gravesen* [1999]. Acidification and outwash increase the porosity, mostly via chalk dissolution. Because this dissolution front coincides with the mould limit and also the maximum frost depth, all these characteristics collapse into a single topsoil unit, see Figure 3.2a. Visual inspection of the auger holes revealed a uniform oxidation depth. A thick capillary fringe preserves a reduced till from this depth down to the watertable minimum. Weathering is thereby divided into the three subunits given in Figure 3.2a.

Boussinesq's equation defines the equilibrium level of the watertable to the logarithm of the distance to the water divide given uniform recharge [*Szilagyi and Parlange*, 1998]. Figure 3.2b shows the recorded watertable minimum in the monitored two years. Comparing the different times when inflow is closest to zero at each well is a simple approach to uniform conditions. Short-range topographic undulation blurs extrapolation of the two regression lines to the hilltop. Taking into account that the watertable had not reached the seasonal minimum uphill when monitoring terminated 1 September 1999, and assuming that the watertable fluctuates in parallel with annual precipitation (Figure 3.13), the all-time minimum in 1996 was roughly 15 m. Figure 3.2a

transfers the downhill decrease in the seasonal minimum to a proportionally thick wedge of reduced till.

Electrical sounding is suitable for interpolation of aquifer depth between the sparse wells in the sedimentary setting of clay over sand. Conductivity increases with porosity, water content, and presence of ion-releasing clay minerals, albeit the low content of clay in Danish clay tills moderates the sand-clay contrast. Induction logging could quantify the formation resistivity at well *754* and *755* after natural gamma logging had confirmed the stratification. Sounding of the only unknown, the aquifer depth, was then executed along the three profiles sketched in Figure 3.1b. Deconvolution with the code of *Dahlin and Loke* [1998] using default numerical settings implies a constant anisotropy. The clearly different aquifer conductivity, however, overshadows the modification of this condition by preferential conduits in the weathered zone. Good contrast in the valley, due to small penetration depth and the origin as homogeneous lodgment till, frames the aquifer level between –7 and 8 m above m.s.l. Its topside matches the peak frequency of the shallowest encountered sand at 5 m above m.s.l. in a regional well database; its relatively small thickness under the catchment matches the transmissivity map of *Christensen* [1994].
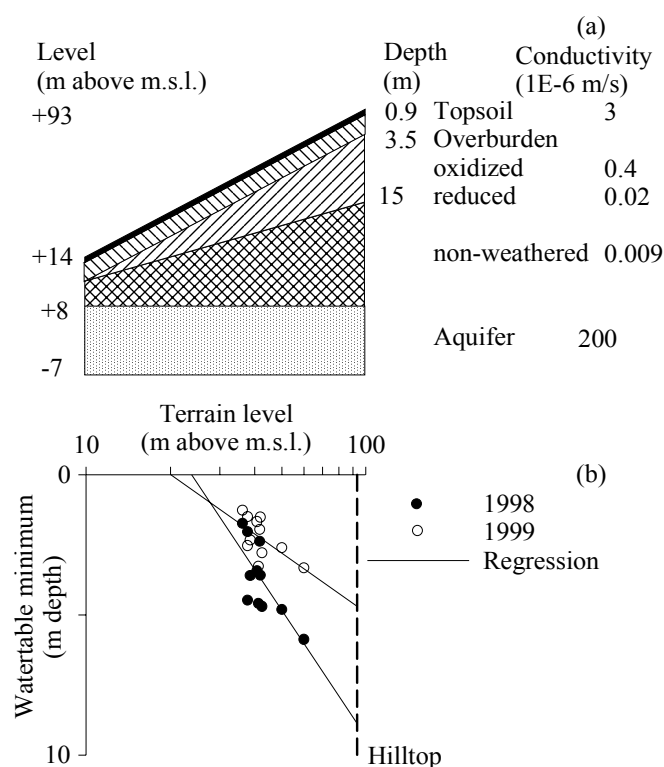

Figure 3.2. (a) Hydrogeological outline for which the aquifer storability is found to 10^{-4}, and (b) regression of the annual minimum watertable indicates the weathering depth.

3.4.2. Hydraulic Conductivity

Slug testing of the weathered overburden, when the watertable was above all screens in the oxidized subunit, infers that the reduced subunit was temporarily confined. Radial outflow from the logarithmically declining disturbance is interpreted according to *Bouwer and Rice* [1976] for the unconfined oxidized till and according to *Hvorslev* [1951] for the confined reduced till. Interpretation for long screens implies an impervious reduced till to eliminate this ambiguity, while interpretation of piezometers in that subunit is insensitive to a change in the estimated weathering depth of a few meters. Partial penetration promotes vertical flow and thereby a logarithmic shape of the decline, but any skin from auger drilling or a too long sand pack would also strengthen such a shape. Interpretation of the slug tail excludes the latter [*Yang and Gates*, 1997], though a regression line was fitted to overcome the limited transducer resolution.

Log-transformation makes the twelve slug tests in the oxidized till plot along a straight line on normal distribution paper. The standard deviation constitutes the same fraction of the mean everywhere on the well site, with a correlation coefficient of 82-86 % depending on its division into two, three, or four portions. Both findings indicate lognormal distribution [*Isaaks and Srivastava*, 1989], for which the mean layer conductivity can be estimated as the geometrical mean. This is implied throughout the glacial till. The waterworks induces ready-made pumping tests of the aquifer. Pumping resumes when the outlet pressure has fallen to a certain threshold. At night, the long rests due to a reduced household consumption make the asymptotic recovery limit evident. Interpretation of net draw down at well *754* was preferred due to the additional quantification of the storativity, but initial delay points to a doubling of the conductivity seen at the pumping well due to unaccounted leakage through the overburden.

Because electric and hydraulic conductivity both follow the pore network, their relationship near wells can be utilized to excerpt the hydraulic counterpart from the electric images. Figure 3.3a shows how their relationship obtains a correlation coefficient of 97 % for identical image blocks and slug tested volumes. Both properties increase power-formed with porosity according to Archie and Kozeny's laws, but the cation exchange decreasing power-formed with porosity in clay must be responsible for the found sign of the relationship [*Purvance and Andricevic*, 2000]. Figure 3.3b shows how imaging has smoothened out the aquifer conductivity, provided that the applied value for the interval between the observational well and the waterworks is valid along all three sounding profiles. Thus the non-weathered overburden is taken at a similarly displaced inflexion tangent of the geometrical mean profile, weighted by the length of each profile. Then the topsoil, constituting one-third of the topmost image block, is taken at its intersection with the surface. These two conductivities are added to the hydraulically tested ones of the oxidized till and the aquifer in Figure 3.2a. The very low conductivity under the aquifer complies with *Christensen* [1994]. Weak transmission has disabled the deeper portion of

the hillside profile, so baseflow modeling must be used to confirm the aquifer delimitation. Such a validation is allowable due to the similar support scale of the two parameterizations [*Gerber and Howard*, 2000].
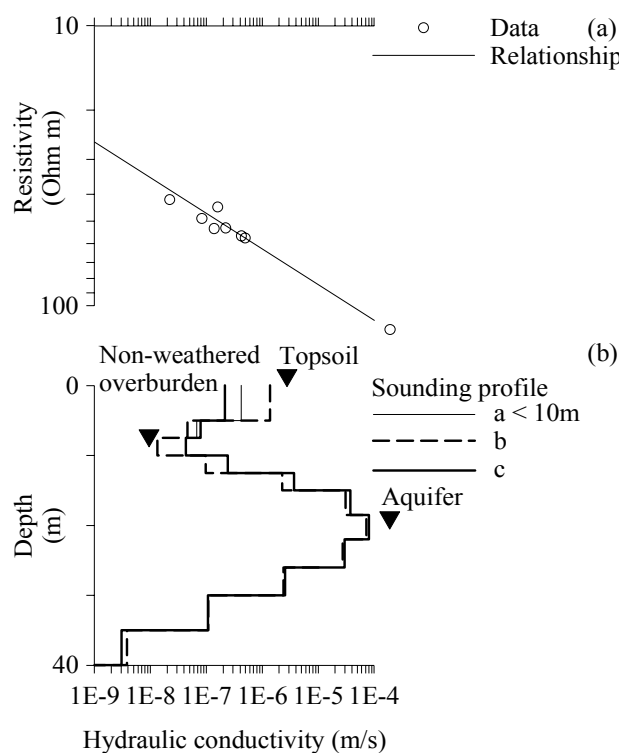
Figure 3.3. (a) Conversion from electric to hydraulic conductivity at examined wells, and (b) application to sounding profiles.

3.5. Streamflow Separation

The first step in building a model of the catchment water cycle is to distinguish discharging groundwater from surface runoff. All discharge stations are scanned for minor quickflow components due to human activity, before baseflow modeling can separate this component and test the aquifer level found by electrical sounding. Watertable monitoring in wells delimit the drainage area in which the watertable resides above the uniformly distributed tile drains. Normalization against this area reveals the drain time and a loss via vertically oriented preferential conduits.

3.5.1. Waterworks and Sewage

Twice per week, the attendant at the waterworks switches group of production wells and flushes ochre out of the precipitation basin. His report times coincide with spikes of 43 ± 3 m^3 at the nearby station *A* and the monitored draw down in well *791*; therefore, this well guides what days to subtract the volume downstream at station *A, B,* and *5602* at the catchment outlet. Drought reveals a diurnal oscillation of 48 ± 6 m^3/d with minimum 8 p.m.

at station *B*. Weir aeration should preclude any daytime decrease due to aquatic plants that rise and break the waters. Evapotranspiration will lessen the daytime discharge, but the source area corresponding to its potential limit extends beyond the meadow into fields around the open reaches of the tributaries, where no oscillation has been observed. Also the waterworks' pumping of the aquifer can be precluded, as its daytime intensification hardly can penetrate the dampening overburden [*van der Kamp and Maathuis*, 1991]. *Larsen et al.* [1995], however, report a sewage plant to which the discharge from another plant was redirected temporarily. In other years, this oscillation amounts to 30 ± 15 m³/d in the record of station *5602*. Provided that the decrease from station *B* corresponds to the dispersion of the waterworks' spikes, the oscillation at the distant sewage plant had the double volume, which is subtracted every day downstream at station *B* and *5602*. Waterworks and sewage account for 1 % of the catchment discharge during monitoring.

3.5.2. Pavement

How precipitation rises quickflow that lasts a day is shown in Figure 3.4a for the heavily influenced station *C*. Bypass via drain schemes did not occur as the watertable was below them, neither did saturation overland flow as the soil infiltration capacity generally exceeds the precipitation intensity in a humid climate. Hence, the paved areas summarized in Table 3.1 could constitute the source area. Idagård's automatic gauge disaggregates a spatially uniform precipitation event, should Antvorskov's manual gauge receive an equal catch. Sixteen events of 2.3-18.8 mm fulfilled this criterion during the monitored two summers. In discharge records, a horizontal baseline suffices to separate what could be the quickflow from baseflow. Figure 3.4b exemplifies for station *C* that normalization against the paved areas makes the non-recovered precipitation proportional to the catch. Linear regression of this loss keeps a correlation coefficient above 89 % for all stations even though onset, duration, and intensity are left uncompensated. Regression works best for station *B*, where the loss remains small due to a large portion of impervious roads.

Table 3.1. Pavement (10 000 m²) and precipitation volume (mm) equivalent to diversion pipes and reservoirs.

Discharge station	*A*	*B*	*C*
Barracks [a]	-	10	10
Asphalt road	1.05	8.03	1.16
Railroad	0.88	2.48	0.80
Precipitation	7	22	19

[a] Squares, roofs, and asphalt roads.

Given quickflow can be convoluted linearly from discretized precipitation, an hourly resolution is a fair compromise between constant intensity and spatial uniformity. Quickflow Q adds up to effective precipitation P_{eff}, *i.e.* precipitation P less predicted loss

$$Q = P_{eff} = P - (a_1 P + a_2) \tag{3.1}$$

where a_1 and a_2 have been defined for each station by a common regression analysis over all events. Detention storage dominates the loss over impermeable areas. In this first case, the event loss is distributed proportionally to the input time series. Infiltration dominates the loss over permeable areas. In this second case, the event loss is distributed according to the Φ–index [*Chow et al.*, 1988], *i.e.* the constant rate at which the effective input equals the output. Figure 3.4c shows the common deconvolution for $N = 24$ hours at station C.
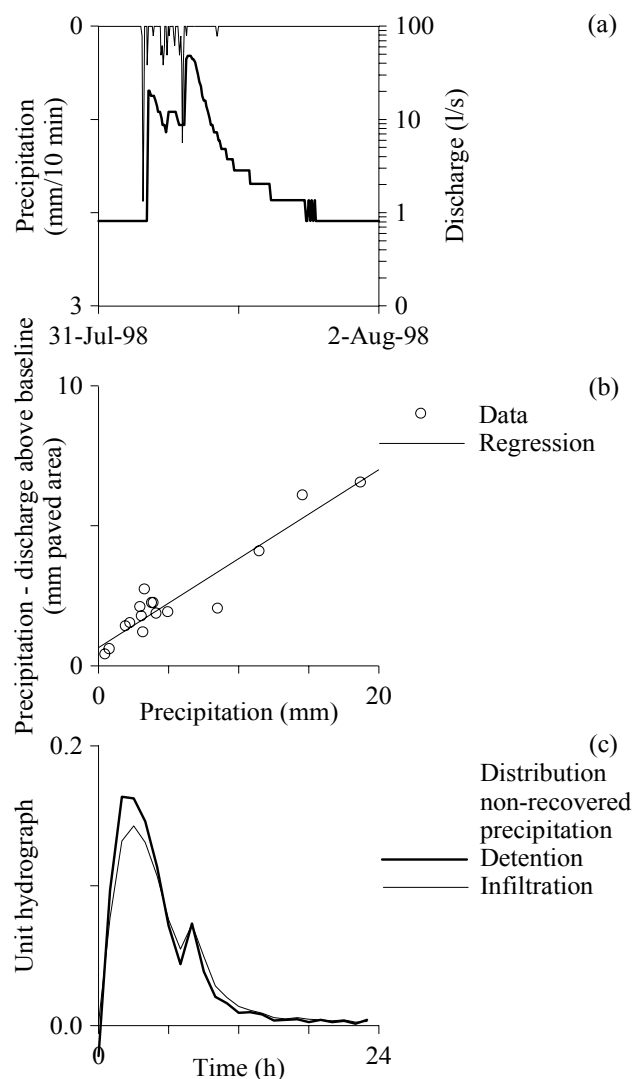

Figure 3.4. Quickflow passing station C: (a) example, (b) regression of non-recovered precipitation for this event and fifteen other, and (c) deconvoluted unit hydrograph.

Though multi-peak storms generate a bumpy recession limb, both cases result in an area under their "unit hydrograph" of 99 and 97 %, respectively, meaning that the input loss and the output tailing by delay reservoirs have been captured. Simulation summarized in Table 3.2 suggests that the first case prevails. The performance is less satisfactorily at station C due to the barracks farthest from the considered precipitation gauge, and at station B and C due to delay reservoirs and collection pipes with a diameter of 0.3-0.6 m and a length of 1-3 km, which are not flushed completely. Separation while Idagård's gauge malfunctioned necessitates a substitution with Antvorskov's daily emptied. A weight has to be determined, since the memory of one day refers some output to the day after precipitation. Minimizing apparently negative discharge after quickflow has been subtracted, partly due to the extrapolation range is extended from 2 to 3 km and non-uniform events are included, results in one quarter pass all internal stations the day after. Further distance to the catchment outlet retards the quickflow there to half the day after. Pavement accounts for 3 % of the catchment discharge during monitoring.

Table 3.2. Correlation coefficient (%) between observed and modeled hourly quickflow from pavement over sixteen events. Unit hydrograph denoted after distribution of non-recovered precipitation.

Discharge station	A	B	C
Detention	93.7	93.4	89.8
Infiltration	94.1	92.8	86.5

3.5.3. Baseflow

Streamflow is governed by the regional aquifer, when drainage fades away late in summer. The thick overburden's four magnitudes lower conductivity precludes seepage from uphill areas, so the aquifer head at the catchment boundary is established by crosschecking databases that contain well geology with soundings at the aquifer level instead of regional groundwater modeling. Preferring the earliest sounding in sectors without observation wells, the kriged aquifer head resembles the regional terrain slope parallel to the water divide in the northern ridge with a southwestward 10 m drop across the catchment. All time series exhibit a sinusoidal variation with minimum in September and an amplitude halving from Flakkebjerg towards well *754*, as the thicker overburden impedes the aquifer replenishment and dampens the seasonal recharge variation to 4 % already at a depth of 15 m [*van der Kamp and Maathuis*, 1991]. A similar overburden thickness sets the boundary amplitude to the 0.4 m of well *754*, while Flakkebjerg's annual increment constructs the boundary history.

The undulating terrain and the meandering streambed require examination of the stream-aquifer contact by distributed groundwater modeling, for which the MIKE SHE code [*DHI*, 1999] is adopted. Assigning the quadratic grid a mesh width of 100 m, dividing the non-weathered overburden into six computational layers, and the compulsory merging of weathered strata into one layer all comply with the convex head. Multiplying the vertical conductivity of Figure 3.2a by a factor of ten in the weathered zone accounts for preferential conduits. A block-kriged terrain model has been established on the basis of contour lines digitized in intervals of 2.5 m. The stream is ascribed to a trapezoidal cross section two magnitudes smaller than the grid size to comply with the nodal presentation. Short distances compared to a daily resolution of the boundary head justify the routing of streamflow as a diffusive wave and of overland flow as a kinematic wave. Manning numbers are set to 20 and 5 $m^{1/3}$/s, respectively, detention storage to 0.01 m. Drilling revealed that sandy deposits cannot release bank storage over longer time. The clayish soil dominates the stream-aquifer contact [*Kaleris*, 1998]. Thus, the exchange with a confined aquifer at finite depth is valid after neutralizing the lining by setting it to the overburden thickness divided by conductivity, for which the harmonic average is 10^{-11} s^{-1}.

Sufficient groundwater discharged in the open reach during the dry August of 1998 to provide a sensitive calibration target [*Kaleris*, 1998]. Figure 3.5 contains point errors on days without spatially uniform precipitation, an acceptable residual of the removed two magnitudes larger quickflow. Calibration starts in steady state for evaluation of the electrical sounding, which was less reliable outside the valley. Precipitation is turned off since baseflow, not drainage, is at stake. Table 3.3 reports how a minor rise of the aquifer topside exaggerates the baseflow, while a lowering of the more remote underside has less impact. Indeed, the aquifer runs in the depicted level instead of following the undulating terrain. In the transient state, twenty identical annual cycles are inserted ahead of the first monitored year to avoid error propagation. The ascent of the boundary head during the wet period raises abundant baseflow. Then, the surface coupling is turned on to account for baseflow being affected by evapotranspiration [*Winter*, 1999]. *Christiansen et al.* [2002] specify the seasonal root depth and leaf area of the vegetation, and the soil database of *Carsel and Parrish* [1988] specifies the unsaturated characteristics in line with the horizontal saturated conductivity. Figure 3.5 shows that permanent grass in the valley withdraws discharge to an acceptable level. Changing the overburden conductivity confirms the magnitude found by electrical sounding, and resetting the aquifer conductivity to what the pumping well indicated lessens the deviation in the observation well to within the seasonal amplitude. Albeit the soil moisture capacity buffers the response to the boundary head, baseflow accounts for 6 % of the catchment discharge during monitoring.
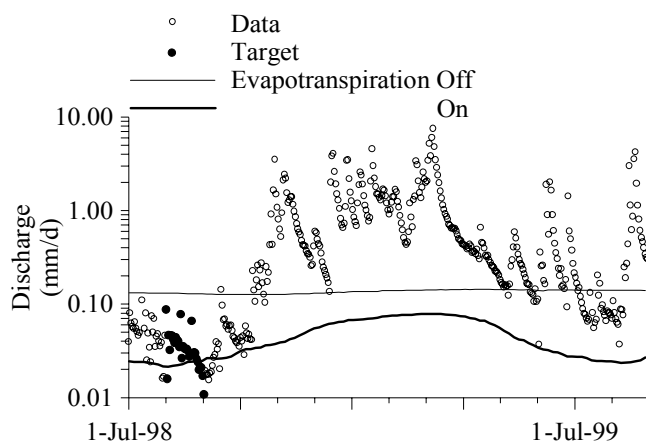
Figure 3.5. Catchment discharge cleared of waterworks, sewage, and pavement, versus simulated aquifer baseflow.

Table 3.3. Calibration of stream-aquifer contact from monthly means.

	Model - Observed [a]	
Steady state	0.051	-0.016
Aquifer top +2m	0.120	-0.015
bottom −4m	0.033	-0.019
Transient	0.098	-0.7
Evapotranspiration [b]	-	-0.5
Conductivity Overburden ·10	0.360	0.0
·0.1	-	-0.6
Aquifer $1 \cdot 10^{-4}$ m/s	-	-0.2

[a] Steady state: discharge station *5602* and *B* (mm/d) August 1998. Transient: *5602* (mm/d) and head well *754* (m above m.s.l.) November 1997 - August 1999.
[b] Accepted subsequently.

3.5.4. Drainage Area

In the variable source concept, quickflow begins with overland flow from initially saturated areas, subsurface flow follows through weathered beds or preferential conduits in these, and ends with return flow from a dynamic area in which soil moisture in excess of the field capacity enables a shallow watertable to respond to precipitation [*Myrabø*, 1997]. Drain schemes form a preferential network that covers all conceivable positions of the dynamic area. Because gravitation makes the position predictable, this drainage area is identifiable from wells provided that no other overland flow than pavement outflow occurs, while seepage and capillarity remain secondary.

Figure 3.6a represents the established terrain model in which the wells span 70 % of subcatchment *B* exclusive of *A* and *C*. According to *Miles and Kitmotto* [1989], who derived the equilibrium watertable with anisotropy and layering present and without intersection of the drain line, a storm with a return period of one month would barely generate waterlogging where the ascent reaches its maximum - right on the midline

between the drain lines. The watertable is more sensitive to drain depth than drain spacing or soil conductivity. Scanning recessions in watertable records, where the capillary fringe acts less dampening, exposes the local drain depth. The recession velocity decreases towards a certain depth at which the observation density increases correspondingly. Each well has one unique equilibrium depth around 0.9-2.1 m, those far below the mean 1.2 m are situated on the edge of a former orchard. Since the mean equals the design depth for drain systems in clay soil, the catchment drain depth is attributed to it. Every well belongs to the drainage area when the watertable resides above the local equilibrium depth, every discharge station does when the recession slope increases one magnitude [*Tallaksen*, 1997]. Figure 3.6b represents monthly means in a compromise between storm frequency and drain time. Gravity governs the seasonal drainage area with a significant expansion from and retreat to lower levels compared to any uncertainty in drain depth or terrain level.

Unaccounted discharge divided by precipitation delimits the drainage area upstream every station. These lines run between the topmost contributing and lowermost noncontributing terrain level, except for well *1* and *2* in March and April 1998 before well development was carried out, subcatchment *C* which saturated rapidly in the fall of 1998 but slowly the following winter, and the sluggish change in subcatchment *A* and the catchment. The reason why *C* could not saturate completely may be the two-third of its terrain model within a narrow level window of 6 m, which lets unresolved undulation
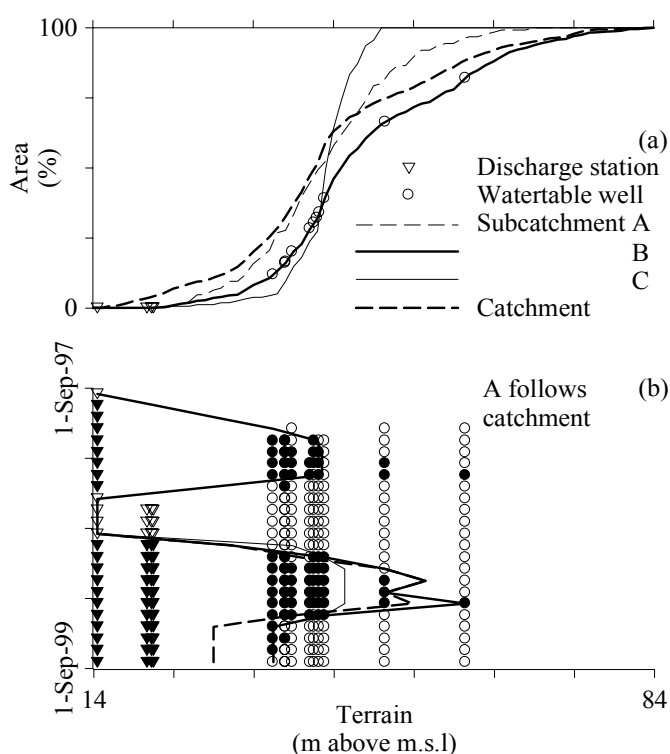

Figure 3.6. (a) Terrain model split in catchment parts. (b) Time series indicating drainage flow at different levels (filled symbols) against discharge cleared of waterworks, sewage, pavement, and aquifer baseflow, divided by precipitation (lines).

introduce an artificial threshold. All other exceptions reflect a drainage area starting from a sloping valley floor. In all parts of the catchment, this drainage area fluctuated from 0-11 % in summer to 73-92 % in January 1999.

3.5.5. Drainage Flow

Station *B*'s milder slope compared to *5602* in Figure 3.7a, apart from the unaccounted weed cut, illustrates how overburden depletion constitutes a larger fraction of the discharge uphill, where the deeper watertable shows that recharge takes place outside the drainage area. Depletion can only be determined as a residual, since drains carry what discharges inside their source area to the stream. *Rorabaugh* [1964] modified the 1D heat flow equation to an unconfined aquifer with a fully penetrating stream, no capillarity, an impervious base and catchment boundary, in which both instant and constant recharge
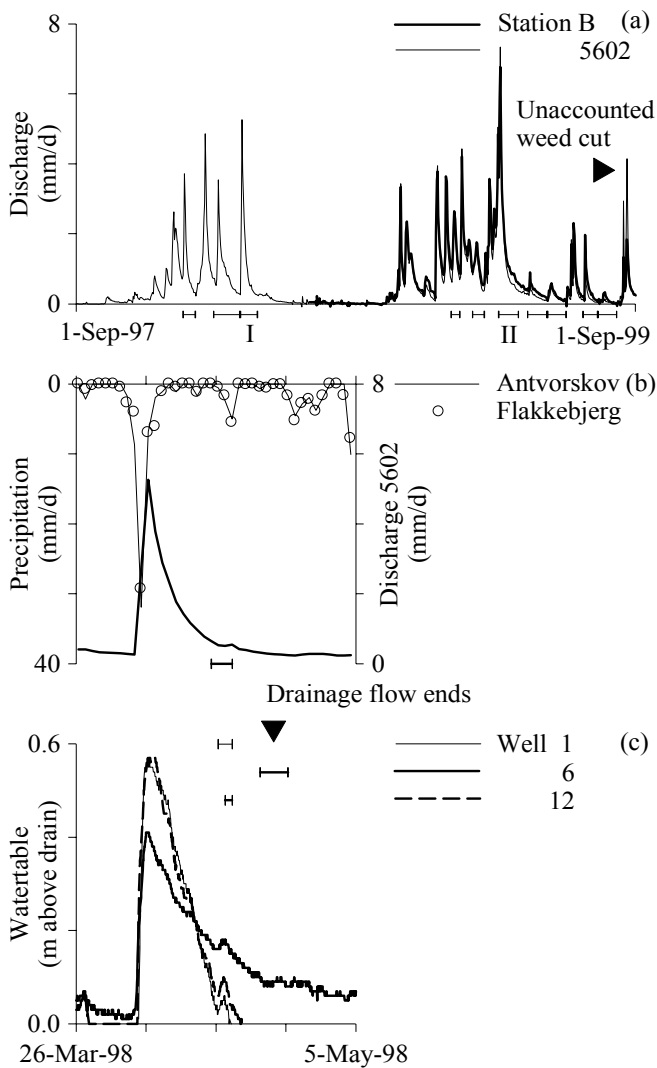

Figure 3.7. (a) Discharge cleared of waterworks, sewage, pavement, and baseflow, and (b) forty days around event *I* with (c) the watertable in three selected wells. Intervals for the end of drainage flow are given for all four records.

leads to exponential recession. He fits the separation point on the recession limb to the point where the antecedent exponential decrease is resumed, whereas *Troch et al.* [1993] identifies the dominant regime by the switch in Dupuit-Boussinesq's equation from a short- to a long-term power function, when the watertable decline, in theory, has reached the catchment boundary. Figure 3.7b shows the uniform precipitation of event *I* for which the two separation methods give an interval for the end of drainage flow around two weeks later. Watertable data inform how long time drainage dominates locally. Figure 3.7c shows for three representative wells the maximum storage one day after precipitation, which marks the time when drainage began, but soil variability and a limited transducer resolution urge a regression to the drain depth. Regression by the two separation methods yields the shown intervals: at the hillside well *1* and at the valley well *12*, the drainage flow ends with the mean catchment response observed in the stream, while groundwater circulation traps the watertable in low-lying depressions above the drain depth. Tailing observed at well *6* postpones the end of drainage flow one week. Starting the long-term power function from this point leads the separation along a horizontal line straight to the minimum before the rising limb, in accord with the great difference in residence time between drainage and groundwater circulation.

Ten events of drainage flow diverting 20-60 mm of precipitation in all seasons have been tagged in Figure 3.7a. Tailing precipitation gives, on average, 6 % scatter around the short-term index and twice as much around the long-term index. Absence of bias indicates unambiguous flow orientation, imperative for linear modeling of the dynamics. The seasonal independence indicates that all loss must be constant in time. Unit hydrographs have been deconvoluted at event *I* for the drainage flow normalized by its source area. Table 3.4 shows a balance between effective precipitation and discharge at a loss of 2 mm. Validation at event *II* confirms the same dynamics for the same loss in all parts of the catchment.

Why the first day diverts 10 % and the second day diverts 30 % in the derived unit hydrograph has to do with discharge records divided at midnight and precipitation records at 8 a.m. Figure 3.8 demonstrates how the two days shift rank when the implicated delay of one-third day is advanced to two-third day ahead, meaning that the intensity has varied during the day of maximum precipitation in event *I*. A linear reservoir starting from rest is characterized by an impulse response function *U(t)*,

$$U(t) = Te^{-Tt} \tag{3.2}$$

where *t* is elapsed time and *T* is drain time [*Chow et al.*, 1988]. Regression over both data pairings converts the many elements into a drain time of 0.28 ± 0.02 d^{-1}.

Table 3.4. Drainage flow normalized to source area (mm). Unit hydrograph for Antvorskov's precipitation with 2 mm loss calibrated at event *I* and applied at event *II*.

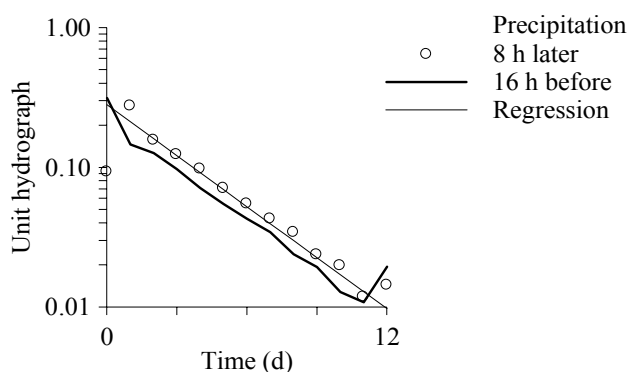| Precipitation		Discharge station			
Total	Effective	*5602*	*A*	*B*	*C*
I April 2-25, 1998					
65	45	44			
II February 14 – April 1, 1999					
126	83	83	80	85	83

Figure 3.8. Drainage unit hydrograph derived from pairing the daily catchment runoff with the daily precipitation at Antvorskov either 8 h later or 16 h before.

3.6. Weathered Soil

Unsaturated bulk modeling outside the drainage area implies a merger of preferential conduits into an anisotropy ratio, confirmation by watertable increments during storm of the slug test as a key to a USDA database of unsaturated characteristics, and calibration of a variably saturated 2D model centered on a single tile drain line to find the anisotropy ratio and the topsoil unchecked by any screen.

3.6.1. Preferential Conduits

Streamflow separation revealed a temporally and spatially constant loss in the drainage area after quickflow from paved areas had been subtracted. Drain scheme recovery of tracers poured over the ground has proved the existence of preferential conduits in clay till [*Villholth et al.*, 1998]. Testing a fraction of the drain spacing only and a prevalently vertical orientation [*Klint and Gravesen*, 1999] could let some recharge from the precipitation the same day escape the drain schemes. Probably, a constant loss of recharge reflects that most conduits penetrate no deeper than the oxidation front, so the subsequent intrusion of the soil matrix returns almost all recharge to the drains. In the drainage area, the watertable rests at the drain level until precipitation begins. The loss may be attributed

to the volume of the preferential conduits in the 1200 mm above the drain level, if drainage flow does not trigger before this macroporosity has been flushed once. A loss of 2 mm corresponds to an active macroporosity of 0.17 %, which matches the upper limit of 0.16 % found by *Villholth et al.* [1998] in a nearby plot study using a similar argument of total displacement. Their tracer-tested lower limit of 0.04 %, however, suggests that the loss simply is redirected to delayed drainage flow.

Heppell et al. [2000] argued that in wintertime conduits form the primary infiltration route through the topsoil of a clay till, in which swelling sealed the surface enough to keep their preference despite an entrance tension of just 4 cm. Why should the capillary fringe above the watertable not bridge the unsaturated zone and thereby widen the infiltration cone for each conduit? Percolating water enters the conduits via this fringe, for instance has well *1*'s watertable recession evidenced active conduits in the reduced till at a depth of 6 m, while the surface tension inhibited infiltration through the conduits from vertical gradients above unity relative to the slug test of the horizontal conductivity. Thus, conduits recharge the groundwater irrespective of depth. *Christiansen et al.* [2002] found from the bypass description in the MIKE SHE code [*DHI*, 1999] applied to a nearby catchment that redistribution by conduits is more important than their 1-2 % of direct recharge; consequently, recharge can be approached by merging glaciotectonic faults and fractures, roots, burrows, freeze-thaw and desiccation cracks into the matrix description. The vertical major axis of the conductivity tensor coincides with the driving gradients of gravity, humidity, and temperature. Fractures and burrows are less unidirectional, but the secondary horizontal orientation [*Klint and Gravesen*, 1999] might coincide with the minor axis of the tensor. The conduit density is assumed to decrease proportionally with the matrix conductivity, corresponding to a single overall anisotropy ratio of the weathered zone.

3.6.2. Unsaturated Characteristics

The potential success of lab investigation is little for clay till, because clay is hard to dry out and till demands extensive sampling for quantification of its heterogeneity. A less troublesome approach is to get unmeasured parameters from lab classification and pedotransfer functions, and calibrate a model from field measurement [*Russo et al.*, 1991]. *Van Genuchten's* formulation [1980] of the retention curve and *Mualem's* [1976] of the conductivity are adopted for compilation with the statistical correlation between their four parameters and the saturated conductivity given by *Carsel and Parrish* [1988] for USDA's twelve soil classes. In winter, the watertable recession adjusts to drainage from a substantial soil volume. The USDA database can be compared to the slug test at the hillside well *1*, where drainage elapses freely (Figure 3.7c). Neglecting overland flow and evapotranspiration equals recharge with precipitation less the 2 mm bypass. Precipitation gauges have been consulted for drought around spatially uniform yet significant storms, where the watertable is checked for an equal rise and fall to preclude intermediate

groundwater flow. Five events with an increment of 110-820 mm exceed the transducer resolution and log interval with one magnitude, at the least.

Before and after inflow, the void pore space equals porosity less detained water. Hydrostatic equilibrium sets tension to the level above the watertable and ties the water content in with the retention curve. Written out, recharge R lowers the watertable depth h from the observed position 0 to 1,

$$R = \theta_s (h_0 - h_1) - \int_{h_1}^{h_0} \theta(z)dz \tag{3.3}$$

where z is level above watertable, θ is water content, and s denotes saturation [*Chu*, 1996]. Clay, Sandy Clay, and Silty Clay Loam with a saturated conductivity of 48, 29, and 17 mm/d, respectively, are the USDA classes closest to the slug test of 28 mm/d for the oxidized till. Figure 3.9 shows that the estimated recharge matches the bypass-corrected precipitation between the two latter classes. Also the three largest precipitation events suggest that oxidized till corresponds to Sandy Clay, if their watertable rise of 180-450 mm up in the topsoil were accounted for a larger pore space there, according to the implied larger conductivity towards the surface. The proximity to Sandy Clay is taken as evidence for slug tests do represent the soil matrix, so the wells intersect an oxidized till that spans the five densest classes.
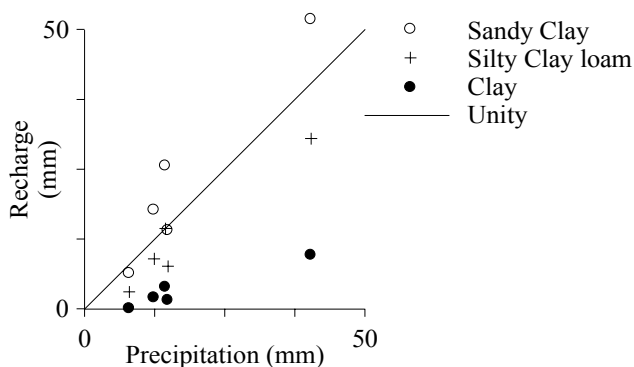
Figure 3.9. Precipitation versus subsequent recharge at well *1*, estimated by Equation 3.3 from the watertable rise and different soils in the database of *Carsel and Parrish* [1988].

3.6.3. Anisotropy Ratio and Topsoil

Four wells, *12* and *C-E,* are scattered over half the spacing between parallel tile drain lines in flat terrain. Their quasi-steady head gradient of 16 % from the oxidized to the reduced till doubles the week after precipitation, and the subsequent recession should adapt to the drainage flow from December to March in the last monitored winter, when the watertable

was above all four screens. Hydrus2D [*Simunek et al.*, 1999] is a suitable code for detailing this setting centered on a single drain line with impervious sides at the midlines 9 m away to mirror division between adjacent drain lines. The drain line is imitated as a seepage face to an atmospheric sink that shuts off when the watertable drops below, and the finite element mesh focus there keeps the relative flux error constant throughout the model domain. The lower boundary is ascribed to piezometer *C*'s head, the upper boundary to precipitation and evapotranspiration until prescribed head at wilting and ponding divert the surplus to overland flow. Hydrus2D applies Richard's equation for unsaturated flow with sink terms for plant uptake and soil evaporation. Wheat, the crop at the site, terminates transpiration before its root zone has saturated. Daily potential rates for transpiration ET_{pt} and evaporation ET_{ps} are derived from the potential evapotranspiration ET_p according to the leaf area index *LAI* [*Jensen*, 1979]

$$\begin{aligned} ET_{ps} &= ET_p e^{-0.4LAI} \\ ET_{pt} &= ET_p - ET_{ps} \end{aligned}$$

(3.4)

Kristensen and Jensen [1975] made a similar approach behind MIKE SHE [*DHI*, 1999], for which *Christiansen et al.* [2002] provide seasonal leaf area index and root depth and a depth distribution constant that resembles an exponentially decreasing root density. Slow growth early in spring justifies the compulsory averaging of the root depth over the considered four months. No major error arises, since the 266 mm of precipitation greatly exceeds the 40 mm of potential evapotranspiration.

Horizontal conductivity, which extracts unsaturated characteristics from the database of *Carsel and Parrish* [1988], is set to the geometrical mean of the implicated screens in the oxidized and the reduced till, but subject to calibration in the topsoil along with the overall anisotropy ratio. Decoupling the soil type from vertical conductivity and considering complete time series detaches saturation, where preferential conduits prevail, from drying, where matrix flow takes over. Four objective functions are investigated: mean head (m) in each well to open for infiltration; daily head (m) to constrain the running state; daily change in each well (m/d) and drainage flow (mm/d) to constrain flow. Tension is extracted from the computational nodes closest to the center of piezometer *D* and *E* and the top of the long screen *12*, and assuming hydrostatic equilibrium converted to head. The streamflow separated drain time sets the target for drainage flow from the plot. This target is only a relative measure, because the number of dimensions has increased by one.

In Figure 3.10a-b, the anisotropy ratio is disengaged with relative errors in daily change and flow to enable plotting against one axis. The mean head falls along both perpendicular trajectories in the objective function spanned by the conductivity, and becomes fulfilled around a ratio of forty in accord with the daily head. The daily change indicates a lower ratio, but its local maximum reflects passage of a layer interface. Integral

outflow is less sensitive to such a complication, so its indication of a ratio of twenty is selected. In Figure 3.10c, the topsoil conductivity is freed along this ratio, and the daily change indicates a distinct optimum at 75 mm/d equivalent to Clay Loam. Pursuing different targets can be defended by initial drainage is sensitive to preferential conduits and the correlated anisotropy ratio, whereas later drainage is sensitive to soil type and the correlated horizontal conductivity.
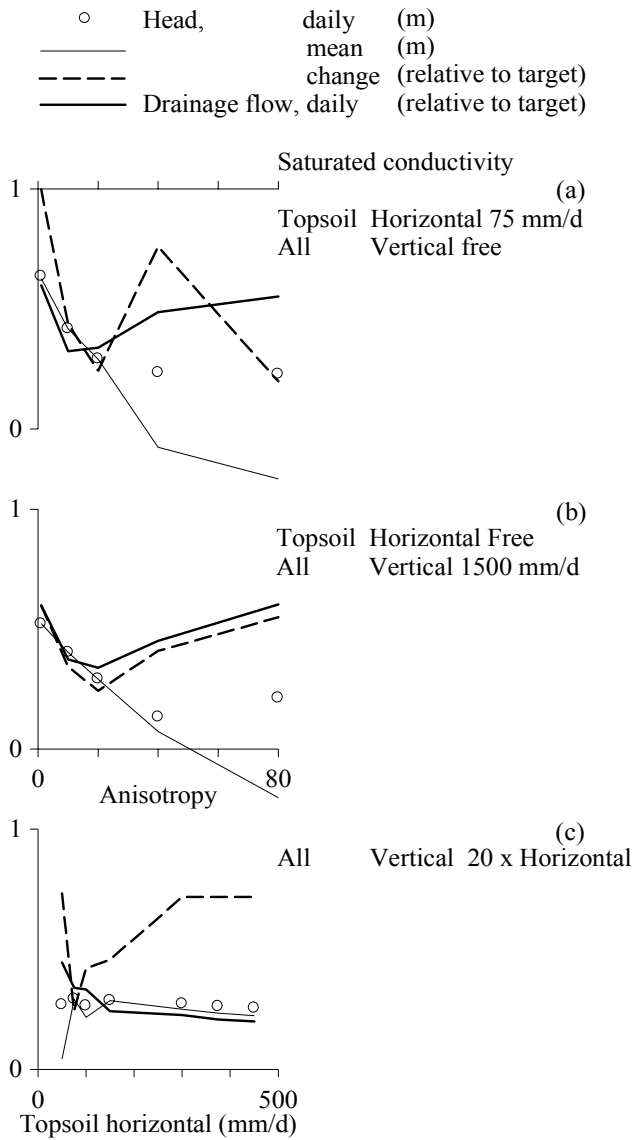

Figure 3.10. Hydrus2D simulation of daily values December 1998 to March 1999 for three wells around a drain line in which flow is compared to the mean catchment drain time. Anisotropy ratio found in (a, b) is used for the topsoil in (c).

3.7. Groundwater Exchange outside Drainage Area

Unsaturated bulk modeling at the wells requires a proper groundwater boundary checked by equilibrium modeling, since precipitation no longer recharges the same day and the surface demand triggers a capillary rise in summer. The outline of a variably saturated 1D model is followed by evidence of the capillary rise to check the screen depth in the reduced till and the time frame used to define the model underside.

3.7.1. Groundwater Boundary

A deep watertable is virtually decoupled from the unsaturated domain, in which the zeroed tension gradient lets gravity govern the flow. Darcy's theorem leads to

$$z \to \infty \Rightarrow \frac{\partial \psi}{\partial z} \to 0 \Rightarrow \frac{Q}{k} \to 1 \qquad (3.5)$$

where z is level above watertable, ψ tension, Q flow rate, and k conductivity. Sandy soil enables such free drainage close to the watertable due to the steep near-residual tail on its retention curve. A less deep watertable yielding perceptible resistance to recharge can only be decoupled from the groundwater domain by calibration of an approximate boundary condition to an acquired watertable record. *Hopmans and Stricker* [1989] defined "deep drainage" as

$$Q = c_1 e^{-c_2|h-h_0|} \qquad (3.6)$$

In a catchment that responds quickly to recharge with the drainage level h_0 being a lake, a stream, or the like, c_1 has to be calibrated for the watertable h in each well, while c_2 can be calibrated synchronously from the discharge record. *De Vries* [1974] formulated recession over time t as

$$Q = \frac{h - h_0}{c_1} + c_2 \frac{\partial h}{\partial t} \qquad (3.7)$$

Resistance c_1 is defined by pattern, path length, and transmissivity of the regional groundwater circulation, c_2 by soil porosity less moisture content at field capacity. His formulation opens for a capillary rise should the watertable fall below the drainage level. Specialized formulations for tile drains as drainage level fall into two similar groups. Only a shallow watertable triggers the full coupling with a hydrostatic equilibrium

$$z \to 0 \Rightarrow \psi = -z \qquad (3.8)$$

which allows for a capillary rise without calibration. Clay soil has the ability to extend equilibrium to far above the watertable due to the thick near-saturated toe on its retention curve.

3.7.2. Equilibrium Modeling

For derivation of the maximum extent of decoupling, we consider steady percolation above the deep watertable in the uphill well *1* equal to the breakthrough in fall, and neglect the high-permeable topsoil. A minor routine was written to unfold the unsaturated profile from the watertable, where saturation ensures convergence. *Van Dam and Feddes* [2000] discretized Darcy's theorem by linking level z and $z+dz$ above the watertable with flow Q defined as positive upwards,

$$Q(z+dz) = \frac{k(z+dz)+k(z)}{2}[1 - \frac{\psi(z+dz)-\psi(z)}{dz}]$$

(3.9)

where k is conductivity, and the bracketed left and right term represents the gradient of gravity and tension ψ, respectively. Only the effective water content S_e has to be searched at the upper level, since it defines tension and conductivity in the applied van Genuchten-Mualem parameterization. Our iterative solution of this implicit formulation utilizes that in equilibrium the function f

$$f = Q(z+dz)-Q \rightarrow 0$$

(3.10)

Iteration leaps to machine precision in a Newton-Raphson scheme, where the slope is calculated from a perturbation $\varepsilon = 10^{-6}$. In the next iteration $i+1$, the updated root is put at the intersection of the slope and the ordinate,

$$S_e^{i+1} = S_e^i - [0 - f(S_e^i)]\frac{(1-\varepsilon)S_e^i - S_e^i}{f((1-\varepsilon)S_e^i) - f(S_e^i)}$$

(3.11)

where the fraction is the slope and $f(S_e^{i+1}) = 0$ has been imposed. After the solution interval has been expanded until the function gets opposite signs at the ends, iteration switches to bisection only if convergence proceeds slowly or the ends have been reached. A 1 mm step is adequate in Equation 3.9's central difference scheme for conductivity, as zero flow results in an unsaturated profile equal to the retention curve.

Again, the slug test result fetches unsaturated characteristics from the database of *Carsel and Parrish* [1988], and vertical conductivity is enlarged with the anisotropy ratio. Lines indicating 10 % deviation from free drainage are given in Figure 3.11 for the oxidized till. Percolation decouples the domain from the watertable by lowering the tension

gradient when it flushes the porosity unoccupied by the immobile water under the retention curve. In Figure 3.7a, catchment discharge shows that percolation exceeds 1 mm/d periodically after the watertable has reached the tile drains. Should such a percolation ever endure to generate equilibrium, the free drainage would still not pervade the lower 1.5 m in terms of tension and 1.9 m in terms of flow. Reduced till has a steeper retention curve that inhibits free drainage more than its smaller conductivity enhances it. During summer, the small percolation rates according to Figure 3.7a and the shallow watertable clarify that full coupling prevails and a capillary rise is present.
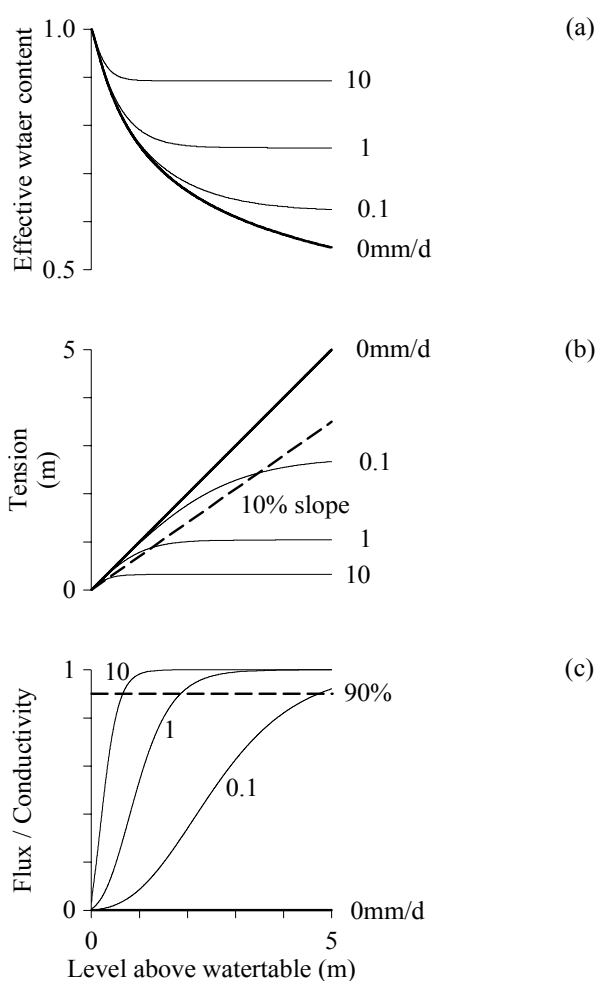
Figure 3.11. Equilibrium profile of the oxidized till at well *1* for different percolation rates (mm/d) in terms of (a) water content, (b) tension, and (c) flux.

3.7.3. Transient Modeling

Richards' equation adds a storage term for root zone budgeting to the lag through the percolation zone in the Darcian theorem. The adopted Hydrus1D code [*Simunek et al.*, 1998] introduces a variable rooting depth at the cost of Hydrus2D's drain presentation, giving them a complementary seasonal adaptation. The seven data points of the seasonal root depth for winter wheat [*Christiansen et al.*, 2002] has to be cut to Hydrus1D's three in

a way that preserves the annual potential transpiration and evaporation of Equation 3.4. This is accomplished by removal of growth in fall and minor bends, and a coordinated harvest time for root depth and leaf area at August 19. The root depth increases from New Year to June 16, and remains constant until harvest; the leaf area increases to May 4, less steeply to June 24, and decreases to zero at harvest. These simplified daily series have a correlation coefficient to their original counterpart of 99 % for transpiration and 90 % for evaporation. Again, the slug test result fetches unsaturated characteristics from the database of *Carsel and Parrish* [1988], the topsoil is Clay Loam and the reduced till, below the measured oxidation depth, is Silty Clay with horizontal conductivities of 75 and 0.21 mm/d, respectively, and vertical conductivity is enlarged with the anisotropy ratio.

Instead of the very watertable, the groundwater boundary has to be induced at the model underside from an assumed hydrostatic equilibrium. This underside is placed below the lowermost monthly watertable in a depth of 6 m for well *1* and 5 m for well *12*. Table 3.5 demonstrates that induction of the reduced till's piezometric head satisfies the measured watertable, bearing in mind the transducer resolution of 14 mm. Those long screens that are not positioned close to such a pressure outtake must have their boundary constructed from the watertable itself. Why well *1* suffers from deplorable dynamics can be grasped by the fact that zero storage capacity would make the boundary push groundwater flow in antiphase of percolation, and thereby swallow recharge and emit chock fronts every time the watertable passes a layer interface. A suite of quasi-steady model runs with a fixed boundary has the chance to escape such extinction. Execution from hydrostatic equilibrium in March does not have to leap extra years to copy the seasonal pattern. Flow is, on average, valid in the interval for which the boundary has been fixed, and reconstruction can be obtained from model runs of all intervals. A daily interval would replicate the resolution of the atmospheric forcing, though a fulfillment of this object would require hundreds of model runs - for each well. A monthly interval improves the dynamics in Table 3.5, but leaves the staircase appearance of Figure 3.12a.

Table 3.5. Watertable error in transient, unsaturated modeling without smoothening of output.

Lower boundary	Model - Observed [a]	
	Well *1*	*12*
Piezometric head screen *C* daily		-0.06±0.12
Watertable daily	0.34±0.59	0.02±0.07
piecewise	0.18±0.32	0.05±0.14

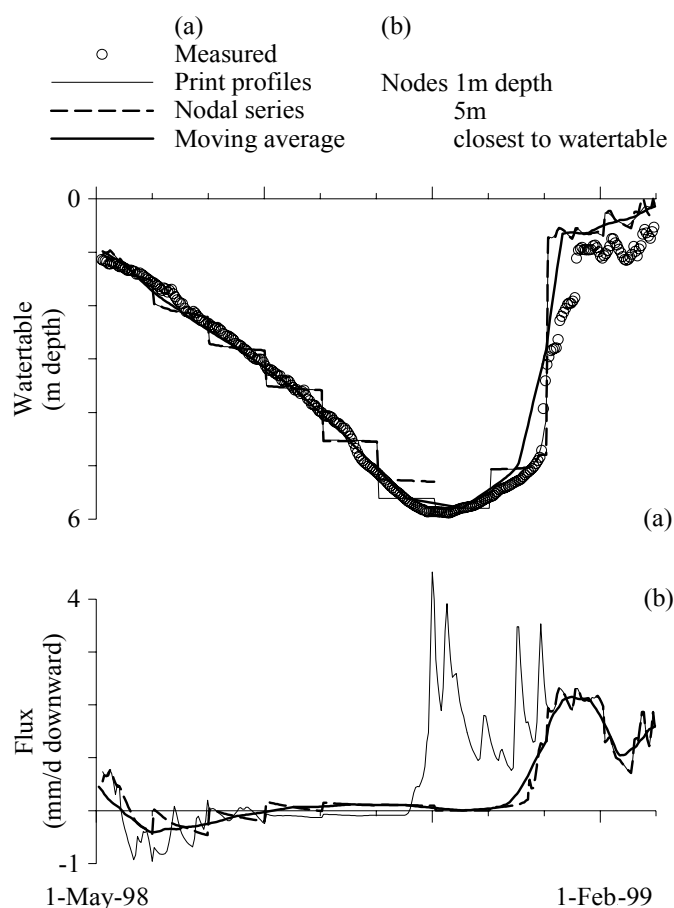[a] Well *1* May 1998 - February 1999, *12* May - October 1998 (m).

Figure 3.12. Hydrus1D simulation of the soil profile at well *1* with the monthly watertable imposed at the lower boundary. (a) Monthly moving average from the two output formats relative to the measured watertable and (b) constructed recharge relative to flow at the shallowest and deepest node pair.

The available two output formats must be elaborated to determine the groundwater exchange. For the one hundred print profiles, the watertable is identified between the two nodes immediately above and below zero tension, and daily values interpolated between the equidistant print times. For the ten nodes paired uniformly below the root zone, the watertable is extrapolated from the node with smallest absolute tension, and daily values weighted according to the time steps. Extrapolation is suspended and replaced with zeroes, however, if drying presses tension beyond 2 m. Figure 3.12a shows that the formats agree until extrapolation provisionally is stopped.

The staircase watertable reflects that the fixed boundary begins overstating and ends understating the downward pressure gradient, vice versa when the watertable rises. Daily values can be sorted out by running a moving average with a bandwidth of one month through the piecewise output. Halfway up the rise during fall, the bandwidth is halved in compliance with a more changeable percolation. Despite terrain-parallel groundwater flow disturbs the 1D framework after the drain level has been reached, the smoothened

watertable can substitute the reduced till's piezometric head in Table 3.5. A similar conclusion is drawn for the intimately related recharge. Flow, computed from Equation 3.9 for each node pair, is seen in Figure 3.12b to dampen away from the surface and over summer, and recharge can be picked from the node pair closest to the monthly watertable.

3.7.4. Evidenced Capillary Rise

Malik et al. [1989] moistened soil columns via an inlet container at the bottom, and *Parlange et al.* [1990] could match all computed filter velocities to Richard's equation. The examined clays had flow rates of 0.20±0.01 mm/d when the wetting front was 1.5 m above the fixed watertable, while suction appeared to persist up to 2.5 m above. Note that suction should persist higher up in clay till according to the unsaturated characteristics of *Carsel and Parrish* [1988]. *Prathapar and Meyer* [1993] examined clay loam in lysimeters with a watertable gradually lowered over a depth of 0.6-1.3 m under a semiarid climate, where surface drying drove the capillary rise to 0.7-1.6 mm/d during the growth season. *Hopmans and van Immerzeel* [1988] examined sandy loam under a humid climate by monitoring the watertable decline from 0.2 to 1.5 m in seven wells during the summer half-year. The modeled evapotranspiration close to its potential limit pulled a capillary rise of 0.6-1.0 mm/d. For a clayey till catchment near the present, *Christiansen et al.* [2002] found by integrated modeling using MIKE SHE [*DHI*, 1999] that the capillary rise amounted to 89 mm/y in the randomly checked grid.

Given time, the imbalances of the study catchment vanish and estimation of net recharge R_{Net} become identical from above and below the watertable,

$$R_{Net} = P - ET = Q + R_{Aq} \tag{3.12}$$

Inflow equals precipitation P less evapotranspiration ET; outflow equals discharge Q cleared of waterworks, sewage, and pavement plus aquifer replenishment R_{Aq}, which *Christiansen et al.* [2002] and *Geological Survey of Denmark and Greenland* [1999] determine to 39 and 28 mm/y for the regional aquifer, respectively. Rearranging for its average gives $ET = P$-Q-R_{Aq} = 710-200-33 = 477 mm/y over 1974-99, or 86 % of the potential limit. Figure 3.13 depicts a fluctuation in their ratio due to annual changes in weather and subsequent underground storage. Figure 3.6b showed that the watertable bursts to the drain level in November and leaps back in April. These months separate grossly the percolation predominantly in winter from the capillary rise predominantly in summer. The discharge record traces how this separation elapsed before monitoring. Annual discharge 1974-99, cleared as above, connects best to the monthly precipitation from November, or December, to April with correlation coefficients of 83 %, or 80 %. Termination in April clocks the onset of plant growth, while the annual differences in

baseflow and time to refill to the drain level expound the gap to a complete match. For the net recharge of 233 mm/y, a percolation closer to 341 than 275 mm/y corresponds to a capillary rise closer to 110 than 44 mm/y.
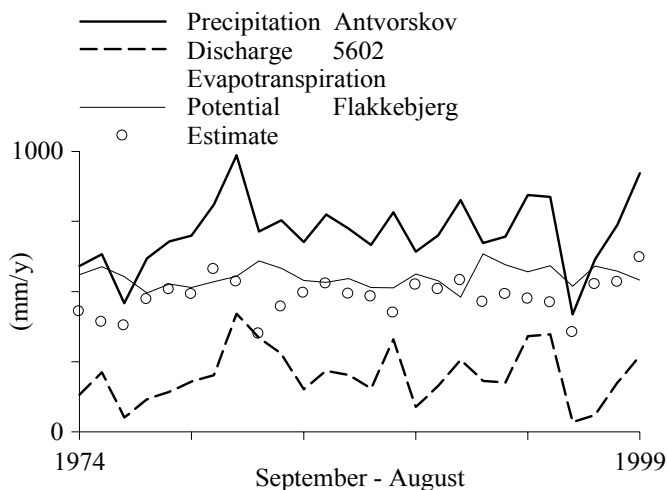

Figure 3.13. Annual evapotranspiration estimated as precipitation less discharge cleared of waterworks, sewage, and pavement, and 33 mm/y of aquifer replenishment.

3.7.5. Reduced Till and Model Underside

These uncertainties must be clarified from the long-term capillary rise versus the summer of 1998 with its normal precipitation and potential evapotranspiration. Comparison is only meaningful for, say, May through August, before watertable deepening at well *1* developed a zero-flux plane that broke the surface connection. Judged from the listed studies and the bell-shaped seasonal evapotranspiration, we should target a capillary rise around 50-60 mm. The model underside is set to the closest integer meters below the lowermost monthly watertable. At the well nests *4A, 9B*, and *12C* the reduced till displays a conductivity on 22±8 % of the oxidized till, corresponding to Silty Clay at the majority of all long screens. Piezometer *A* and *B* resides at a depth of 3½ m, *C* at a depth of 6 m. Their slug test results are attached to all positions of the long screens as either one-fifth the locally tested of the oxidized till or uniformly as that of piezometer *C* multiplied by the anisotropy ratio to 4.2 mm/d in the vertical direction. Replacement of the distributed conductivity with the uniform halves the deviation from the target in Table 3.6. Thus, the installation depth of the piezometer has to accommodate the watertable minimum, or else the slug test will probably bias the conductivity ascribed to the model underside from its exponential decrease with depth. In our case, the other too shallow piezometers allow for an artificially large capillary rise. Also the time frame for the watertable minimum has biased the model underside to be too shallow. Taking the chance of weather into account by neglecting the wet 1999 deepens the model underside to 5 m everywhere, except for 6 m in well *1*, and brings an acceptable capillary rise.

Table 3.6. Transiently modeled capillary rise
May - August 1998 (mm) for which the wells
are listed after terrain level. Flush empty
entries from left.

Reduced till [a] Moel underside [b]	Distributed 1998-9	Uniform	1998
1	105	23	
2	55	46	
3	103	24	
12	29		23
11	1		
4	149	145	85
5	103	94	69
7	131	42	
754	150	148	93
9	153	152	92
6	174	126	87
Mean	105	75	53

[a] Conductivity one-fifth the oxidized till, or as pizeometer *C*.
[b] Integer meters below lowermost monthly watertable.

3.8. Results

Rainfall-runoff modeling is the traditional approach to link catchment discharge with atmospheric forcing. Consideration of an ensemble of storms serves to remove weather variability from the model's correlation to topography, land cover, soil, and geology. If the selected storms are similar or the mapping improper, the validity of the calibration may be jeopardized. Getting to the catchment water balance requires a model that represents the underground well. One may even avoid some subjective calibration, depending on how sound its physical rationale is. Unfortunately, the depth-dependent entrance on the retention and conductivity curves governed by topography and the correlated watertable, the soil dependence of these curve sets, and tension building up to equalization for passage of layer interfaces all lead to a potentially overwhelming variability in the unsaturated zone compared to the groundwater below. Difficulties in quantifying effective watertable depths and curve sets have lead many to deduce recharge from root zone budgeting on top of a groundwater model, and, at the most, consider the capillary rise as an unchecked refinement. We emphasize that attempts to parameterize a numerical code comprising unsaturated flow should be evaluated at suitably located wells. *Grayson et al.* [1997] pointed out how soil moisture switches relatively fast between a wet state with water moving along the terrain and a dry state with water moving vertically, *i.e.* a shift between non-local topographical control and local soil control. Tile drains made it possible to map the extent of the wet state as the drainage area in Section 5, and dry state modeling was prepared in Section 7.

Table 3.6 indicates a downhill increase in the capillary rise. Well *6* in a depression, *754* in a flat area, and *9* on a hillslope located 1 km apart illustrates how strong the feedback can be under normal weather conditions and the little influence of the soil variability for a shallow watertable. Watertable deepening under the hillslope edge at well *11* cuts the feedback compared to the nearby well *12* with an equal conductivity and terrain level. Well scarcity against the topographical variability, and soil variability emerging during the dry state imply that the distinction between wet and dry states can be made only on a monthly basis for the six level intervals defined in Table 3.7. Neither the wet state nor the capillary rise during the dry state reaches the uppermost interval without any well. This interval is attributed to well *1* except in March 1999, where it remains in the dry state and is represented by the Hydrus1D run of the well for the following month. The lowermost interval contains the 5 % of the catchment covered by permanent grass. Hydrus1D runs carried out both for permanent grass and winter wheat against the low-lying well *6* result in an annual difference in recharge of 5 %, as permanent grass continues transpiration after winter wheat has been harvested. A merger in the dry state, June to September 1998, is free of this bias. Table 3.7 summarizes the zonated groundwater exchange as of 1998, which has aimed at maintaining the well density per unit area. A doubled precipitation in October lifts the annual recharge above normal. The exceptional large precipitation the following twelve months and its diversion through tile drains may explain why recharge increases downhill. Figure 3.14 gives an impression of how successive winter precipitation and summer evapotranspiration drive the groundwater exchange for the catchment as a whole. Net recharge runs between incoming precipitation and outgoing discharge, but falls below in normal summers due to the capillary rise ignited by evapotranspiration.

Table 3.7. Topographically zonated groundwater exchange, accumulated for 1998.

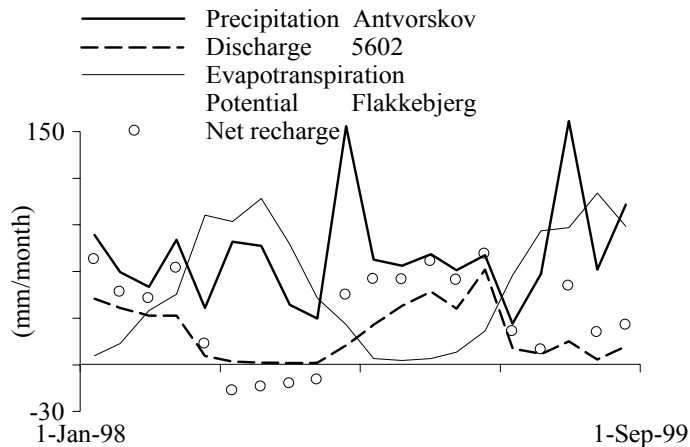| Zone	Well	Terrain (m above m.s.l)	Area (%)	Recharge (mm)	Capillary rise (mm)
I		66-84	6	102	18
II	*1*	56-66	12	102	18
III	*2*	46-56	14	196	48
IV	*3, 12, 11*	41-46	21	412	20
V	*4, 5, 7*	36-41	22	356	77
VI	*754, 9, 6*	14-36	25	494	106
Catchment			100	334	57

Figure 3.14. Monthly net recharge against discharge cleared of waterworks, sewage, and pavement, and atmospheric forcing.

3.9. Conclusions

We have investigated the magnitude of the capillary rise in clay till under a humid climate by mapping the monthly value of this and groundwater recharge for six topographical intervals in an underdrained 16 km^2 Danish catchment. In 1998, we find that the capillary rise stabilizes at 0.7 mm/d during four months in the valley, resulting in totally 57 mm against the 334 mm of recharge. Clay till transmits the drying demand from the surface to the groundwater until the watertable has fallen below a depth of 3-4 m. Ignoring the capillary rise markedly understates the water movement, even though the climate is humid.

Our sequential parameterization of physically based models applies watertable data to circumvent the ambiguity inherent in spatial variability and confine any bias introduced by the user. Owing to the excessive wetness from October 1998, a dozen of wells were adequate for the established distinction between the dry state area and the complementary pulsating wet state area from which tile drains divert recharge to the stream. Separation of contributions from pavement and baseflow revealed the drain time and a loss, which has been attributed to the existence of vertically oriented preferential conduits. According to watertable increments during storm, the slug test can be used to access soil characteristics in a USDA database. The database and the drain time could transform the description of preferential conduits from a streamflow loss to a bulk anisotropy by calibration of a variably saturated 2D model centered on a single drain line. Variably saturated 1D modeling used the monitored watertable depth to determine the lag before infiltration recharges in the dry state. Moreover, the model must be fully coupled to the watertable to reproduce the capillary rise without calibration. The depth at which piezometers are installed in the reduced till and the time frame of the minimum watertable are both crucial issues for a true model underside.

References

Abbaspour, K. C., M. T. van Genuchten, R. Schulin, and E. Schlappi, A sequential uncertainty domain inverse procedure for estimating subsurface flow and transport parameters, *Water Resour. Res.*, *33*, 1.879-1.892, 1997.

Allerup, P., and H. Madsen, Accuracy of point precipitation measurements, *Nordic Hydrol.*, *11*, 57-70, 1980.

Bos, M. G. (Ed.), Working group on small hydraulic structures, *Discharge measurement structures*, Int. Institute for Land Reclamation and Improvement, Wageningen, Netherlands, 1976.

Bouwer, H., and R. C. Rice, A slug test for determining hydraulic conductivity of unconfined aquifers with completely or partially penetrating wells, *Water Resour. Res.*, *12*, 423-428, 1976.

Carsel, R. F., and R. S. Parrish, Developing joint probability distributions of soil water retention characteristics, *Water Resour. Res.*, *24*, 755-769, 1988.

Chow, V. T., D. R. Maidment, and L. W. Mays, *Applied hydrology*, McGraw-Hill Inc., Singapore, 1988.

Chu, S. T., Groundwater recharge and water table rise under equilibrium condition, *Trans. Am. Soc. Agric. Eng.*, *39*, 981-984, 1996.

Christensen, S., Hydrological model for the Tude å catchment, *Nordic Hydrol.*, *25*, 145-166, 1994.

Christiansen, J. S., J. C. Refsgaard, and M. Thorsen, Modelling of pesticide transport and fate at catchment scale, methodology and case study, *submitted*, *J. Hydrol.*, 2002.

Dahlin, T., and M. H. Loke, Resolution of 2D Wenner resistivity imaging as assessed by numerical modeling, *J. Applied Geophysics*, *38*, 237-249, 1998.

de Vries, J. J., *Groundwater flow systems and stream nets in the Netherlands*, Ph.D. Thesis, Vrije Univ. Amsterdam, Netherlands, 1974.

DHI, Water & Environment, *MIKE SHE 1999 Water movement, User manual*, Denmark, 1999.

Geological Survey of Denmark and Greenland, *National vandressource model, midtvejsrapport, Status – maj 1999* (Danish), Denmark, 1999.

Gerber, R. E., and K. Howard, Recharge through a regional till aquitard: three-dimensional flow model water balance approach, *Ground Water*, *38*, 410-422, 2000.

Gillham, R. W., The capillary fringe and its effect on water-table response, *J. Hydrol.*, *67*, 307-324, 1984.

Grayson, R. B., A. W. Western, F. H. S. Chiew, and G. Blöschl, Preferred states in spatial soil moisture patterns: local and nonlocal controls, *Water Resour. Res.*, *33*, 2.897-2.908, 1997.

Hansen, E., and M. Dyhr-Nielsen, The hydrological Suså-study, *Nordic Hydrol.*, *13*, 257-262, 1982.

Heppell, C. M., T. P. Burt, and R. J. Williams, Variations in the hydrology of an underdrained clay hillslope, *J. Hydrol.*, *227*, 236-256, 2000.

Hinton, M. J., S. L. Schiff, and M. C. English, Physical properties governing groundwater flow in a glacial till catchment, *J. Hydrol.*, *142*, 229-249, 1993.

Hopmans, J. W., and C. H. van Immerzeel, Variation in evapotranspiration and capillary rise with changing soil profile characteristics, *Agric. Water Management*, *13*, 297-305, 1988.

Hopmans, J. W., and J. N. M. Stricker, Stochastic analysis of soil water regime in a watershed, *J. Hydrol.*, *105*, 57-84, 1989.

Hvorslev, M. J., *Time lag and soil permeability in ground water observations*, Bull. 36, US Army corps of Eng., Waterways Exp. Stn. Vicksburg, MS, 1951.

Isaaks, E. H., and R. M. Srivastava, *Applied geostatistics*, Oxford Univ. Press, New York, NY, 1989.

Jensen, S. E., Model ETFOREST for calculating actual evapotranspiration, *Comparison of forest water and energy exchange models*, Int. Soc. for Ecological Modelling, 165-172, Ed. Halldin, S., Denmark, 1979.

Kaleris, V., Quantifying the exchange rate between groundwater and small streams, *J. Hydraulic Res.*, *36*, 913-932, 1998.

Klint, K. E. S., and P. Gravesen, Fractures and biopores in Weichselian clayey till aquitards at Flakkebjerg,

Denmark, *Nordic Hydrol.*, *30*, 267-284, 1999.

Kristensen, K. J., and S. E. Jensen, A model for estimating actual evapotranspiration from potential evapotranspiration, *Nordic Hydrol.*, *6*, 170-188, 1975.

Larsen, T. E., K. Hansen, and E. Iversen, *Synkronmålinger i Vårby Å-systemet 1994* (Danish), Waterconsult, County of Western Zealand, Denmark, 1995.

Lerner, D. N., A. S. Issar, and I. Simmers, *Groundwater recharge, a guide to understanding and estimating natural recharge*, Int. Contributions to Hydrogeology, 8, Int. Ass. Hydrogeologists, Verlag Heinz Heise, Hannover, Germany, 1990.

Malik, R. S., S. Kumar, and R. K. Malik, Maximal capillary rise flux as a function of height from the water table, *Soil Sci. J.*, *148*, 322-326, 1989.

Mikkelsen, H. E., and J. E. Olesen, *Sammenligning af metoder til bestemmelse af potentiel fordampning* (Danish), Rep. S 2157, Danish Institute of Agricultural Sciences, Denmark, 1991.

Miles, J. C., and K. Kitmotto, New drain flow formula, *J. Irrigation and Drainage Eng.*, *115*, 215-230, 1989.

Mualem, Y., A new model for predicting the hydraulic conductivity of unsaturated porous media, *Water Resour. Res.*, *12*, 513-522, 1976.

Myrabø, S., Temporal and spatial scale of response area and groundwater variation in till, *Hydrol. Processes*, *11*, 1.861-1.880, 1997.

Parlange, J. Y., R. Haverkamp, J. L. Starr, C. Fuentes, R. S. Malik, S. Kumar, and R. K. Malik, Note on maximal capillary rise flux as a function of height from the water table, *Soil Sci. J.*, *150*, 896-898, 1990.

Prathapar, S. A., and W. S. Meyer, Measurement and estimation of capillary upflow from watertables under maize on irrigated soils, *Aus. J. Soil Res.*, *31*, 119-130, 1993.

Purvance, D. T., and R. Andricevic, On the electrical-hydraulic conductivity correlation in aquifers, Geoelectrical characterization of the hydraulic conductivity field and its spatial structure at variable scales, *Water Resour. Res.*, *36*, 2.905-2.914, 2000.

Rorabaugh, M. I., Estimating changes in bank storage and groundwater contribution to streamflow, *Int. Ass. Sci. Hydrol.*, *63*, 432-441, 1964.

Russo, D., E. Bresler, U. Shani, and J. C. Parker, Analysis of infiltration events in relation to determining soil hydraulic-properties by inverse problem methodolody, *Water Resour. Res.*, *27*, 1.361-1.373, 1991.

Simunek, J., M. Sejna, and M. T. van Genuchten, *The HYDRUS-1D software package for simulating the one-dimensional movement of water, heat, and multiple solutes in variably-saturated media*, version 2.0, IGWMC-TPS 70, Int. Ground Water Modelling Center, Colorado School of Mines, Golden, CO, 1998.

Simunek, J., M. Sejna, and M. T. van Genuchten, *The HYDRUS-2D software package for simulating the two-dimensional movement of water, heat, and multiple solutes in variably-saturated media*, version 2.0, IGWMC-TPS 53, Int. Ground Water Modelling Center, Colorado School of Mines, Golden, CO, 1999.

Sophocleous, M. A., Combining the soil-water balance and water-level fluctuation to estimate natural groundwater recharge, practical aspects, *J. Hydrol.*, *124*, 229-241, 1991.

Szilagyi, J., and M. B. Parlange, Baseflow separation based on analytical solutions of the Boussinesq equation, *J. Hydrol.*, *204*, 251-260, 1998.

Tallaksen, L. M., A review of recession analysis, *J. Hydrol.*, *165*, 349-370, 1997.

Troch, P. A., F. P. de Troch, and W. Brutsaert, Effective water table depth to describe initial conditions prior to storm rainfall in humid regions, *Water Resour. Res.*, *29*, 427-434, 1993.

van Dam, J. C., and R. A. Feddes, Numerical simulation of infiltration, evaporation and shallow groundwater levels with the Richards equation, *J. Hydrol.*, *233*, 72-85, 2000.

van der Kamp, G., and H. Maathuis, Annual fluctuations of groundwater levels as a result of loading by

surface moisture, *J. Hydrol.*, *127*, 137-152, 1991.

van Genuchten, M. T., A closed-form equation for predicting the hydraulic conductivity of unsaturated soils, *Soil Sci. Soc. Am. J.*, *44*, 892-898, 1980.

Villholth, K. G., K. H. Jensen, and J. Fredericia, Flow and transport processes in a macroporous subsurface-drained glacial till soil, I: Field investigations, *J. Hydrol.*, *207*, 98-120, 1998.

Winter, T. C., Relation of streams, lakes, and wetlands to groundwater flow systems, *Hydrologeol. J.*, *7*, 28-45, 1999.

Yang, Y. J., and T. M. Gates, Wellbore skin effect in slug-test data analysis for low-permeability geologic materials, *Ground Water*, *36*, 931-937, 1997.

Chapter 4

Response of a Clayey Till Catchment to Two Decades of Atmospheric Forcing

Thomas Schrøder

Danish Meteorological Institute

Dan Rosbjerg

Technical University of Denmark

Abstract. We investigate the influence of the commonly ignored capillary rise from groundwater on the water balance in a Danish catchment of 16 km^2. Hydrological modeling for 1980-99 substantiates its, on the average, uphill decrease and corresponding increase in net recharge of 30 %. The groundwater feedback is responsible for a correlation coefficient of 30 % between annual evapotranspiration and the North Atlantic Oscillation, which governs Europe's weather, particularly in winter and perhaps over a large part of the northern hemisphere. Generally, hydrological modeling of clayey catchments with a similar size may characterize the oscillation's historical coverage better than what sparse long precipitation records have traced. Runoff from comparable catchments indicates good model performance after a parameterization based on electrical sounding, streamflow separation, and modeling of watertable wells.

4.1. Introduction

Glacial thrusts during the ice ages formed a large part of the surface in the present humid climate belt. These till units appear to be clayey even for minor clay contents, because extensive mixing has decreased the permeability. Little is known about the tortuous water circulation inside glacial till [*Hinton et al.*, 1993] and bulk modeling remains a prerequisite for mapping groundwater recharge in these deposits [*Gerber and Howard*, 2000].

Basin hydrology applies to a regional scale with an almost steady net recharge percolating to confined aquifers [*Halford*, 1999], whereas hillslope hydrology applies to a local scale with a mass balance of the unconfined aquifer that takes account of streamflow generation but treats deeper circulation as a loss [*Wigmosta and Burges*, 1997]. Integrated modeling bridges the two scales by including the watertable as an internal state and the water circulation that streams do not intersect, so it may reduce the recharge uncertainty by one order [*Lerner et al.*, 1990]. Extending the model boundaries, however, implies increasing ambiguity as more circulation mechanisms are brought into play. One must therefore decide whether parameterization of a given mechanism is worth the effort.

Solar heating dries the soil surface and makes plants grow. The moisture depletion will eventually encounter the unconfined groundwater body and trigger an upward flow from its watertable, which we refer to as the capillary rise. Laboratory studies [*Malik et al.*, 1989] and field studies undertaken in semiarid areas [*Prathapar and Meyer*, 1993] have

verified the potential of this feedback to evapotranspiration, a mechanism which persists for a rather deep watertable in a clay soil due to its relatively straight retention curve.

Levine and Salvucci [1999] found from statistics for hillslope circulation against steady-state groundwater modeling that the uphill falling watertable decreases the capillary rise and increases the net recharge correspondingly. Integrated modeling has an advantage in its minor dependence on statistical inference, but a disadvantage in its extensive parameterization. We have monitored a Danish, clayey till catchment that also lies in the westerly wind belt. Low pressures bring rain from the Atlantic and generates a humid climate characterized by mild winters, changeable summers, and a weak monsoon. Our watertable measurement enabled a sequential parameterization that has resolved the daily recharge and capillary rise in six terrain intervals [*Schrøder and Rosbjerg*, 2002].

In this paper, we include a time period before monitoring took place in our examination of the surface-groundwater contact with the assistance of integrated modeling. First, we accentuate snow storage in the precipitation description and use the mapped net recharge to tie the sequentially determined groundwater parameters together. Second, we elaborate the unsaturated conductivity. Third, we perform nineteen years of integrated modeling to uncover how the capillary rise adjusts the average net recharge to terrain and how the annual evapotranspiration resembles to the North Atlantic Oscillation.

4.2. Study Catchment

Harrested catchment is located in Denmark south of the town Slagelse in the rural southwestern Zealand with a ridge running on its northern and western flank. Topographical delimitation indicates a drainage area of 16.01 km^2 upstream discharge station *5602* with a relief 14-93 m above the mean sea level (m.s.l.), as reproduced in Figure 4.1b. In the catchment, 95-98 % of the soil has been classified as clay till. Our two years of monitoring from September 1997 comprised eleven watertable wells spanning two-third of the catchment in terms of terrain level, the three internal discharge weirs *A*, *B*, and *C*, and an automatic tipping-bucket rain gauge at Idagård, which like the manual gauge at Antvorskov is corrected for wind and wetting following *Allerup and Madsen* [1980]. Global radiation, temperature, wind, and humidity recorded at Flakkebjerg underlie a modified Penman estimate of the potential evapotranspiration [*Mikkelsen and Olesen*, 1991].

4.2.1. Hydrogeology

Glaciofluvial sediments form a regional confined aquifer with practically no deeper exchange through the tertiary clay underneath [*Christensen*, 1994], and its overburden of later deposited glacial till forms an unconfined aquifer. These till units comprise a lodgment till that propagated over the ridge of terminal till, and a flow till that left its
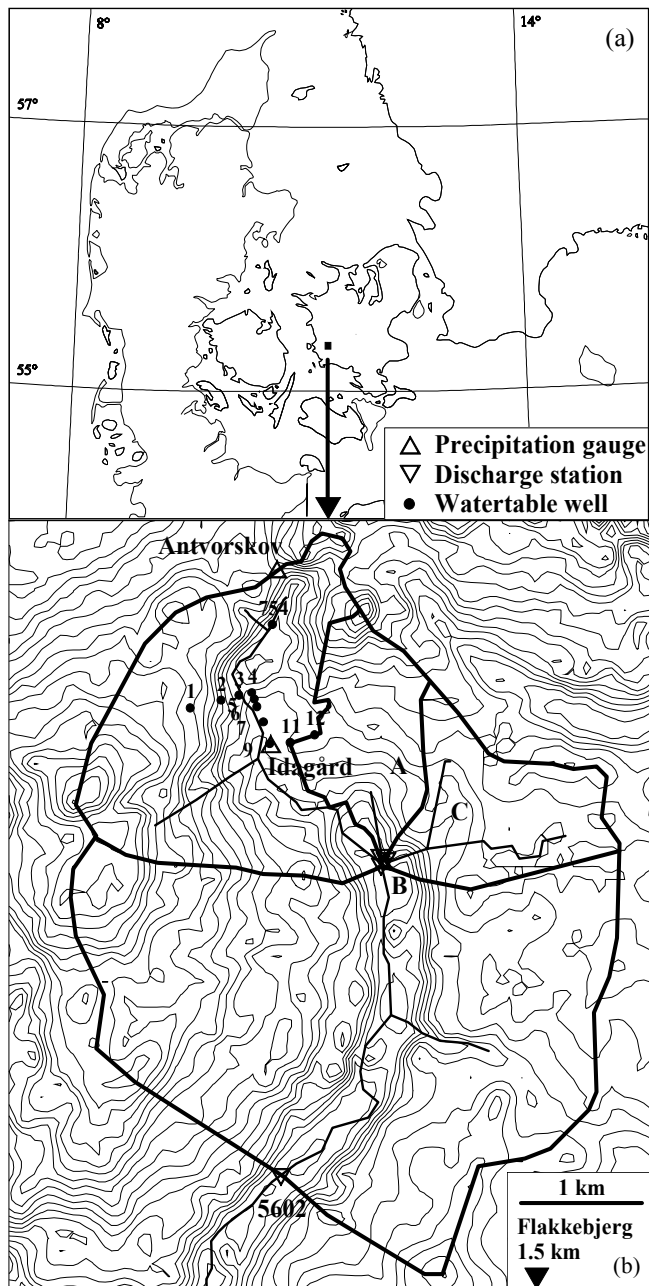
Figure 4.1. (a) Location of study catchment with (b) terrain contours in 2.5 m intervals and relevant instrumentation.

northern part with an irregular surface. Groundwater crosses the catchment boundary mainly via the regional aquifer, as the northern ridge coincides with a major water divide. Figure 4.2 shows how a reduced till with an uphill increasing thickness has been added to the uniformly weathered strata to account for the capillary fringe, which separates the visible oxidation front from the watertable minimum [*Schrøder and Rosbjerg*, 2002]. Hydraulic conductivity and the level of the regional aquifer have been interpolated between the sparse wells using a combination of borehole logging, electrical sounding, and baseflow modeling.
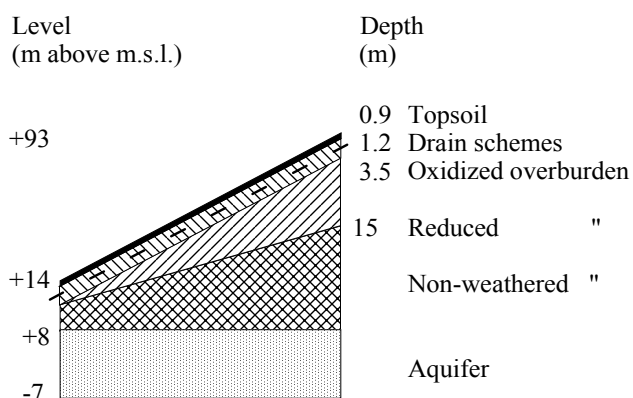
Level
(m above m.s.l.)

Depth
(m)

0.9 Topsoil
+93
1.2 Drain schemes
3.5 Oxidized overburden

15 Reduced   "

+14
Non-weathered "

+8

Aquifer

-7

Figure 4.2. Conceptual geology and subsurface drainage.

4.2.2. Vegetation

The agricultural area that in 1991 constituted 99 % of the catchment had changed little over the past six decades [*Waagepetersen et al*., 1991], though bare winter fields should be covered with crops, narrow stretches along streams laid fallow, and wetlands reestablished after the water protection act of 1987. Figure 4.3 shows how the farmland of the county has decreased slightly and grains were standardized from spring barley to winter wheat. The county trend applies in the catchment, because winter wheat indeed prevailed during monitoring and the municipality never deviated more than a few percent from either of them. While pasture and meadow that covered the area around the open stream (5 % of the catchment) can be merged as permanent grass in the lowermost terrain, the unknown outside distribution of grains requires a simplification with two model scenarios: one for winter wheat and one for spring barley. The county trend indicates for 1980-99 that the first has to be weighted one-third and the second two-third.
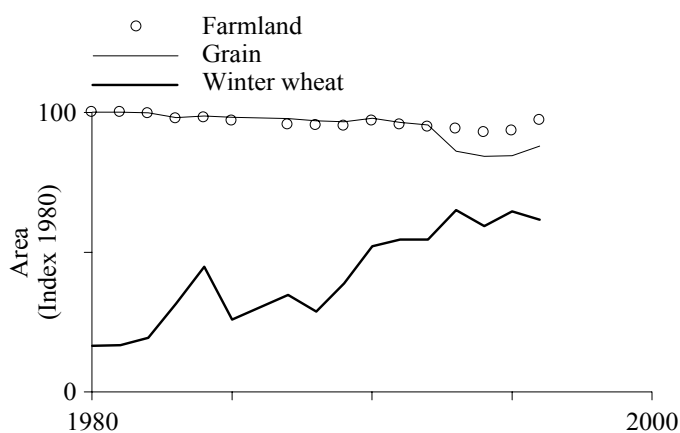

Figure 4.3. Western Zealand's development of farmland and how much winter wheat constituted of the area covered by grain [*Statistics Denmark*, 1986-99].

4.2.3. Snow Storage

Both rain gauges are of the Hellmann kind, aluminum fabricated, and with a cross inserted in winter to prevent snowdrift. The coastal proximity makes the air temperature a robust index of the energy available for snowmelt [*Maidment*, 1993]. Provided that the degree-day model applies, the manual gauge reveals the daily input and the automatic gauge the output of the snow pack. If so, the infiltration I [mm/d] should be retarded when the air temperature T [°C] drops below a threshold $T^{'}$ and released proportional to the degree-day factor D [mm/d/°C] when it rises above

$$I = \begin{cases} 0 & ; T \leq T^{'} \\ D(T - T^{'}) & ; T > T^{'} \end{cases} \tag{4.1}$$

Temperature records divide at midnight whereas precipitation records divide at 8 am. A shift in the less variable temperature by weighting the day of collection one-third (0-8 am) and the preceding day two-third (8 am-12 pm) introduces a random error with a standard deviation of 0.6 °C according to hourly measurements at Flakkebjerg.

From November 1998 to February 1999, 257 mm of precipitation was recorded and the daily temperature ranged –8 - +7 °C with an average of +1 °C. A difference in the catch of 2 % suggests that mass errors due to snowdrift and sporadic rainstorms can be neglected. Figure 4.4a shows the calibration towards a threshold of –1 °C, its negative
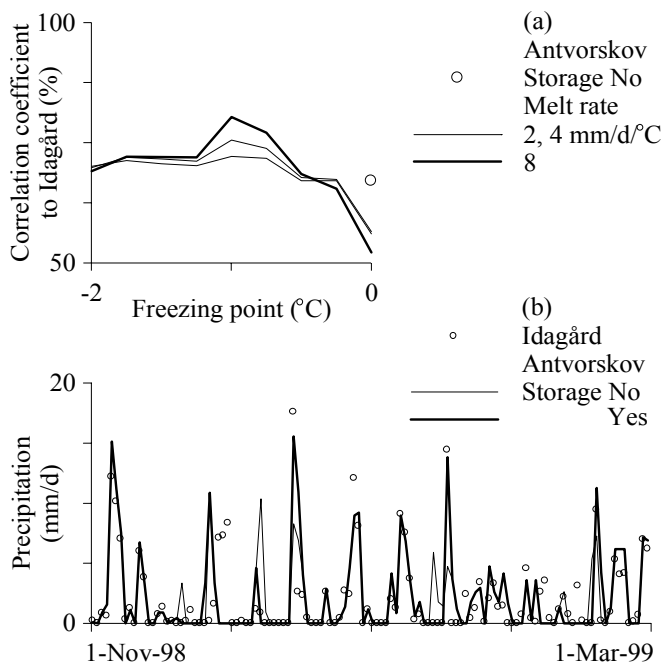

Figure 4.4. (a) Antvorskov's daily emptied gauge conditioned to Idågård's automatic using snow storage with a freezing point and a melt rate, and (b) underlying time series.

value reflects precipitation during the, on the average, colder night. The factor is settled at 8 mm/d/°C, as infinity is sought above this value on the basis of a single day. It exceeds 6 mm/d/°C near coasts on a low latitude, where buffering due to the rarely ice-covered sea results in frequent passage of the freezing point [*Maidment*, 1993]. The low albedo of old, dirty snow and the increasing radiation in springtime should make the factor seasonally dependent, but this may not be an issue due to the frequent thaw and the short winter season.

Figure 4.4b shows the time series. Observe for the manual record how heavy showers at the time of emptying mask the early November and late December peaks, while the flat top in late February is an equal distribution of a shower over a weekend without daily emptying. The last major error appears in late November, where application of the temperature ahead of a passing cold front has cancelled the detention at the manual gauge. Of the precipitation in the winter half-year, 12 % was retarded as snow during 1980-99.

4.3. Hydrological Model

The adopted code MIKE SHE [*DHI*, 1999] encloses sinks for abstraction and stream exchange in its groundwater description based on Boussinesq's equation. Terrain has been block-kriged from digitized contour lines onto its quadratic grid with an assigned mesh width of 100 m. Between the regional aquifer and the compulsory merged weathered strata, the non-weathered overburden is split into six equally thick computational layers. The stream has been ascribed to a trapezoidal cross section that is two magnitudes smaller than the grid size to comply with its nodal presentation, and its exchange has been ascribed to a neutral lining over the confined aquifer at a finite depth by setting the lining equal to the average overburden thickness divided by its conductivity. Streamflow can be routed as a diffusive wave and overland flow as a kinematic wave due to the daily resolution of the atmospheric forcing, or net recharge in its place. Tile drains are described as a lumped sink with bypass to the stream delayed through a linear reservoir without initial storage. Table 4.1 lists all key parameters.

First, we parameterize the groundwater domain from the mapped net recharge and the boundary head of the regional aquifer, also accounting for the waterworks in the stream valley that extracts 70 000 m^3/y. Later, we can exploit its surface coupling in which the vertical unsaturated flow based on Richard's equation contains a sink for evapotranspiration and recharge is derived via an iterative procedure over five steps by matching the watertable change in every grid with the storage change above and below.

Table 4.1. Groundwater and surface parameters from *Schrøder and Rosbjerg* [2002]. Bold figures are subject to calibration.

	Conductivity (mm/d)		Storage (%)	
	Horizontal	Vertical	Unconfined	Confined
Topsoil	75	20 x	5.5	0.010
Oxidized overburden		"	**5.0**	"
Reduced	**0.21**	"	**0.59**	"
Non-weathered	**0.78**	**0.78**	"	"
Aquifer	8600	1 x	37	"
Drain time			**0.28** d^{-1}	
Detention storage			0.01 m	
Stream lining			10^{-11} s^{-1}	
Manning number Streamflow			20 m$^{1/3}$/s	
Overland flow			5 m$^{1/3}$/s	

4.4. Groundwater Parameters

Recharge varies less with scale than routing and storage parameters, and consequently it is safer to upscale recharge from the previously investigated watertable wells. After correction for snow storage, the a priori defined net recharge for January 1998 through August 1999 can be used for calibration of the model parameters. The overburden requires transient calibration due to its low-permeable character [*Halford*, 1999], but the considered period should be long enough to characterize the uniform strata due to the fact that weathered pore space is flushed roughly five times in the lower half of the catchment. The a priori definition breaks the non-linear coupling of the parameters to the unsaturated flow through omitting this part of the integrated modeling, preserves the perceived capillary rise, and accelerates the runtime by two magnitudes.

Calibration by inversion will search the parameters according to an objective function that accumulates the least square fit between modeled and measured time series. Linear inversion has been outlined for models that form their output from a linear combination of their parameters by collecting the first-order derivatives of each parameter against each measurement in a Jacobian matrix and letting a Marquardt-Levenberg scheme inspect its eigenvectors to turn the search away from the steepest descent in case of parameter correlation. The adopted code Pest [*Doherty*, 1999] allows for central difference iteration and parallel MIKE SHE runs on a computer network.

Non-linear prediction did not alter the solution for another non-linear Boussinesq model in the neighboring Tude catchment [*Christensen and Cooley*, 1999]. Electrical sounding and streamflow separation constrain the scalar gap and facilitate the linear inversion together with a log transformation of the drain time, which implies a logarithmic decrease of the watertable against time, and of the usually lognormal-distributed conductivity [*Isaaks and Srivastava*, 1989]. The horizontal conductivity locks its vertical

counterpart in the weathered strata via the anisotropy ratio that accounts for preferential conduits and provides an estimate of the specific yield from the textural database of *Carsel and Parrish* [1988]. The later fully integrated model cannot represent a watertable that falls into the non-weathered overburden. To circumvent this unaccounted threshold in the objective function, the specific yield is copied from the reduced till to the non-weathered overburden. Owing to the fact that drains make the watertable fall rapidly below the topsoil in winter, the number of parameters for calibration narrows to the seven shown in Figure 4.5.

The initial watertable is ascribed to the drain depth inside the area that contributed to drainage flow and it deepens uphill along the slope of its topographically dependent minimum. Calibration must be deactivated for the first three months, since test runs indicate that the piezometric head adjusts to abrupt changes caused by an erroneous initial guess within two months. Subsequent daily averages for the four discharge stations
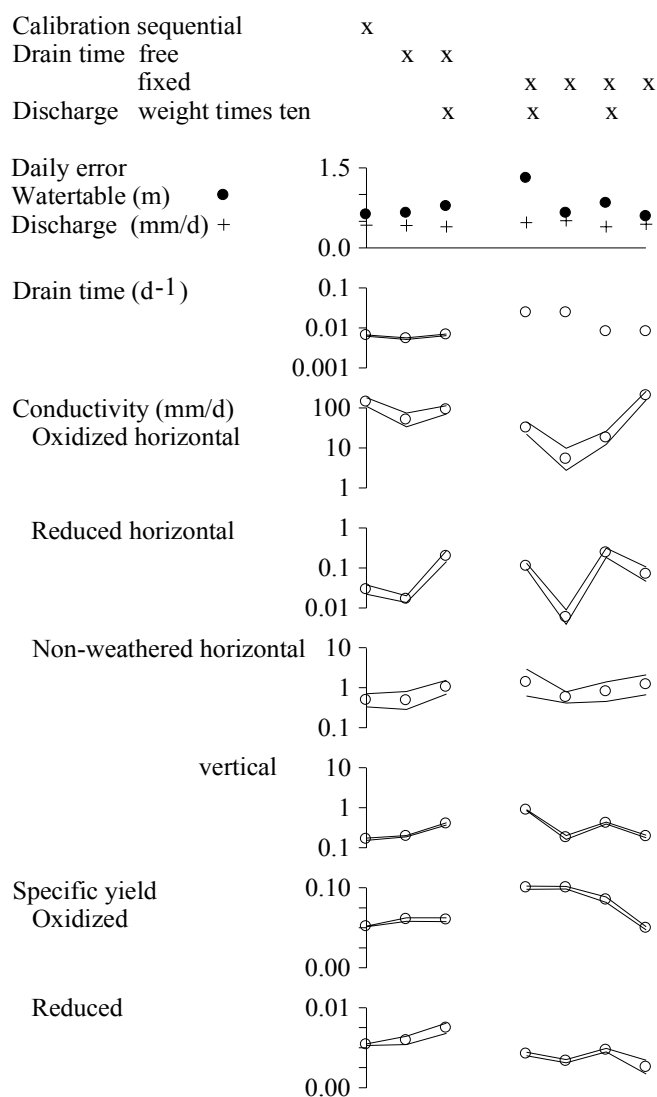
Figure 4.5. Results for seven calibrations of the groundwater parameters with 95 % linear confidence bands to indicate the solution sensitivity.

and the six watertable wells *1, 2, 5, 9, 12,* and *754* suffice in the objective function, because they provide the widest possible control of where and when the drain schemes and the layers contribute to the catchment discharge, and the inversion improves marginally for more measurements compared to the number of addressed parameters [*Duan et al.*, 1992]. Relative weights *w* make the watertable *h* and the discharge *Q* comparable through their number *N* and standard deviation σ,

$$w_Q = 1$$
$$w_h = \frac{N_Q}{N_h} \frac{\sigma_Q}{\sigma_h} = \frac{1639}{3028} \frac{0.11mm/d}{1.06m} = 0.06 \tag{4.2}$$

for which the compound objective function reads

$$\phi = \sum_{i=1}^{N_Q} (w_Q(Q_{sim} - Q_{obs}))^2 + \sum_{j=1}^{N_h} (w_h(h_{sim} - h_{obs}))^2 \tag{4.3}$$

sim denotes simulation and *obs* observation [*Carrera and Neumann*, 1986]. Our depth normalization emphasizes the contributing terrain level through the internal discharge stations and the uphill wells. Seven calibrations are tested to circumvent that the shared starting point encounters a local minimum or a threshold in the objective function. A sequential calibration pursues the parameter type according to its impact by calibrating the drain time, then conductivity, and lastly the specific yield. The six other calibrations of Figure 4.5 arise from either freeing all addressed parameters or freezing the drain time at one of the two last iteration levels in the sequential, and weighting the discharge data as Equation 4.2 or ten times more.

Inspection of all seven calibrations reveals that the drain time and the vertical conductivity of the non-weathered overburden are resolved with their own eigenvector, as they govern the topographical and vertical diversion, while the conductivity and the specific yield of the reduced till are not, as this layer constitutes a transition zone for the flow orientation. Figure 4.5 shows how the stepwise slower drain time leads to a stepwise larger conductivity and smaller specific yield in the surrounding oxidized till, as the soil type influences the drain time [*DHI*, 1999]. Extra weight on discharge turns some outflow from the drains to the regional aquifer by increasing the vertical conductivity of the non-weathered overburden and the correlated, ill-posed parameters of the reduced till. The watertable data are best matched in the rightmost calibration, which differ from the leftmost, the sequential, only by its simultaneous calibration of the specific yield. Their disengagement of the oxidized till from the other parameter's correlation to the weight suggests that extra weight on discharge has magnified a threshold in this layer. Also the poor watertable simulation of the fourth calibration supports that wells contain valuable information on thresholds like the drain level and the layer interfaces.

Only the drain time changes significantly for the selected rightmost calibration: it slows down by a factor of thirty. This factor bulks drain density and soil conductivity into a linear reservoir with a storage that is proportional to outflow. Streamflow separation gave the initial value for strictly vertical flow down to the drain, but the groundwater may circulate from the ten times more distant midline between the drains and down into and back from the several times thicker, more low-permeable reduced till.

The selected calibration simulates the watertable with an error of one-tenth the seasonal amplitude, and Figure 4.6 shows its slightly deteriorated simulation of the streamflow part that comprises drainage flow and baseflow. Errors like the May 1998 bulge arise from the prior recharge mapping, which only had enough watertable wells to resolve the monthly mean area that contributes to drainage flow. Apart from the fact that the applied rain gauge cannot capture all convectional rain, the snow storage and the merging of preferential conduits into a weathered anisotropy appear to be proper.
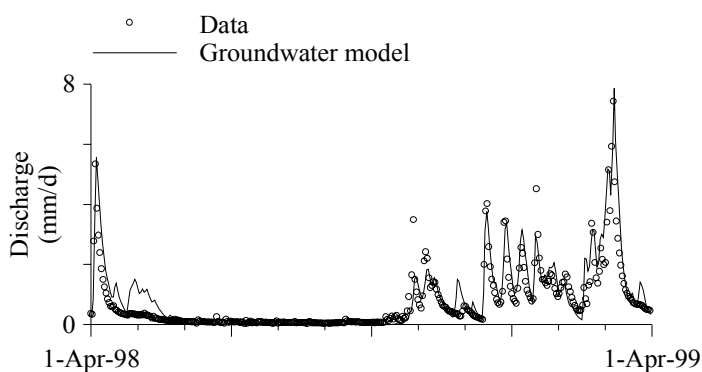

Figure 4.6. Catchment discharge cleared of waterworks, sewage, and pavement against the calibrated groundwater model.

4.5. Unsaturated Parameters

The integrated model will, like the prior recharge mapping, apply vegetation characteristics from *Christiansen et al.* [2002] and use the saturated horizontal conductivity to extract unsaturated soil characteristics from the database of *Carsel and Parrish* [1988]. MIKE SHE permits *van Genuchten*'s [1980] parameterization of the retention curve, but replaces *Mualem*'s [1976] extension to conductivity with Kozeny's approach. Figure 4.7 shows two least square fits of Kozeny's exponent to the soil database at log tensions equally spaced above wilting: one with and one without the toe near saturation. The latter achieves a tighter fit for all three weathered layers by introducing a one magnitude lower saturated conductivity, an assumption which is of minor importance where saturated conditions is rarely met.

Model execution for 1981-92 includes the wet start year and the warm end year in a provisional catchment water balance from two model runs weighted according to Figure 4.3 to circumvent the unknown distribution between spring barley and winter wheat.
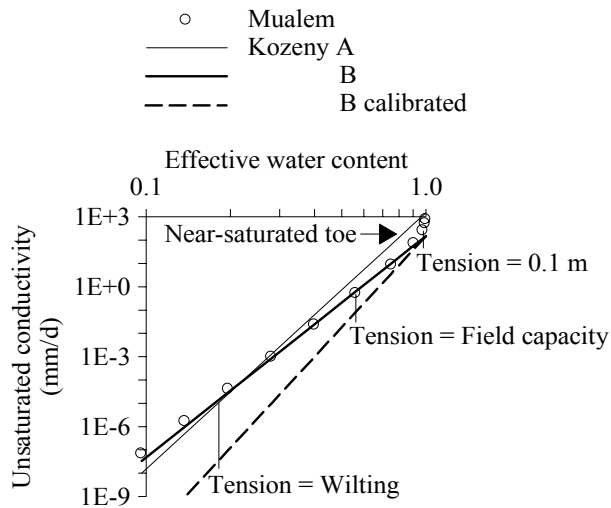
Figure 4.7. Kozeny's exponent is fitted for the topsoil to Mualem's expression from wilting to saturation (*A*) or to 0.1 m tension (*B*).

Starting from field capacity and the said January 1998 watertable, the monthly recharge copies onto itself after three years of warm-up. Table 4.2 shows that fitting without the toe helps in reproducing the discharge, but the improvement stops when the implied dry state also is chosen below the topsoil. Further improvement can be achieved by projecting Kozeny's exponent from the layer below, but the too shallow watertable repeats that the dry state should not be chosen below the topsoil. Thus, Kozeny's exponent is upscaled for the topsoil alone, and its calibrated conductivity below the database predicted value implies no major impact on the watertable.

Plowing generates a pan at the base of the furrows. Insertion of a plough pan in a depth of 0.25-0.3 m with a conductivity two magnitudes below the surrounding topsoil had no effect on the discharge and is therefore not responsible for the conductivity discordance. Figure 4.7 suggests that the discordance increases to two magnitudes as the topsoil dries out over the late summer and early fall, where the watertable declines many meters. We stipulate from *Mualem*'s [1976] argumentation for using only his extension in clay soil that the discordance is generated by a seasonal switch from below to within the near-saturated toe in the hydraulic conductivity of the thick, underlying weathered till. The impact on the water balance must be small, however, as the maximum error in the watertable simulation occurs during its minimum in the fall, where the capillary rise and the drainage flow remain insignificant.

Table 4.2. Kozeny's exponent for unsaturated conductivity calibrated 1981-92 against discharge clear of waterworks, sewage, and pavement (*Q*) and well *1*'s deepest watertable compared to August 1998 (*h*).

	Topsoil	Oxidized	Reduced	Q(mm/y)	h(m depth)
Measured				231	3.7
Fit [a]	A	A	A	192	
	B	A	A	202	
	B	B	A	203	
Layer below [b]	B	Bn	A	206	2.4
	B	An	A	208	2.3
	Bn	A	A	212	3.3
	An	A	A	205	3.5
Calibration [c]	B(13)		A	232	3.3

[a] To Mualems's expression from wilting to saturation (*A*) or to a tension of 0.1 m (*B*), [b] indicated by *n*, [c] final exponent.

4.6. Results

Production runs can be made from September 1980, where the well that monitors the annual trend in the regional aquifer's boundary head was installed in Flakkebjerg, to the end of our monitoring in August 1999. Table 4.3 shows an annual turnover in the water balance that is quite insensitive to the gradual replacement of spring barley with winter wheat, since the watertable remains shallow enough in winter to enable a capillary rise to feed a soil evaporation from bare fields almost as efficiently as any plant transpiration from a rudimentary root network. The replenishment of the regional aquifer is similar to 22 mm/y in the northwestern 450 km^2 Tude catchment [*Christensen*, 1994], 39 mm/y in the southern 65 km^2 Bjerge catchment [*Christiansen et al.*, 2002], and 28 mm/y for the 7215 km^2 Zealand as a whole [*Geological Survey of Denmark and Greenland*, 1999]. Against the relevant discharge shown in Figure 4.8, the total deviates 0.4 % and the largest discrepancy is a horizontal displacement from September to November 1987, when construction works redirected diversion from additional paved areas to the studied stream.
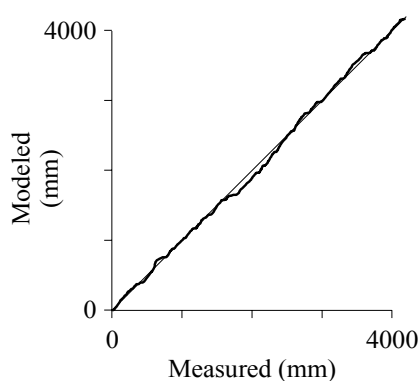
Figure 4.8. Catchment discharge cleared of waterworks, sewage, and pavement against the integrated model for 1980-99.

Table 4.3. The water balance 1981-99 weights a model run for spring barley (*B*) two-third and a model run for winter wheat (*W*) one-third.

	B	*W*	Total
Precipitation			736
Potential evapotranspiration			557
Evapotranspiration	486	495	489
Canopy	13	23	17
Pond	0	0	0
Evaporation	54	30	46
Transpiration	33	47	38
Groundwater	0	0	0
Net recharge	247	238	244
Aquifer replenishment	31	31	31
Discharge	222	212	219

4.6.1. Runoff

The prior recharge mapping applied the variable source concept to identify the area in which the watertable was shallow enough to trigger recharge and subsequent drainage flow on the day of precipitation. This contributing area is ascribed to gravity and therefore taken as a continuum that expands uphill from the stream. A good indication of the concept is a runoff coefficient, defined as discharge divided by precipitation, which varies proportionally to the catch.

Conventionally, the runoff coefficient has been compiled for the storm response. It must also hold for their annual average provided that reference is made to discharge instead of the catch, because a clay soil's annual net recharge is harder to quantify from the catch less the estimated evapotranspiration, which varies from year to year due to the capillary rise from a variable watertable depth. Figure 4.9 confirms a proper modeling of

the concept from other fully underdrained clayey catchments that range two magnitudes in size and steepness. The runoff coefficient reveals a tremendous variability in the contributing area - an indication of the prevalence of its monthly variability of 0-88 % during the monitored two years and conversely the applicability of the concept for recharge mapping. MIKE SHE's merging of drain schemes and weathered layers and its seasonally problematic unsaturated conductivity seem to have no major impact on the annual water balance.
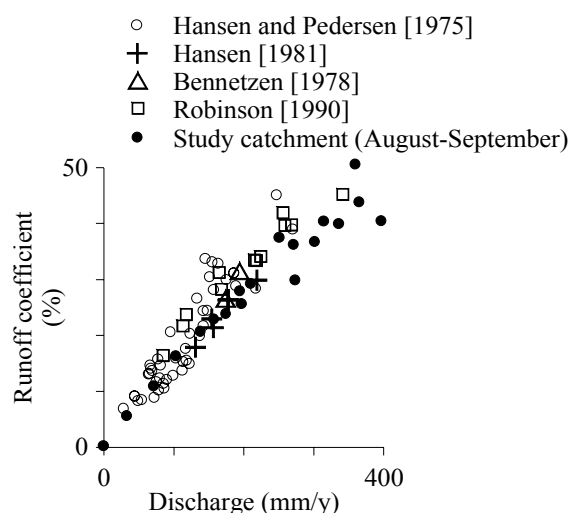

Figure 4.9. Annual discharge versus runoff, defined as discharge divided by precipitation.

4.6.2. Net Recharge

Winter [1999] has outlined qualitatively how recharge adjusts to topography, and *Levine and Salvucci* [1999] made a statistical approach to this observation. Their modeling of the unsaturated exchange between a plant cover and a watertable in an idealized hillslope cross section gave them an event-based partitioning of the atmospheric forcing and the responding capillary rise, which lead to a correlation between the long-term net recharge and its corresponding watertable depth. The correlation furnished their groundwater model with a lookup table that could balance the equilibrium watertable against the influx.

Equilibrium is hard to assert from the monitored transient watertable, but the established integrated model has provided a one magnitude longer time frame. Figure 4.10 reproduces the anticipated uphill increase in net recharge. The average 244 mm/y depicts the precipitation surplus in the humid climate and the permeable substratum that deepens the watertable and thereby impedes the capillary rise. The groundwater focus in the stream valley maintains a shallow watertable at the cost of a deeper one at the water divide. This topographically determined groundwater flow limits the capillary rise from 90 to 20 mm/y, which in turn explains the uphill increase in the net recharge. A zero-flux plane will develop when the watertable deepens more than 3-4 m. Uphill, the topographical

undulations induce a greater dispersion in the net recharge through the greater dispersion in how frequently the capillary rise becomes extinguished.

Dry years aggravate the soil moisture deficit in summer, which pushes the developed zero-flux planes further downhill and postpones the watertable rise at the winter onset. The required additional filling of the vadose zone increases the uphill area free of capillary rise and thereby maximizes the net recharge compared to the available recharge. This unsaturated feedback mechanism ensures a flexible groundwater "catch zone" that sweeps up- and downhill with the annual weather. How volatile this zone is can be illustrated from the monitoring. Monitoring took place at a time of excessive rainfall, which turned the net recharge to be largest downhill in agreement with the variable source concept. It seems to be the luck of the draw that monitoring coincided with a weather window, in which the dozen of watertable wells sufficed for a monthly recharge mapping based on this concept.
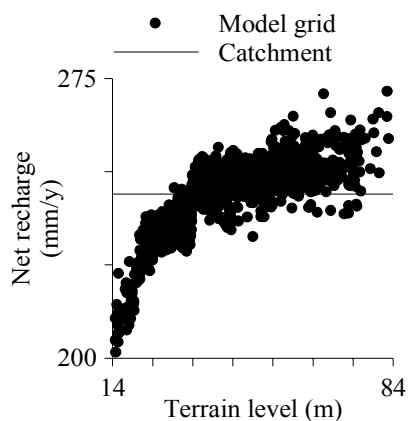

Figure 4.10. Net recharge 1980-99 for each model grid and for the catchment mean as a whole.

4.6.3. Evapotranspiration

The North Atlantic Oscillation (NAO) designates a barotropic, latitudinal oscillation in atmospheric mass centered on the dipole between the Icelandic low and the Azores high pressure. It shifts the longitudinal storm tracks and associated eddy activity, which govern the moisture transport of most frontal rain to European westerlies. Because this perennial oscillation accounts for more than one-third of the variability in the, in a meteorological sense, regional sea level and is most pronounced in winter, *Hurrell* [1995] institutionalized the use of a NAO index based on the time-averaged difference in the winter's sea level between two specific measurement stations in Iceland and Portugal, normalized against a certain range of years. His index enabled the meteorological community to trace the regional oscillation back to 1864, far beyond what can be achieved by reanalysis of numerical weather prediction models. Reanalysis offers, on the other hand, the best detection of global-scale climate trends during the past five decades, as its assimilation of many more data reduces the noise level, and it reveals a NAO dipole in the Atlantic sector

that not always centers on the considered two stations. Hence, the first principal component of its sea level pressure anomalies is a more physical index [*Marshall et al.*, 2001].

NAO contains a slight maximum in its power spectrum around the mode of 2-3 years, though the decadal mode has gained significance over the past few decades. Figure 4.11 presents evapotranspiration and relevant streamflow on an annual basis, which suffices to resolve the dominating part of the spectrum, against the NAO index and its substitute made from reanalysis. Their amplitudes are not comparable due to different noise levels and reference years for variability, but the trend signs must be identical in years of significant oscillation. Reanalysis deviates three times when the trend is small, evapotranspiration five, including 1983 and 1985, and discharge nine, including 1985, 1986, 1989, 1990, and 1995. The discharge of the underdrained, clayey catchment responds proportionally to the local rain, but each year includes contributions from two winter seasons and baseflow reflecting inter-annual storage. Evapotranspiration peaks in summer and is supplied by the capillary rise until zero-flux planes develop in fall, which makes it a better measure for the rain of the antecedent winter. This feedback is strong enough to maintain a ratio of 88 ± 8 % of the annual potential value.

Generally, catchments capture the area mean moisture flux. The flux must be interpreted from evapotranspiration based on a model that has been calibrated to discharge, when discharge is not the best measure in itself. Then, the derived flux will constrain the local outcome for numerical weather prediction models. *Hurrell and van Loon* [1997] mapped the NAO's extent from the correlation coefficient of its index to long precipitations records, and found from *e.g.* the poor 14 % to the considered Danish rain gauge that Denmark is in the trough between a positive correlation in Scandinavia and a negative on the continent. With reservation for brevity and increasingly wet conditions over northern Europe, we find a correlation coefficient of 30 % to the evapotranspiration of the study catchment.

Thompson and Wallace [1998] responded to a newly discovered relation between the NAO and the surface temperature across the entire northern hemisphere above mid-latitudes with their concept of the Arctic Oscillation. This oscillation may exceed the El Ninõ Southern Oscillation regarding the impact on global weather, if it really is hemispheric. Mapping how both indexes correlate to the evapotranspiration in clayey catchments can therefore contribute to the vivid debate on its geographical extension. At least, such mapping can be a good control of its spatial coverage before reanalysis as long as precipitation, temperature, cloud cover or another scale for radiation, and discharge were recorded.
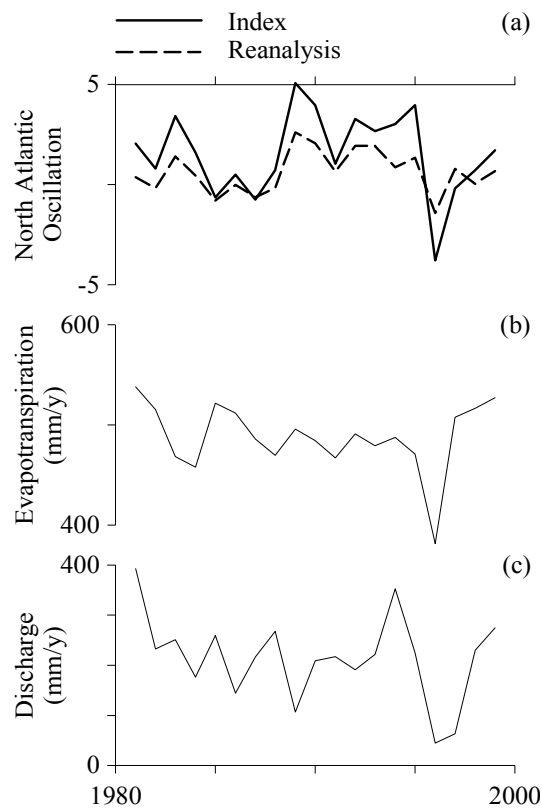
Figure 4.11. Evapotranspiration and discharge cleared of waterworks, sewage, and pavement against the North Atlantic Oscillation, both its index and the first principal component of the sea level pressure according to reanalysis (http://www.cgd.ucar.edu /~jhurrell/nao.pc.winter.html).

4.7. Conclusions

We have explored how a feedback mechanism in clay soil, referred to as the capillary rise, influences the water balance in a catchment of 16 km^2. Suction by the drying surface and plants powers this gradually stronger response from groundwater over the summer until the watertable falls too deep and interstitial zero-flux planes develop. Seen over many years, it accounts for an uphill increase in the net recharge of 30 %.

Also, it ties the annual evapotranspiration to the North Atlantic Oscillation. The correlation coefficient of 30 % is perhaps better than thought of for Denmark, implying that hydrological modeling can establish area-integrated values for the oscillation's spatial coverage - even beyond the available reanalysis of numerical weather prediction models, which precipitation gauges and the index based on sea level pressure are unable of.

Literature values for runoff from comparable clayey, fully underdrained catchments indicate that our modeling has performed satisfactorily, though the applied code contains some shortcomings in its merging of drain schemes and weathered layers and its exponential unsaturated conductivity. No literature values were not found for the suction flux under a humid climate, so this has been parameterized from an elsewhere reported recharge mapping covering two years.

References

Allerup, P., and H. Madsen, Accuracy of point precipitation measurements, *Nordic Hydrol.*, *11*, 57-70, 1980.

Bennetzen, F., Vandbalance og kvælstofbalance ved optimal planteproduktion, 3. Modeller og resultater (Danish), *Tidsskrift for planteavl*, *82*, 191-220, 1978.

Carrera, J., and S. P. Neuman, Estimation of aquifer parameters under transient and steady-state conditions, 1. Maximum likelihood method incorporating prior information, *Water Resour. Res.*, *22*, 199-210, 1986.

Carsel, R. F., and R. S. Parrish, Developing joint probability distributions of soil water retention characteristics, *Water Resour. Res.*, *24*, 755-769, 1988.

Christensen, S., Hydrological model for the Tude å catchment, *Nordic Hydrol.*, *25*, 145-166, 1994.

Christensen, S., and R. L. Cooley, Evaluation of prediction intervals for expressing uncertainties in groundwater flow model predictions, *Water Resour. Res.*, *35*, 2.627-2.639, 1999.

Christiansen, J. S., J. C. Refsgaard, and M. Thorsen, Modelling of pesticide transport and fate at catchment scale, methodology and case study, *submitted*, *J. Hydrol.*, 2002.

DHI, Water & Environment, *MIKE SHE 1999 Water movement*, *User manual*, Denmark, 1999.

Doherty, J., *Pest, model-independent parameter estimation*, Watermark Computing, Brisbane, Australia, 1999.

Duan, Q., S. Sorooshian, and V. Gupta, Effective and efficient global optimization for conceptual rainfall-runoff models, *Water Resour. Res.*, *28*, 1.015-1.031, 1992.

Geological Survey of Denmark and Greenland, *National vandressource model, midtvejsrapport, Status – maj 1999* (Danish), Denmark, 1999.

Gerber, R. E., and K. Howard, Recharge through a regional till aquitard: three-dimensional flow model water balance approach, *Ground Water*, *38*, 410-422, 2000.

Halford, K. J., Effects of steady-state assumption on hydraulic conductivity and recharge estimates in a surficial aquifer system, *Ground Water*, *37*, 70-79, 1999.

Hansen, B., *Drænvandskvantitet og kvalitet i Susåens opland* (Danish), Rep. Suså H 19, Danish Committee for Hydrology, Denmark, 1981.

Hansen, L., and E. F. Pedersen, Drænvandsundersøgelser 1971-74 (Danish), *Tidsskrift for planteavl*, *79*, 670-688, 1975.

Hinton, M. J., S. L. Schiff, and M. C. English, Physical properties governing groundwater flow in a glacial till catchment, *J. Hydrol.*, *142*, 229-249, 1993.

Hurrell, J. W., Decadal Trends in the North Atlantic Oscillation: Regional Temperatures and Precipitation, *Science*, *269*, 676-679, 1995.

Hurrell, J. W., and H. van Loon, Decadal variations in climate associated with the North Atlantic Oscillation, *Climatic Change*, *36*, 301-326, 1997.

Isaaks, E. H., and R. M. Srivastava, *Applied geostatistics*, Oxford Univ. Press, New York, NY, 1989.

Lerner, D. N., A. S. Issar, and I. Simmers, *Groundwater recharge, a guide to understanding and estimating natural recharge*, Int. Contributions to Hydrogeology, 8, Int. Ass. Hydrogeologists, Verlag Heinz Heise, Hannover, Germany, 1990.

Levine, J. B., and G. D. Salvucci, Equilibrium analysis of groundwater-vadose zone interactions and the resulting spatial distribution of hydrologic fluxes across a Canadian prairie, *Water Resour. Res.*, *35*, 1.369-1.383, 1999.

Maidment, D. R., Handbook of hydrology, McGraw-Hill Inc., New York, 1993.

Malik, R. S., S. Kumar, and R. K. Malik, Maximal capillary rise flux as a function of height from the water table, *Soil Sci. J.*, *148*, 322-326, 1989.

Marshall, J., Y. Kushnir, D. Battisti, P. Chang, A. Czaja, R. Dickson, J. Hurrel, M. McCartney, R. Saravanan,

M. Visbeck, North Atlantic climate variability: phenomena, impacts and mechanisms, *Int. J. Climatology*, *21*, 1.863-1.898, 2001.

Mikkelsen, H. E., and J. E. Olesen, *Sammenligning af metoder til bestemmelse af potentiel fordampning* (Danish), Rep. S 2157, Danish Institute of Agricultural Sciences, Denmark, 1991.

Mualem, Y., A new model for predicting the hydraulic conductivity of unsaturated porous media, *Water Resour. Res.*, *12*, 513-522, 1976.

Nash, J. E., and J. V. Sutcliffe, River flow forecasting through conceptual models, part I: a discussion of principles, *J. Hydrol.*, *10*, 282-290, 1970.

Prathapar, S. A., and W. S. Meyer, Measurement and estimation of capillary upflow from watertables under maize on irrigated soils, *Aus. J. Soil Res.*, *31*, 119-130, 1993.

Robinson, M., *Impact of improved land drainage on river flows*, Rep. 113, Institute of Hydrology, Wallingford, UK, 1990.

Schrøder, T. M., and D. Rosbjerg, Assessment of capillary rise in a clayey till catchment using streamflow and watertable data, *submitted*, *J. Hydrol.*, 2003.

Statistics Denmark, *Agricultural statistics annuals*, Copenhagen, Denmark, 1986-99.

Thompson, D. W. J., and J. M. Wallace, The Arctic Oscillation signature in the winter geopotential height and temperature fields, *Geophys. Res. Let.*, *25*, 1.297-1.300, 1998.

van Genuchten, M. T., A closed-form equation for predicting the hydraulic conductivity of unsaturated soils, *Soil Sci. Soc. Am.J.*, *44*, 892-898, 1980.

Waagepetersen, J., S. U. Clausen, K. Schlünsen, D. R. Clark, J. E. Olesen, and H. E. Mikkelsen, *Drainage and runoff in 9 minor water courses from the 1929's until today* (English summary), Rep. 48, Danish Land Development Service, Roskilde, Denmark, 1991.

Wigmosta, M. S., and S. J. Burges, An adaptive modeling and monitoring approach to describe the hydrologic behavior of small catchments, *J. Hydrol.*, *202*, 48-77, 1997.

Winter, T. C., Relation of streams, lakes, and wetlands to groundwater flow systems, *Hydrologeol. J.*, *7*, 28-45, 1999.

Chapter 5
Subsurface Drainage

The discussion on whether the removal of artificial drainage and subsequent restoration of wetlands would increase the exploitable groundwater resource has for many been based on the assumption that artificial drainage decreases the aquifer replenishment. On Zealand, where the groundwater abstraction has been driven close to the edge of sustainable use, the study catchment is very suitable for such an examination due to its exceptionally long discharge record compared to its limited size.

The fieldwork took place in a time that was much wetter than the antecedent twenty years. We have calibrated an integrated model to this wet period and what turns out to be the driest year of the past century, 1996. Such a parameterization, which embraces the transition regime, makes the model more appropriate for examination of the water balance
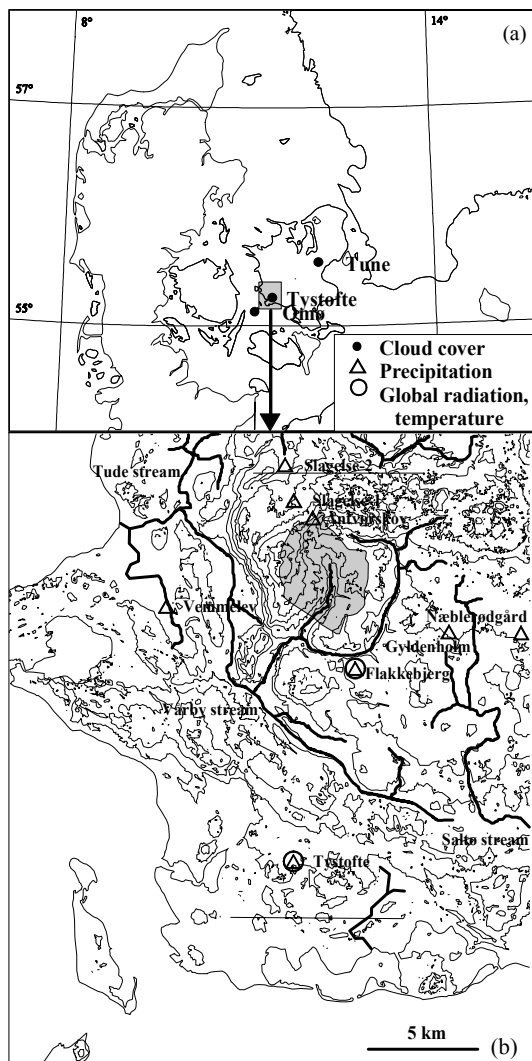

Figure 5.1. (a) Location of study catchment and applied weather stations on Zealand, and (b) regional topography contoured in 10 m intervals around the open streams.

prior to drainage works. Of course, we cannot adjust the drain coverage for the earliest recorded discharge, back in the twenties, without substantiating the atmospheric forcing and the correlated boundary head of the aquifer. Let us begin with the historical data and make some simplifying assumptions before rerunning for nowadays weather.

Generally, the annual division should refer to the start of the month with largest rainfall, the start of the month with largest increase in rainfall, or the end of the month with smallest discharge. While the rainy season changes over time [*Frich et al.*, 1997], the regular solar drying and the responding capillary rise retain the discharge season. Over the past century, the small catchment discharge in August refers the start of the "Hydrological year" to September 1.

5.1. Precipitation

Figure 5.1b shows the longest operated precipitation gauges in the region, where Slagelse was moved to a new location in 1973 after it had been out of service for twelve years. Quality control discloses an excessive catch at Flakkebjerg after an automatic gauge had become its primary instrument in 1987. Some days contain peculiar storms relative to the manual control gauge and other gauges, including the likewise automatic at Tystofte. Their frequent occurrence precludes a physical cause such as local convective rain. Probably, they are spikes caused by electronic malfunctioning, and those larger than 50 mm/d have been replaced with the average of the regional gauges. In the period of operation up till 1990 and after 1995, the control gauge makes a better alternative.

Table 5.1 compares the five gauges with fewest data gaps after their filling. Since no one-sided trend could be inferred from double mass curves, the employed changes due to lee, snow correction, and quality control bear physical meaning, and the stationary means can be determined from linear regression. Surface roughness forces rain out of passing clouds, which implies an increasing long-term mean with distance to the sea along the prevailing west-southwesterly wind [*Frich et al.*, 1997]. Whether the hills attract rain or give lee is not discernible, so the spatial dependence is fitted from the regression means to a plane that slopes 10 % per 18 km towards west-southwest. Figure 5.2 shows how the

Table 5.1. Precipitation gauges relative to Antvorskov in the hydrological years 1974-99, sorted along the prevailing wind orientation.

Station	[a]	[b]	[c]		Patched months [e]	
Tystofte	92.4	93.1	16.3	12	3	3 Flakkebjerg
Flakkebjerg	95.4	94.7	7.5	33	0	0
Slagelse-2	97.5	98.3	2.8	24	7	28 Vemmelev
Antvorskov	100.	100.0	0.0	55	0	1 Slagelse-2
Næblerødgår	94.3	101.3	12.1	45	0	2 Gyldenholm

[a] Monthly correlation coefficient (%), [b] ratio according to regression through origo in double mass curve (%), [c] distance (km), [d] terrain level (m), [e] daily distribution, also monthly volume, and origin.
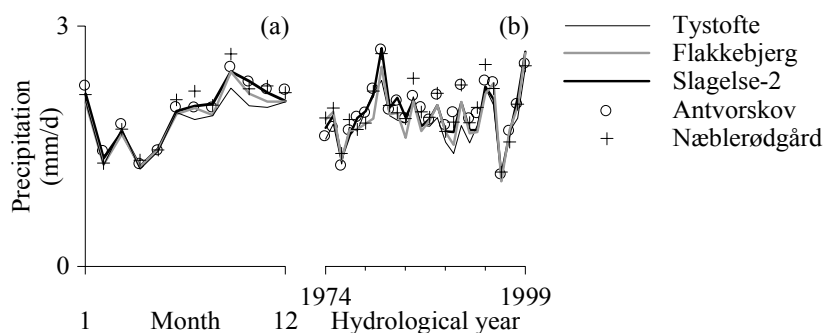
Figure 5.2. (a) Seasonal and (b) annual precipitation captured by regional gauges 1974-99.
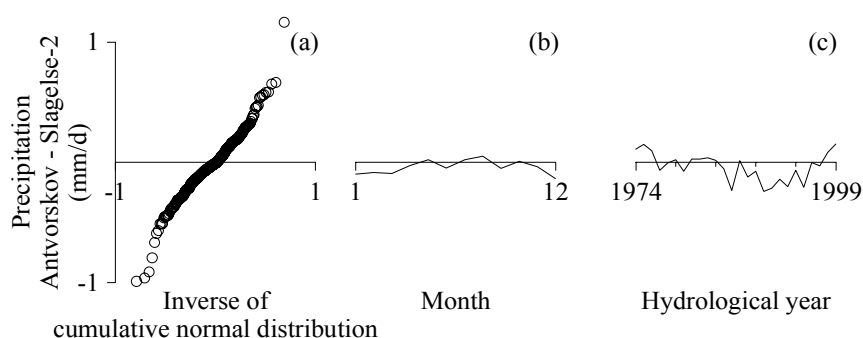

Figure 5.3. Antvorskov's monthly precipitation volume less that of the nearest gauge 1974-99, after correction for the spatially dependent mean.

inter-annual variability that reflects the North Atlantic Oscillation exceeds the weak monsoon of the humid climate with its minor September peak.

A substitute has to be found for the gauge at Antvorskov before its installation in 1957. Figure 5.3 reproduces how the substitution from Slagelse-2 performs in 1974-99, after correction for the spatially dependent mean. Presumably, the North Atlantic Oscillation modulates the prevailing wind orientation and the higher positioned Antvorskov receives a larger catch when the wind turns westerly in winter, but a normal distribution test can only identify the 2 % outliers that convective storms generate outside the bands of white noise. Thus, the long-term mean remains the only systematic drift to be accounted for [*Hipel and McLeod*, 1994].

Tystofte, Slagelse-1, and Vemmelev were operated in the twenties, but lee conditions have not been measured before the sixties. These lee conditions divide in three sheltering classes, in which the catch has to be multiplied with a monthly dependent factor that exceeds unity [*Allerup and Madsen*, 1980]. The annual increase for sheltering class *A* is 12 %, for *B* 16 %, and for *C* 20 %, meaning that a subjective choice has an impact similar to the distance between the regional gauges. Provided the wind orientation has not changed immensely, the coastline determines that the catch at Slagelse-1 remains largest on average. From this rule of thumb, Tystofte's sheltering class was *A* against *C* today and the other way around for the other gauges. Keeping these sheltering classes until lee

measurement began accumulates into a discrepancy below 2 % for interpolation to Antvorskov's location. Figure 5.4 shows the more pronounced peak one month earlier in the twenties than today, as *Frich et al.* [1997] have recovered for all Danish gauges from 1931-60 to 1961-90.
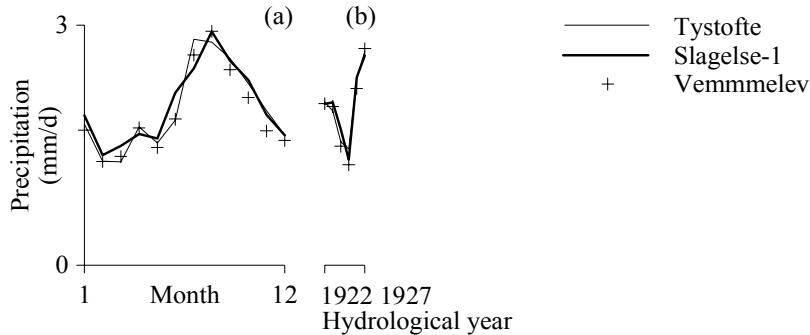

Figure 5.4. (a) Seasonal and (b) annual precipitation captured by regional gauges 1922-27.

5.2. Potential Evapotranspiration

Stress by sun and wind on soils and plants, merged into the quantity denoted potential evapotranspiration, also has to be estimated from the records at hand.

5.2.1. Modeling Approach

Net radiation received at the surface R_{net} comprises direct short- and diffuse long-wave components, R and L, where the incoming short-wave radiation is referred to as global radiation Ra. The radiation balance reads

$$R_{net} = Ra - R_o + L_i - L_o \qquad (5.1)$$

Index *i* denotes incoming and *o* outgoing. *Penman*'s [1956] energy balance, compare to Equation 2.2, contains transport terms for latent heat λET_a, sensible heat H, and heat G vanishing into the ground,

$$R_{net} = \lambda ET_a + H + G + P + M \qquad (5.2)$$

where $\lambda = 2.465$ MJ/kg is water's vaporization heat, P is energy for plant photosynthesis, and M is energy for snowmelt. He eliminated surface temperature, connected latent heat transport to the atmospheric resistance based on temperature, vapor content, and wind speed, and neglected photosynthesis and snowmelt. *De Bruin* [1987] found for farmland in a humid climate that neglecting *Penman*'s explicit account of transport by latent heat induces an error of maximum one-fourth the net radiation. Since the measurable quantity, global radiation, correlates to the sum of net radiation and lost soil flux

$$Ra = f(R_{net} + G) \tag{5.3}$$

he revived *Makkink's* [1957] description of the daily potential limit

$$ET_p = c_0 + c_1 \frac{\frac{\partial e_s}{\partial T} Ra}{\lambda(\frac{\partial e_s}{\partial T} + \gamma)} \tag{5.4}$$

where $\gamma = 0.667$ mb/°C is the psychrometer constant, and $\partial e_s/\partial T$ is the gradient of saturated vapor pressure with respect to temperature, which has been fitted from a table given by *Wilson* [1991]. *De Bruin* [1987] emphasized that this formulation only has physical meaning for the summer half-year, as Equation 5.3's imperfect correlation modifies the two coefficients via the seasonally dependent latent heat, though application for the winter only implies a small absolute error. *Mikkelsen and Olesen* [1991] adopt $c_0 = 0$ and $c_1 = 0.7$ for Danish conditions.

Temperature has been recorded at synoptic weather stations 8 am, 2 pm, and 9 pm. Regression analysis for Flakkebjerg indicates that the daily mean can be estimated to 95 % of their average with a standard deviation of 0.3 °C. Global radiation has been estimated from daily evaporation, but not before 1957 in Denmark [*Mikkelsen and Olesen*, 1991]. It was instead estimated from the ratio between actually occurring and potential sunshine duration, in accord with its approach on clear days to the short-wave radiation received at the atmospheric boundary. Measurement of monthly "bright sunshine" on Campbell recorders was however not upgraded to daily values on Fuess and Cassela recorders before the seventies [*Clark et al.*, 1992]. Cloud cover, which has been recorded at Tystofte's synoptic weather station in the twenties along with temperature, may be considered for improving the monthly resolution of the non-linear evapotranspiration close to the potential limit in the study catchment, but it remains a proxy as it may suffer from the observer's judgment and his averaging over cloud distance, altitude, and thickness.

The latitude dependent radiation level and the atmospheric transparency, which also depends on whether the climate is coastal or continental, govern the actually received short-wave radiation at the surface. Tentative studies for building insulation and air-conditioning pursued a description of the global radiation as a product of clear sky radiation governed by the solar altitude and a reduction factor governed by the bulk cloud cover, therein assuming that ground absorption makes a strictly proportional transformation of short-wave radiation into long-wave emission. *Kimura and Stephenson* [1969] could describe the reduction factor by a second order polynomial with monthly dependent coefficients, when they accumulated the global radiation from hourly solar

altitudes. *Lund* [1979] calibrated their polynomial to the Danish climate from three years of measurement. He extended the day length due to the refraction of 0.5° at the horizon and accounted the geographical determination of the solar altitude for Earth's orbit in terms of its rotational axis is not perpendicular to the ecliptic, its orbital eccentricity, and the solar noon deviation from the meridian. Yet, an absolute error remained in his modeled global radiation that runs sinusoidal through the year and peaks in August with an underestimation of 7 %. This systematical error was attributed to the measurement of the long-wave radiation, which is concentrated by clouds near the horizon and the solar disc. Thus, the overcast sky induces an anisotropy that impeded a separation from the short-wave counterpart.

5.2.2. Model Correction

Let us validate *Lund*'s procedure [1979] for the three years 1988-90. The lack of measured global radiation (Figure 5.5a) and cloud cover at the same location should not be a major drawback, since modeling from cloud cover over either the inland Tune or the coastal Omø, see Figure 5.1a, makes a smaller difference than his reported error. Cloud cover observation every third hour has replaced the three times per day at the manual synoptic stations. Resembling passing clouds from three daily readings requires an interpolation of the intermediate hourly values with a moving average that barely reaches the preceding and subsequent observation, *i.e.* one bandwidth for day and another for night. A
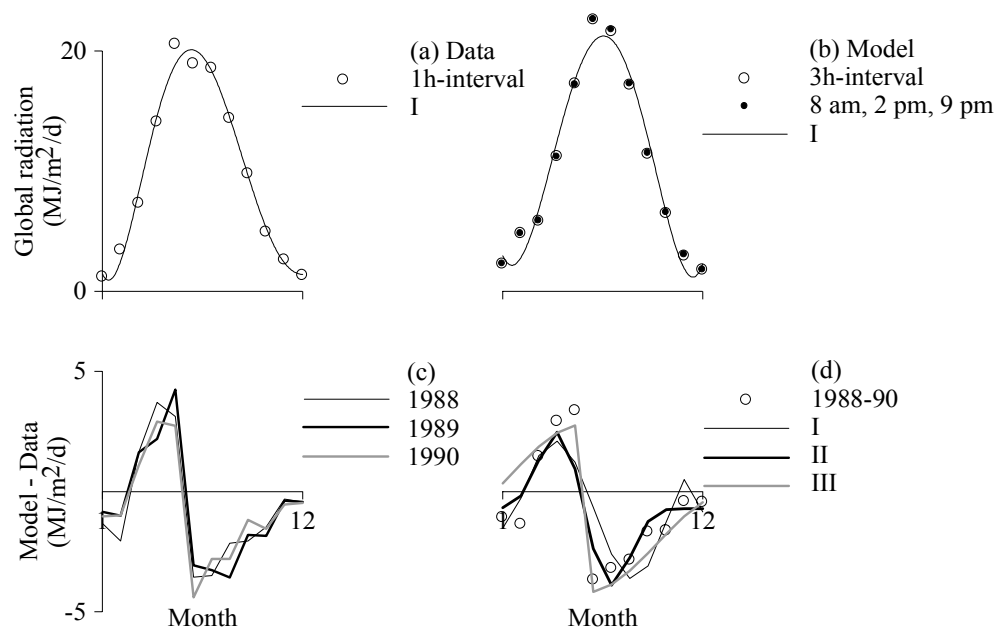

Figure 5.5. Global radiation 1988-90: (a) hourly measured at Flakkebjerg with empirical fit *I*, (b) modeled from Tune's cloud cover, either by its 3 hour measurement or by a moving average through synoptic times, with empirical fit *I*. Model less data (c) seasonally each year and (d) seasonally all years versus the three empirical fits *I-III*.

comparison with the observations every three hours shows that the interpolation breaks down mostly during night. The minor impact due to the small radiation level at night appears from the unbiased modeling in Figure 5.5b.

Long calibration series are an asset to overcome the randomness of the cloud cover during three specific years. *Lund* [1979] may be right about his proposed sinusoidal correction, but the dependence of long-wave radiation to temperature in the fourth power, according to Stefan-Boltzmann's law, and the polynomial extinction by clouds could favor another generalization from the maximum error in summer. We have attempted to describe the monthly difference in Figure 5.5d (*x*) by a fifth order polynomial (*I*), a higher order sine $3 \sin^5 x$ (*II*), and an inverse function $2 / |x-5\frac{1}{2}|$ (*III*), but none of them are superior all of the year and their misfit of 0.41-0.30 $MJ/m^2/d$ are not convincingly better than the inter-annual spread of 0.44 $MJ/m^2/d$ in Figure 5.5c. Only the average of the test period can be defended, but the marginal 4 % error of the average radiation level is acceptable.

Figure 5.6a shows a neat match with Makkink's potential evapotranspiration after the corrected global radiation has been linked with temperature. All underlying months are matched to within 1 %. The range for 38 years of measurement demonstrates that simple statistics would perform poorly, even for a monthly resolution, while *Penman*'s estimation [1956] is given for illustration of the neglected explicit accounting of transport by latent heat. Figure 5.6b fails to track all daily changes due to convective clouds growing over the 100 km between the global radiation observation at Flakkebjerg and the cloud cover observation at Tune, but this inconsistency is greatly relieved in the twenties by application of both cloud cover and temperature data from Tystofte - less than 15 km from the study catchment.
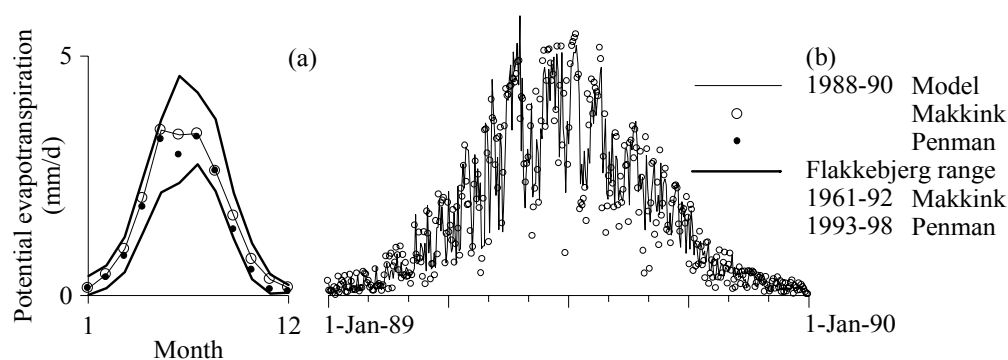

Figure 5.6. Modeled potential evapotranspiration against (a) monthly and (b) daily measurements, after the cloud cover predicted global radiation has been corrected for its seasonal discrepancy.
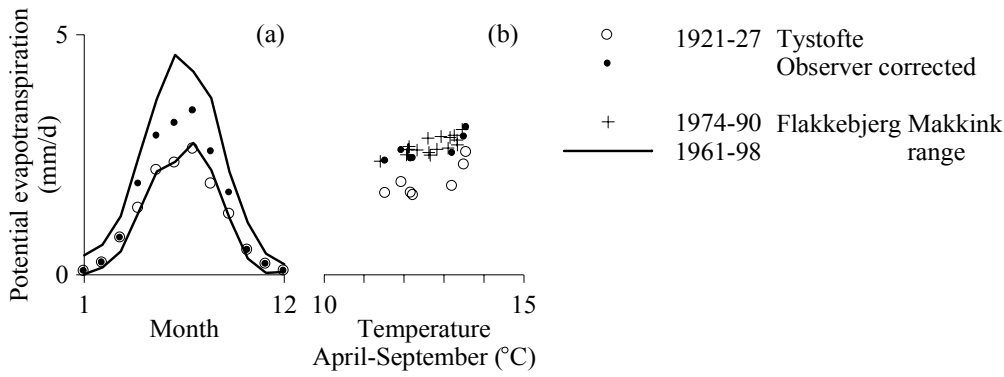
Figure 5.7. Potential evapotranspiration 1921-27, without and with correction for the observer through his cloud cover tabulation, against historical limits and summer temperature.

5.2.3. Observer Correction

Figure 5.7a reveals that uncritical application in the twenties pushes the potential evapotranspiration to the lower boundary of what we can expect. How the Makkink estimate should correlate to the measurable summer temperature appears from the simultaneous measurement of global radiation at Flakkebjerg in 1974-90. Figure 5.7b evidences a bias introduced via the observed cloud cover, a conclusion the complementary instrument for sunshine duration supports with an indication of normal conditions [*Clark et al.*, 1992].

Today's closest cloud cover stations with a long record of monthly means are Omø and Tune with an overall mean of 61 and 65 %, respectively [*Laursen et al.*, 1999]. Their coastal and inland position along the dominant wind direction on each side of the questioned Tystofte delimits its probable outcome. They should be comparable despite their different measurement periods, since each year deviates no more than 5 % from the long-term mean. Figure 5.8a shows that their perennial gap, which reflects convective clouds arising over land, equals Tystofte's mean of 67 % outside the above range with an
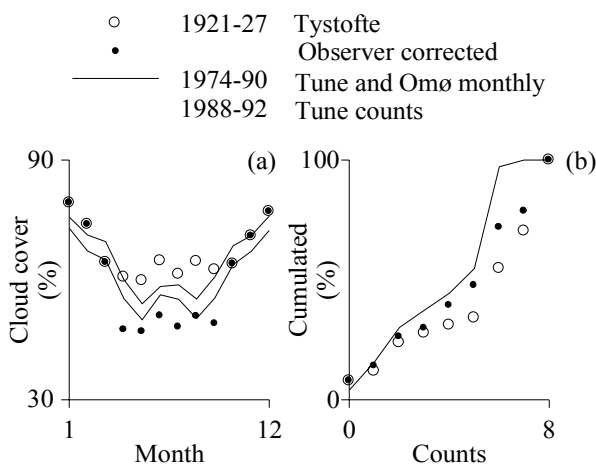

Figure 5.8. Cloud cover 1921-27, without and with correction for the observer through his cloud cover tabulation, against historical limits.

unrealistically overcast summer. Photographers refer to the apparently darkening background while they face the sun as backlight. Anybody would tend to exaggerate the degree of overcast when the sun gains altitude, unless they have an illustrated reference at hand. Figure 5.8b exemplifies the underlying count distribution for five years at Tune, where zero corresponds to clear sky and eight to overcast. This scale for modeling purposes applies a standard conversion from the observation scale to ten.

We develop a rigorous cure from the maximum count where backlight may influence strongest and those counts where the conversion truncates most relative to proportionality. Nested reduction brings an acceptable mean in Table 5.2 (A), a slightly extended reduction for summer months only improves the seasonal fit (B), an all-weather reduction displaces the mean to the nearby station Omø (C), and resetting the largest truncations around the unaffected clear sky gives a final improvement of the count distribution (D). Figure 5.8 shows how the remedied seasonal distribution and mean value compares best to Omø: a typical station for inner Danish waters [*Laursen et al*., 1999]. Figure 5.7 shows that the simplistic procedure has achieved a proper correlation with temperature and lies well within the expectation bands for potential evapotranspiration. Generally speaking, one should always validate an observer's skills from instruments and recent cloud cover data. The remaining error in the seasonal distribution and in the counts near overcast indicate that additional entries for spring and fall would benefit the overall fit, but such a fine-tuning adds more ambiguity to the conversion which cannot be relieved by matrix inversion alone, since the constraints for season and overcast have greater effect.

Table 5.2. Correction of observer's cloud cover record for Tystofte 1921-27 by modifying the conversion in four steps A-D according to the correlation coefficient to the monthly distribution at Omø and Tune 1974-90 and the count distribution at Tune 1988-92.

Measured	[a]	A	B [b]	C [b]	D [b]
0	0				
1	1			0	
2	2			1	1
3	2			1	
4	3			2	2
5	4			3	3
6	5		4	4	4
7	6	5	5	5	4
8	6		5	5	5
9	7	6	6	6	6
10	8	7	7	7	6
Mean (%)	67	60	63	61	61
R^2 monthly	87.2	85.1	95.6	96.3	96.5
R^2 count (%)	92.2	96.9	95.8	95.3	97.4

[a] Danish Meteorological Institute standard conversion from observer's record, [b] April-September only.

5.3. Historical Drain Coverage

Extensive drainage works have been undertaken during the past century and detailed inventories of their coverage have been archived by the dominant contractor, *Danish Land Development Service* [1997]. Since the sixties, the drainage works have consisted of reparations only due to abolition of subsidies, falling grain prices [*Waagepetersen et al.*, 1991]*,* and the water act of 1987. *Aslyng* [1980] estimated the provincial coverage and its history from tile drain production and inspection of randomly picked 1 % of the arable land, as done abroad [*Robinson*, 1990]. From 1929, the drain coverage had doubled to 49 % for the country as a whole, while it was unchanged on the densely populated islands. Alternative estimation including a drain lifetime of around eighty years suggested a doubling on the islands as well. Our streamflow separation indicates that 83 % of the study catchment contributed to drainage flow during the wet spring of 1999, whereas *Danish Land Development Service* [1997] has archived 30 % coverage. *Hansen* [1981] argued that the archives were not representative for the nearby Suså catchment, and we note that the value is below the national average and the, due to the dense clayish soil, recommended full coverage by *Waagepetersen et al.* [1991].

    Waagepetersen et al. [1991] explored the seasonal rainfall-runoff relationship for nine of *Danish Land Development Service*'s [1978] discharge records, including the study catchment, but could not identify a change over time. *Clark et al.* [1992] established from a monthly root zone budget that runoff increased from 35 to 37 % of the rainfall in the study catchment, a rather insignificant change compared to an underlying discharge increase of 15 %, a rainfall increase of 10 %, and an evapotranspiration decrease of 6 %. They used the rain gauge at Tystofte due to its digitized record and ascribed a mean lee correction for the time before such measurement was carried out. Our check against the spatially dependent mean catch determines the lee class and enables substitution of Antvorskov's record before its installation with the little uncertainty indicated in Figure 5.9. This leads to
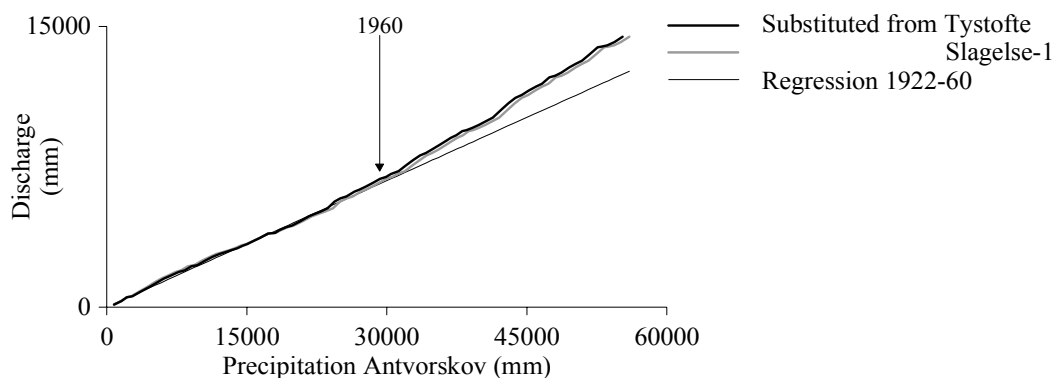

Figure 5.9. Double mass curve 1922-99 for precipitation that has been substituted from adjacent gauges before 1957 against catchment discharge clear of waterworks, sewage, and pavement.

a rainfall increase of only a few percent, in accord with *Frich et al.* [1997]. The slope increase for the rainfall-runoff from 23 to 30 % becomes equivalent to the discharge increase after the contribution from waterworks, sewage, and pavement has been subtracted. The rainfall does not introduce any persistence on a scale above twenty years according the annual catch, which approaches normal distribution, so the runoff enhancement should be significant.

Because the runoff enhancement coincides with the last known drainage works, a conversion of roughly 2 km^2 at Idagård in 1960, it motivates our attempt on modeling the changed water balance. A plotting paper from a continuous float device that had been installed in the study catchment in 1926 was recovered at a visit to the operator. This supports that the recorded daily values constitute a proper objective function for calibration of the drain coverage. The first drainage work after discharge measurement had begun was in 1927 [*Schrøder*, 1991], and the preceding period from 1921 contains the smallest constant drain coverage for which discharge has been recorded.

5.4. Calibration of Integrated Model

Compared to 1981-99, the weather of 1922-26 was equally wet but slightly colder with a 5 % lower potential evapotranspiration. We start from today's full drain coverage, an estimate based on streamflow separation. Grains covered three quarter of Denmark's cultivated areas in the twenties, and spring barley prevailed [*Statistics Denmark*, 1968]. The fraction of cultivated land has not changed in the study catchment since then [*Waagepetersen et al.*, 1991], and assuming that spring barley covered the cultivated 95 % while permanent grass covered the 5 % around the open stream introduces no major error, as model runs only show a 2 % increase in evapotranspiration during the thorough change to winter wheat in 1981-99 (Table 4.3). *Christiansen et al.* [2002] provide seasonal series of leaf area and rooting depth for all model runs.

5.4.1. Aquifer Head and Precipitation Revisited

The aquifer head has been decomposed into a spatial pattern, a seasonal sine, and an annual trend taken from a well that was installed 1980 in Flakkebjerg. Before then, the trend might be correlated to the annual surface load due to the thick overburden [*van der Kamp and Maathuis*, 1991]. This surface load can be divided into a primary winter precipitation and a secondary summer precipitation, less the potential evapotranspiration in response to the capillary rise, but the changed rainy season could degrade this approach. The trend might also be correlated to the annual baseflow at the catchment outlet, just 3 km from the well. While the unknown changeable source area makes the drain scheme contribution inseparable before our monitoring, it is easy to subtract the contribution of waterworks, sewage, and pavement from the recorded discharge. Discharge correlates with

Table 5.3. Increasing the aquifer head and substituting Antvorskov's precipitation gauge 1922-26.

Aquifer head	+0	+2	+4	+0	+2	+4
Precipitation gauge [a]	Slagelse-1 (695)			Tystofte (729)		
Aquifer replenishment	30	25	20	30	25	20
Discharge [b]	0.04	0.04	0.05	0.12	0.12	0.13

[a] Substituted Antvorskov, where the mean volume is bracketed, and [b] measured to 0.12 mm/d June-September.

the annual head in the well to within 10 % of its seasonal amplitude apart from 1990-91 and 1998-99, where dryness and wetness may have hampered the attributed discharge via the unaccounted drain scheme contribution.

The reduced drain coverage may raise the aquifer head more than the trend hindcast from today indicates. Table 5.3 shows that the aquifer replenishment decreases 5 mm/y every time the aquifer head is raised additionally 2 m, whereas an unchanged hindcast yields an increase of 2 mm/y for a removal of all drainage. In other words: the generated waterlogging changes the hydraulic gradient through the overburden less than the 2 m imposed at its bottom. Thus, the discharge remains our best approach to a hindcast. Table 5.3 also shows that substituting Antvorskov's gauge from Slagelse-1 and Tystofte implicates a 5 % discrepancy in the mean precipitation over the considered five years, after the spatial dependence of the long-term mean has been withdrawn. Albeit the summer rain was larger, see Figure 5.2 and 5.4, the summer discharge was presumably still dominated by baseflow and rather unaffected by the unknown drain coverage. Why the more distant Tystofte performs best could be ascribed either the lee giving hills between the catchment and Slagelse-1, or a more northward summer wind due to continental warming [*Frich et al*., 1997].

5.4.2. Drain Coverage in the Twenties

The survey map of *Danish Land Development Service* [1997] plots most drainage works in the valley, where the flat areas are concentrated. Whether these works are new installations or just renovations are impossible to judge, because the map does not contain works that are older than the drain lifetime around eighty years. Removal of drain schemes should generate waterlogging and in turn overland flow, which modeling did not detect for the eighties and nineties. The relatively slow discharge recession in the twenties implies that the generated overland flow, if it was present, has been captured in surface depressions before it could reach the stream. Model runs with a sufficient network of ditches from the underdrained fields to the stream, *i.e.* the drain constant of the model is attributed to all model grids continuously uphill from the stream to avoid delayed drainage, generates an excessive volume of overland flow in the hills that surface depressions cannot intercept

and the downhill drainage system then carries to the stream. The erroneously large discharge peaks supports that existing drains, if present, were installed mostly in the hills - not in the valley. We simplify calibration with the assumption of a continuous drainage area above a certain terrain level, instead of guessing the probable mosaic of drained and undrained fields.

Overland flow can be triggered before waterlogging occurs if the precipitation intensity exceeds the soil infiltration capacity. The daily reading of the precipitation gauge understates the intensity during short convective storms, but this sampling error is blurred in the validated streamflow by the drain scheme contribution over several weeks. Decisive errors might be embedded in the terrain model. Neglected details smaller than the contoured interval of 2.5 m lead to an artificially smooth surface that does not represent all surface depressions and consequently generates too much overland flow. Extra error may arise from MIKE SHE's modeling of overland flow, as both its peak and volume are very sensitive to the Manning number [*Xevi et al.*, 1997]. We pursue two different calibration targets due to the topographical smoothening. Modeled discharge is evaluated *I*) with and *II*) without overland flow, where the latter gives an upper limit of what unaccounted hollows can retard. Figure 5.10a shows how these two targets match the required 11 % discharge reduction from what full coverage predicts at a drain coverage of 31 % and 95 %, respectively. Figure 5.10b depicts the tail of the resulting daily series, which achieves an efficiency coefficient [*Nash and Sutcliffe*, 1970] of −78 % and 42 %.
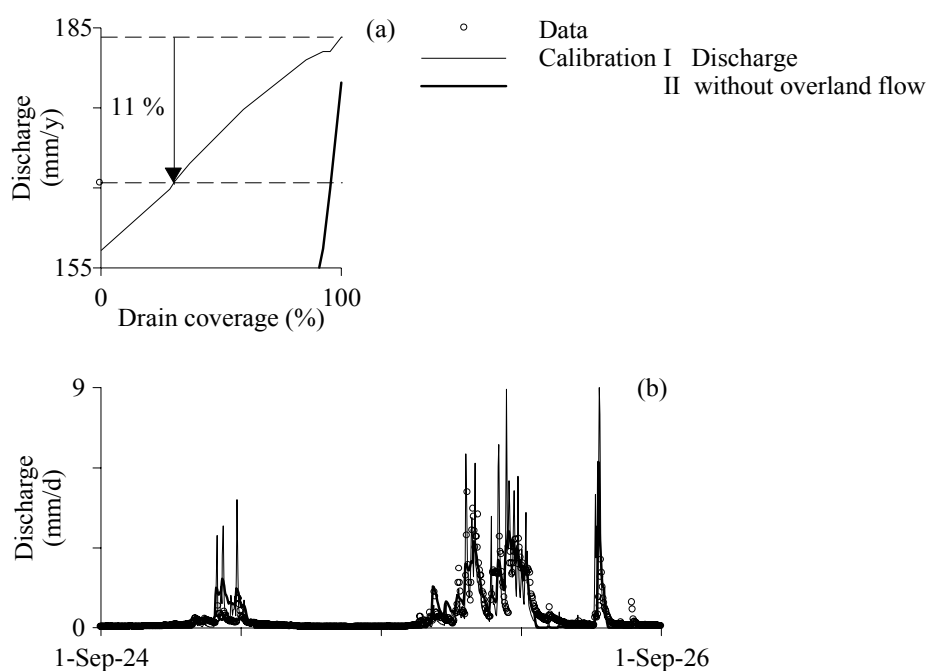

Figure 5.10. (a) Two reductions of the drain coverage reestablish the average discharge of 1922-26, but (b) model the daily discharge differently.

For optimum *II* speaks the daily match. Perhaps the dense rural population from the times of the medieval manor and convent initiated some early drainage works. For optimum *I* speaks that it is most compatible with *Aslyng*'s [1980] estimate given a limited drain lifetime and *Schrøder* [1991] who reported an unaccounted lake on the meadow, which was dammed "until around World War one". A dam of just 1 m would delay the winter peaks enough to sustain the underestimated spring recession and thereby gain the best daily dynamics, including no overshooting in dry years like 1925 as the alternative optimum did. Manmade drainage works prepare an area for farming by excavating a canal network, add ditches around fields, level the terrain, and finally install the subsurface drainage. Such drainage is essential for easy access to the fields in a short growing season where timely sowing and harvesting are critical. The drainage work in 1926 consisted of deepening the natural stream [*Danish Land Development Service*, 1997]. Its initial character indicates that the bulk of the subsurface drainage was installed later on. The preferred optimum *I* turns misrepresented overland flow and convective storms into minor issues. As shown in Figure 5.10a, the discharge reduction is 11 % from 1981-99 back to 1922-26. Rerun for 1981-99 eliminates uncertainty due to atmospheric forcing and vegetation type, and regenerates the 11 % reduction. Figure 5.11 points out how subsurface drainage works undertaken between 1926 and 1980 have reduced the aquifer replenishment less than its annual changes due to weather. Further removal of all subsurface drainage reduces the discharge by 15 % relative to present conditions.
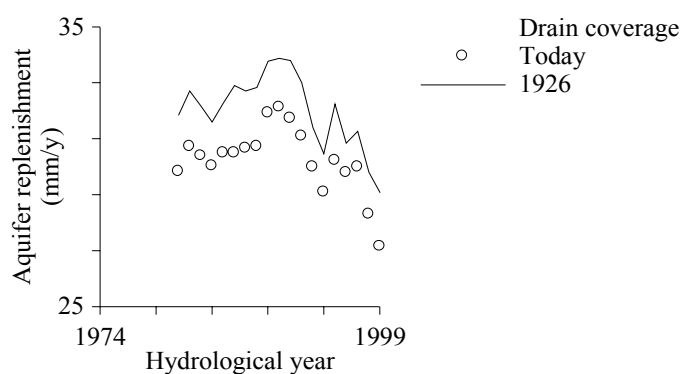

Figure 5.11. Aquifer replenishment lost due to subsurface drainage works 1926-80.

5.4.3. Outlook

Most studies state that subsurface drainage increases the baseflow under the storm peaks by reducing the overland flow, but omit a statement on whether the total discharge increases. *Bengtson et al.* [1988] monitored a drained and an undrained neighboring parcel for two years. *Skaggs et al.* [1994] who reviewed many studies did not find simulations showing a 10 % increase in total discharge convincing. They paid attention to the fact that drainage decreases the storm peak and thereby reduces the erosion in winter, whereas *Waagepetersen et al.* [1991] paid attention to the fact that drainage increases the total

discharge one-third. They compiled an increase for drained areas on 17±15 % using Danish discharge records that range several decades. The increase was largest in clay soil, but also stream deepening contributed in a flat catchment by intercepting a larger groundwater volume. Though their interval could change, if they performed streamflow separation and checked the wind exposure of the rain gauges, it agrees with our study.

Al-Khudhairy et al. [1999] calibrated MIKE SHE to a minor marsh catchment, turned the subsurface drainage off and noticed a waterlogging similar to observations in a neighboring undrained catchment. Reproduction of these watertable fluctuations suggests that this modeling tool offers insight on the implicated changes in the water balance. *Dumbrauskas et al.* [1998] used MIKE SHE to model a clayey catchment for which subsurface drainage must have transformed overland flow into slower but more discharge, while evapotranspiration has decreased. *Robinson* [1990] found similar yet smaller changes, which he attributed to the chance of weather. He thought that improved plant growth in the drier soil would enhance the transpiration and thereby eventually extinguish all change. We applied a plant growth that repeats every year unaffected by weather and the correlated watertable. Modeling of a nearby catchment by *Christiansen et al.* [2002] suggests that our simplification moves the evapotranspiration roughly 3 %. Hopefully, this answers *Robinson*'s scepticism.

Figure 5.12 illustrates the modeled change for a gradual removal of the subsurface drainage, given the weather of 1981-99. Waterlogging occurs in wintertime and generates a perennial lake in the terrain focus in the valley around the reported milldam at our discharge stations *A-C*. Waterlogging moves one-fourth of the mean catchment soil evaporation to surface ponds, its persistence until midsummer moves some plant transpiration below the watertable, and the canopy remains unaffected. Removal of all
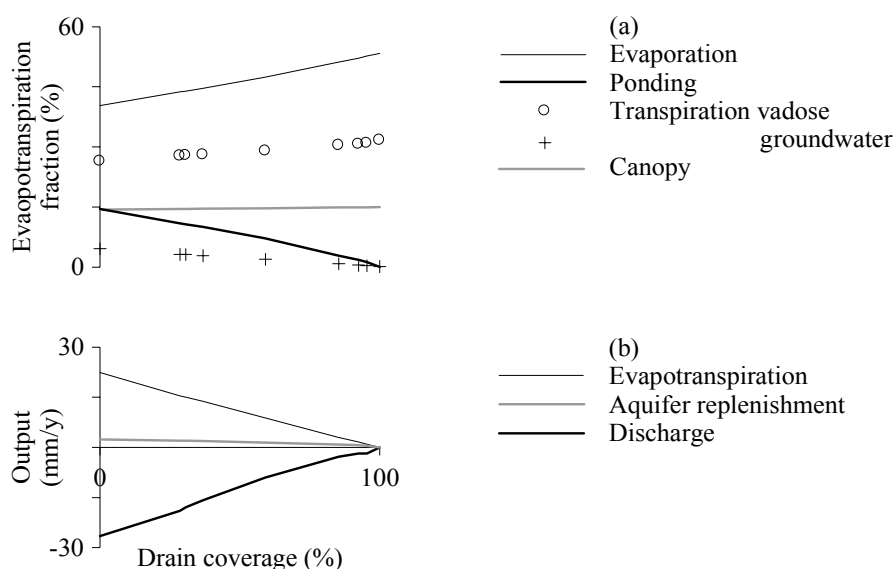

Figure 5.12. Water balance changes when the subsurface drainage is removed gradually.

drain schemes leads to substantial waterlogging. Evaporation from the generated surface ponds increases as much as discharge via drain schemes decreases, except for the slightly larger hydraulic gradient does push 2.4 mm/y more aquifer replenishment through the overburden.

5.5. Summary

We find that an increase in the drained area from 31 % in 1926 to above 83 % in 1981 is responsible for the intermediate runoff enhancement. The 11 % increase in discharge substitutes evaporation from waterlogged areas and to a lesser extent the 7 % decrease in the one magnitude smaller aquifer replenishment.

Evapotranspiration close to its potential limit, due to the capillary rise, demands a careful prior estimation of the atmospheric forcing. Potential evapotranspiration was estimated from temperature and cloud cover records using an extension of Makkink's formulation in which global radiation is modeled from the cloud cover. It was important to check the observer's judgment for the influence of backlight. The spatial dependence of the long-term catch provides a good check of the otherwise unknown lee class for the precipitation records.

References

Al-Khudhairy, D. H. A., J. R. Thompson, H. Gavin, and N. A. S. Hamm, Hydrological modelling of a drained grazing marsh under agricultural land use and the simulation of restoration management scenarios, *Hydrol. Sci. J.*, *44*, 943-971, 1999.

Allerup, P.. and H. Madsen, Accuracy of point precipitation measurements, *Nordic Hydrol.*, *11*, 57-70, 1980.

Aslyng H. C., *Afvanding i jordbruget* (Danish), Royal Veterinary and Agricultural University of Denmark, Denmark, 1980.

Bengtson, R. L., C. E. Carter, H. F. Morris, and S. A. Bartkiewicz, The influence of subsurface drainage practices on nitrogen and phosphorous losses in a warm humid climate, *Trans. Am. Soc. Agric. Eng.*, *31*, 729-733, 1988.

Clark, D. R., J. E. Olesen, H. E. Mikkelsen, S. U. Clausen, and J. Waagepetersen, *Historical trends in precipitation, evapotranspiration and runoff from nine Danish catchments*, Rep. S 2177, Danish Institute of Agricultural Sciences, Denmark, 1992.

Christiansen, J. S., J. C. Refsgaard, and M. Thorsen, Modelling of pesticide transport and fate at catchment scale, methodology and case study, *submitted*, *J. Hydrol.*, 2002.

Danish Land Development Service, *Discharge data for Danish streams 1917-70*, Denmark, 1978.

Danish Land Development Service, *Archive maps of undertaken drainage works*, Denmark, 1997.

de Bruin, H. A. R., From Penman to Makkink, *Evaporation and weather; Tech. Meeting 44, Ede, Netherlands, 25 Mar 1987*, *Proceedings and information*, TNO Committee on hydrological research 39, 5-31, Ed. Hoogart, J. C., Netherlands, 1987.

Dumbrauskas, A., L. Iritz, R. Larsson, and A. Povilaitis, *Environmental effects of agriculture practices, hydrology and nutrient transport, part 1: water cycle*, Rep. 3218, Univ. of Lund, Sweden, 1998.

Frich, P., S. Rosenørn, H. Madsen, and J. J. Jensen, *Observed precipitation in Denmark 1961-90*, Tech. Rep. 97-8, Danish Meteorological Institute, Denmark, 1997.

Hansen, B., *Drænvandskvantitet og kvalitet i Susåens opland* (Danish), Rep. Suså H 19, Danish Committee for Hydrology, Denmark, 1981.

Hipel, K. W., and A. I. McLeod, *Time series modelling of water resources and environmental systems*, Elsevier, Amsterdam, Netherlands, 1994.

Kimura, K., and D. G. Stephenson, Solar radiation on cloudy days, *ASHRAE Trans.*, *2106*, 1969/II, New York, NY, 1969.

Laursen, E. V., Thomsen, R. S., and J. Cappelen, *Observed air temperature, humidity, pressure, cloud cover and weather in Denmark – with climatological standard normals 1961-90*, Tech. Rep. 99-5, Danish Meteorological Institute, Denmark, 1999.

Lund, H., *Revised splitting procedure for calculation of direct normal radiation and diffuse radiation*, Thermal Insulation Laboratory, Technical University of Denmark, Denmark, 1979.

Makkink, G. F., Ekzameno de la formulo de Penman, *Repr. Neth. J. Agric. Sci.*, 5, 290-305, 1957.

Mikkelsen, H. E., and J. E. Olesen, *Sammenligning af metoder til bestemmelse af potentiel fordampning* (Danish), Rep. S 2157, Danish Institute of Agricultural Sciences, Denmark, 1991.

Nash, J. E., and J. V. Sutcliffe, River flow forecasting through conceptual models, part I: a discussion of principles, *J. Hydrol.*, *10*, 282-290, 1970.

Penman, H. L., Evaporation: an introductory survey, *Neth. J. Agric. Sci.*, 4, 8-29, 1956.

Robinson, M., *Impact of improved land drainage on river flows*, Rep. 113, Institute of Hydrology, Wallingford, UK, 1990.

Schrøder, J., *Harrested sø, forprojekt til naturgenopretning* (Danish), Danish Land Development Service, County of Western Zealand, Denmark, 1991.

Skaggs, R. W, M. A. Brevé, and J. W. Gilliam, Hydrologic and water quality impacts of agricultural drainage, *Critical Reviews in Environmental Sci. and Tech.*, *24*, 1-32, 1994.

Statistics Denmark, *Agricultural statistics 1900-1965*, I, 10, Denmark, 1968.

van der Kamp, G,. and H. Maathuis, Annual fluctuations of groundwater levels as a result of loading by surface moisture, *J. Hydrol.*, *127*, 137-152, 1991.

Waagepetersen, J., S. U. Clausen, K. Schlünsen, D. R. Clark, J. E. Olesen, and H. E. Mikkelsen, *Drainage and runoff in 9 minor water courses from the 1929's until today* (English summary), Rep. 48, Danish Land Development Service, Denmark, 1991.

Wilson, E. M., *Engineering hydrology*, McMillan, London, UK, 1991.

Xevi, E., K. Christiaens, A. Espino, W. Sewnandan, D. Mallants, H. Sørensen, and J. Feyen, Calibration, validation and sensitivity analysis of the MIKE-SHE model using the Neuenkirchen catchment as case study, *Water Resour. Management*, *11*, 219-242, 1997.

Chapter 6
Conclusions

This study investigates the magnitude of the capillary rise, *i.e.* the upward flux from the watertable, in a clayey till catchment under a humid climate, and how it helps to adjust groundwater to topography and annual weather. Historical records enable a spin-off study of subsurface drainage.

A literature survey of methods for determination of groundwater recharge made it clear that usually only the percolation at some level above the watertable is considered, and the subsequent capillary rise is neglected. Clay soil may have a lag phase from infiltration to recharge that becomes magnitudes larger during fall, when the watertable uphill deepens many meters, and a capillary rise during summer in response to surface drying. Monitoring the very watertable by a number of wells captures the lag phase of recharge, its spatial distribution, and allows for model interpretation of also the capillary rise. We installed a monitoring network comprising eleven wells in an underdrained catchment. Though the number of wells was limited, they covered two-third of the 16 km^2 catchment in terms of terrain level. Adopting the variable source concept, they sufficed for a monthly distinction in six terrain intervals between the dry state area and the wet state area from which tile drains divert recharge to the stream. Baseflow modeling confirmed the geological layering imaged by electrical sounding and borehole logging, including hydraulic conductivity. Separation of contributions from pavement and baseflow gave drain time and a loss. Assuming that the loss equals the volume of preferential conduits above drain level, their volume is 0.17 %. Watertable increments during storm confirmed the use of slug tests to access to soil characteristics from a USDA database. Then, calibration of a variably saturated 2D model centered on a single drain line could describe the preferential conduits as a bulk anisotropy ratio. Equilibrium scenarios confirmed that variably saturated 1D modeling of the wells in their dry state can adopt full coupling to the monitored watertable to reproduce the capillary rise without calibration. The piezometer depth in the reduced till and the time frame of the minimum watertable are, however, both crucial issues.

The second part of the work applied an integrated model to explore how the capillary rise adjusted the catchment circulation to two decades of atmospheric forcing. A steepest descent search algorithm corrected by the Marquardt-Levenberg scheme was used for calibration of the groundwater parameters. No major changes arose from the sequential parameterization of the monitoring, apart from the expansion of the drain time from 1D to 3D. Discharge and watertable data of also dry years, and later literature values for runoff from comparable catchments, indicated that among the unsaturated parameters it was only necessary to condition Kozeny's exponent for unsaturated conductivity to Mualem's formulation with its parameters in the adopted soil database. Moreover, the storage of precipitation as snow before it infiltrates could be calibrated from the presence of both a

daily emptied manual gauge and an automatic gauge.

The third part of the work applied the established integrated model to elucidate that an increase in the drained area from 31 % in 1926 to above 83 % in 1981 has lead to the observed runoff enhancement. Evapotranspiration close to its potential limit, due to the capillary rise, necessitated careful estimation in the twenties. The potential was estimated from temperature and cloud cover records using an extension of Makkink's formulation in which global radiation is modeled from cloud cover. It was important to check the observer's judgment for the influence of backlight. The spatial dependence of the long-term catch checks the unrecorded lee class for precipitation.

The main conclusions are:

- Watertable monitoring renders other calibration of a groundwater model's surface contact than drain time, preferential conduits, and snow storage superfluous, if conductivity found by electrical sounding or hydraulic tests is not considered to be calibration.

- In 1998, evapotranspiration drove the capillary rise to 0.7 mm/d during four months in the valley, resulting in totally 57 mm against the 334 mm of recharge.

- The capillary rise accounts for an uphill increase in the long-term net recharge of 30 %, from 200 to 260 mm/y, implying that local topography is mirrored into the aquifer circulation faster than found by regional modeling without this feedback.

- The capillary rise ties annual evapotranspiration to the North Atlantic Oscillation. The correlation coefficient of 30 % is perhaps better than thought of for Denmark, implying that hydrological modeling can establish area-integrated values for the oscillation's spatial coverage beyond the available reanalysis of numerical weather prediction models, which precipitation gauges and the index based on sea level pressure are unable of. This will contribute to the discussion on its spatial extent.

- Subsurface drainage installed after 1926 reduces evaporation from waterlogged areas and, to a lesser extent, the one magnitude smaller aquifer replenishment, resulting in an 11 % increase in discharge. Complete removal would only increase the aquifer replenishment by 2 mm/y.

The following is suggested for future work:

- Quantification of the error in reproducing the watertable with long screens.

- Evidence of the capillary flux by large lysimeters with a controlled watertable.

- Compiling a database with van Genuchten-Mualem characteristics for tills alone.

- Studies of the calibration issues, *viz.* drain time, bulk presentation of preferential conduits, and snow storage.

- Terrain-parallel flow, maybe a perched watertable, in the weathered soil requires revision of the MIKE SHE code, so the watertable can drop below the top layer and unsaturated conductivity can be expressed by Mualem's formulation.

Appendix A

Streamflow Monitoring

Design

Discharge from the well site has been monitored at the outlet of the piped stream downstream two tributaries, where the placement of the three stations 40 m apart eliminates intermediate storage (Figure 3.1b). Two metering campaigns confirmed that discharge would not exceed the precipitation over their topographically delimitated drainage areas, constituting 8-40 % of the catchment in terms of runoff. A peak rate amplification of one-fourth for these subcatchments agrees with studies compiled by *Kirkby* [1980], so amplification of the study catchment's extremes with a return period of ten years and subsequent reduction proportional to the area lead to design rates from minimum 0.1 l/s at station *A* to maximum 800 l/s at station *B*.

Continuous discharge measurement can be based upon electromagnetic particle tracking, Doppler particle tracking, or the energy transform over a specific structure. A structure driven into the streambed precludes the escape of low-flow and requires a cheaper datalogger with little power consumption, two advantages carrying greater weight than resistance to high-flow. Side- or bottom contraction controls the cross-sectional area and its velocity field, but the flat meadow can only support a pond of 10-15 % at station *B*, which necessitates either a long-throated flume or a broad-crested weir [*Replogle and Wahlin*, 1997]. A weir minimizes the material cost, as calculation according to *Bos et al.* [1976] points to a 10 m long flume. High-flow requires a submersible weir to be resolved. Both the upstream and downstream energy level must be monitored, because the Froude number of the natural regime below unity implies that discharge depends on the energy level in both directions, whereas a value above unity makes downstream monitoring in the tributaries unnecessary, reducing the material cost there to thin-plated, or sharp-crested, fully aerated weirs.

Rating Curves

The left side of Figure A.1 shows the approach channels, which are reasonably uniform, straight, and one magnitude longer than wide. *Bos et al.* [1976] thought that their results for rectangular laboratory flumes apply to a weir crest remaining adequately distant above the frictional streambed in such a natural channel. Discharge relates to the energy gradient via mass conservation and Bernoulli's equation for equilibrium. The upstream energy loss has to be avoided, and either full aeration of the weir or critical flow over its crest must be established. Then, integration over the geometrically determined cross-sections derives weir discharge from the upstream energy level. The chosen triangular geometry that

ensures the same relative error for all flowrates dominates the integration via the index. A narrow angle would give a small relative error but also a small capacity. To allow for torrents of surface water, weir C's accuracy has to be reduced by a trapezoidal geometry with a wide angle. Discharge Q for the three weirs A, B, and C follows

$$Q_A = C_e \frac{8}{15} \sqrt{2g} \tan\frac{\theta}{2} H^{\frac{5}{2}}$$

$$Q_B = C_d C_v \frac{16}{25} \sqrt{\frac{2}{5}g} \tan\frac{\theta}{2} H^{\frac{5}{2}} \qquad\text{(A.1)}$$

$$Q_C = C_e \frac{2}{3} \sqrt{2g} [b + \frac{4}{5} H \tan\frac{\theta}{2}] H^{\frac{3}{2}}$$

where H is the upstream energy level above the weir nose monitored in a stilling well, θ is notch angle, b is crest width, g is acceleration of gravity, C_e denotes effective discharge for a sharp-crested weir, while C_d and C_v denote discharge and velocity for a broad-crested weir, respectively. Diagrams for these coefficients that describe the upstream concave velocity field and an extra coefficient for submersion of a broad-crested weir have been digitized and polynomially fitted to automate the conversion to discharge.
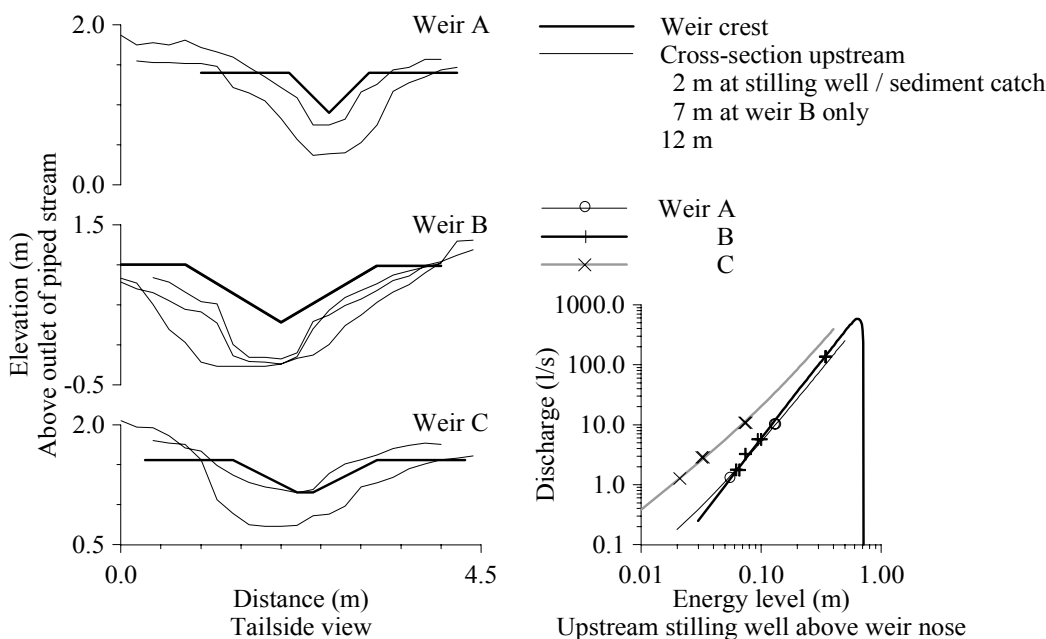

Figure A.1. The broad-crested weir B is orientated to within 1 cm from the flow axis in its approach channel, and all calibration points match the theoretical rating curves.

Figure A.2. Rounding of weir *B* carries the upstream energy level to its long crest, where hydrostatic conditions prevail until a submersion of 80 %, as monitored by the downstream stilling well. Braces, shelters, pebbles, and plastic membranes retard the erosion.

Workmanship

Drilling substantiated that the weirs should be 1-2 m high to be driven through the streambed deposits into the clay till and made by 10 mm steel sheets to prevent bending, while a crest beveling to 2 mm should maintain the aeration of weir *A* and C. The watercourses have been deepened 0.2-0.3 m and widened 0.5 m over 5 m to secure aeration and create sediment catches. Pebbles, reinforced plastic, a concrete plate downstream, and rings sheltering the stilling wells postpone erosion [*Kraatz and Mahajan*, 1975]. Additional tailside braces, evident in Figure A.2, serve to absorb momentum. Water voles undermined weir *A*. Bentonite in sackcloth were filled into their holes, but winter storms continued to push these plugs out until a 3.2 m^2 plate was driven through their gallery system on 23 February 1999.

Quality Control

Streambed undulation modifies any rating curve, especially its correction coefficients. Discharge rates smaller than 5 l/s were controlled with the filling time of a 25 l bucket, larger rates with a current meter (OTT, Germany) running one minute. Tripled measurement has reduced the impact of flow perturbation, and the linear relation between propeller revolution and current speed had been calibrated in a laboratory flume. The right side of Figure A.1 demonstrates a match with the theoretical rating curves, though error combination following *Bos et al.* [1976] suggests an uncertainty of 5 % for the control against the 2-3 % of the monitoring system.

Comparison of the discharge records confirms that the stilling wells do not suffer from resonance and storage delay between the readings every 15 minutes, or over-icing. Backup transducers verified that the electric-pressure transducers preserve their calibration slope, and, due to their larger measurement interval, the weirs were never flooded, except for violation of weir *C*'s aeration twice according to the downstream transducer at weir *B*.

These two peak levels have been subtracted the level of flooding. Weir *B* submerged more than the critical 80 % in eleven hours, where the discharge decreased less than 20 %. Cross-section measurement after the weirs had been taken down indicated that wandering dunes had entered the sediment catches, but not the stilling wells, and altered the initially established rating curves. The records are not revised, since the largest change was the 0.5 % decrease of weir *B*'s correction coefficient for velocity.

Figure A.3 reveals three shifts at station *A* due to the water voles. Station *5602*'s record contains one shift the last month. Inspection of its water level showed an abrupt decrease, which could be a weed cut that was not yet accounted for in its stage-discharge relationship. The other stations were fully aerated during the growth season and their approach channels kept free of plants; therefore, their rating curves are intact [*Ovesen*, 1998]. The accomplished rectilinear curves indicate that the prevailing streamflow generating processes remained unchanged during the cause of our monitoring [*Dingman*, 1994], except for a discernible bulge for station *C* in the fall of 1998, when its flat drainage area saturated before the rest of the study catchment.
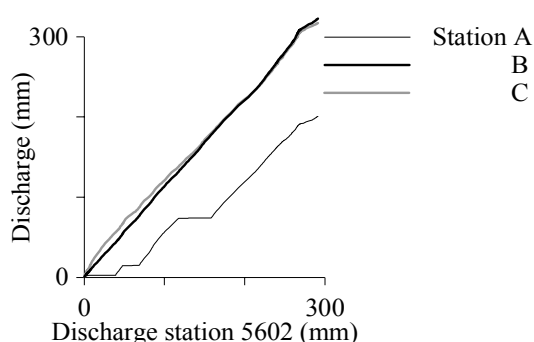

Figure A.3. Double mass curves for 10 July 1998 – 1 September 1999, normalized by the topographically delimitated drainage area.

References

Bos, M. G. (Ed.), *Working group on small hydraulic structures, Discharge measurement structures*, Int. Institute for Land Reclamation and Improvement, Wageningen, Netherlands, 1976.

Dingman, S. L., *Physical hydrology*, Prentice-Hall, Upper Saddle River, NJ, 1994.

Kirkby, M. J. (Ed.), *Hillslope hydrology*, John Wiley & Sons Ltd, Chichester, UK, 1980.

Kraatz, D. B., and I. K. Mahajan, *Small hydraulic structures*, Irrigation and drainage paper 26, Vol. 2, Food and Agriculture Org. of the United Nations, Rome, Italy, 1975.

Ovesen, N. B., Diurnal fluctuation in stage and discharge induced by aquatic plants in a Danish lowland stream, *Proceedings of the SIL-conference*, Dublin, Ireland, 1998.

Replogle, J. A., and B. Wahlin, Portable and permanent flumes for channel flow measurement, *Int. Water and Irrigation Review*, *17*, 8-12, 1997.

Appendix B

Watertable Monitoring

Table B.1 summarizes the geometry of the wells shown in Figure 3.1 and how frequently the below explained two types of error were encountered. In addition, well *754*'s daily value, but not monthly, is disregarded from June 1999 where soil compression at a new construction site smoothened the infiltration. Figure B.1 presents the corrected daily watertable, averaged over hourly readings. Each well is installed in an access tube of concrete that was buried and protected against traffic by a steel lid. In spite of the lid and a bottom sealing of bentonite, these tubes were flooded occasionally by either surface water or a rising watertable, so the casing had to be extended almost up to terrain to prevent intrusion of the very screen. Failure peaked the wet fall of 1998, where particularly well *4* and *7* were flooded due to their position at the foot of small hillslopes.

In 1998, error type *I*, see Table B.1, occurred during the operation of Orphimedes bubbling-pressure instruments (OTT, Germany). Albeit hung in a bottom-sealed cylinder next to the well with the airing tube just below the lid, the diurnal temperature oscillation kept pushing humidity into their insufficiently protected datalogger. Function terminates earlier for the shallow access tubes due to rapid saturation of the air, and in frosty weather due to disproportionately emptying of the battery. Moreover, fine sediments and air bubbles in its measuring tube induce instability and subsequent error messages. The lost readings have been patched by linear regression against the nearest well having similar screen length and watertable depth, an example is given in Figure B.2a. Hysteresis among the wells that results from a different watertable depth due to terrain undulation and the slope towards the drain lines decreases the correlation coefficient to 80-85 %.

Table B.1. Well geometry and error frequency.

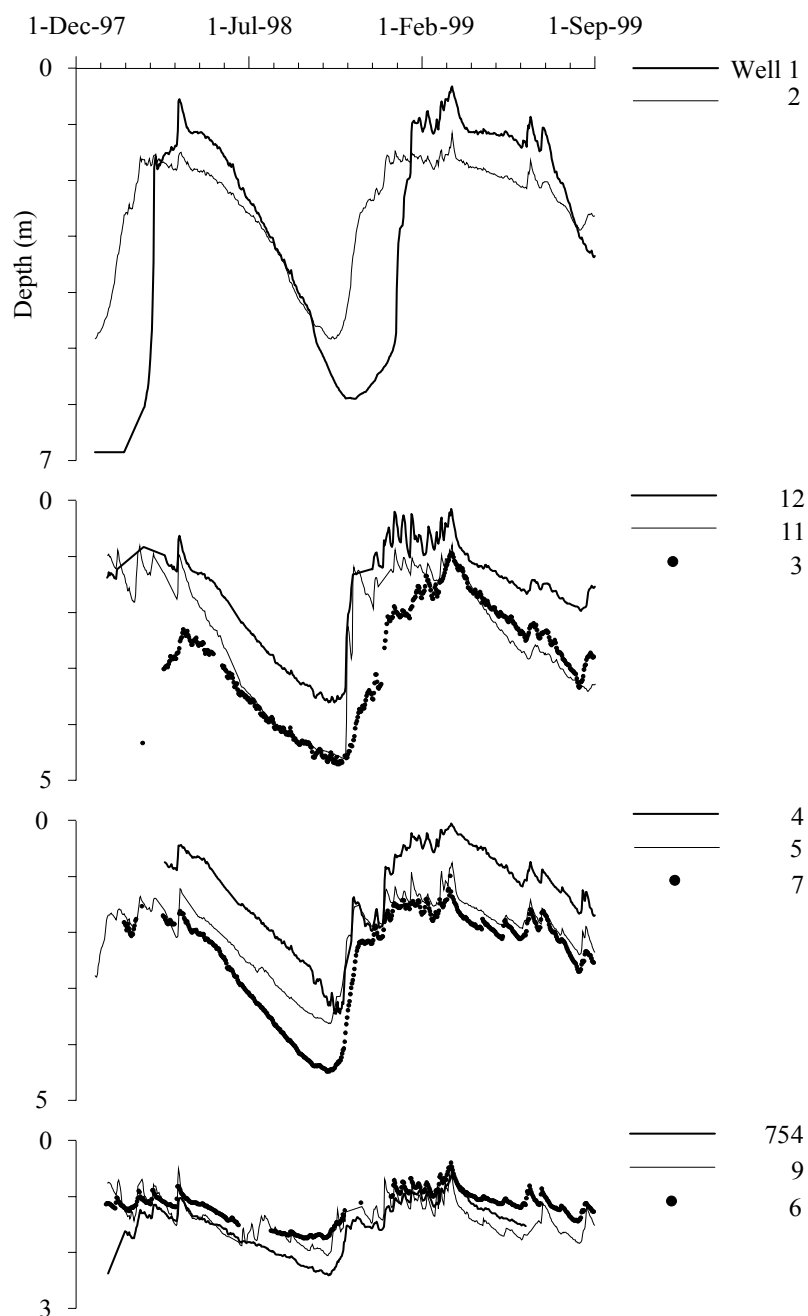| Well	Terrain Level m	Screen Length m	Depth m	Casing top Depth m	Error I 1998 %	Error II 1999 %
1	60.51	5.0	6.85	0.10	2	0
2	50.48	,,	6.98	0.05	2	9
3	42.90	,,	7.01	,,	24	0
4	41.14	,,	6.93	0.02	36	19
5	38.89	,,	6.90	0.05	18	0
6	36.51	6.0	7.98	0.06	37	0
7	38.01	5.0	6.90	0.05	23	32
9	38.05	,,	6.85	0.03	15	9
11	41.62	,,	6.97	0.06	22	0
12	42.25	,,	6.92	,,	37	0
754[1]	42.0	2.0	10.0	0.09	10	0
					21±13	6±11

[1] Adopted as unconfined.

Figure B.1. Corrected daily watertable, sorted according to terrain level. One-fourth of error *I* has been filled in, all of error *II*. Daily changes below 0.1 m jump to 0.8 m at the winter onset and 0.5 m whenever drainage flow sets in.

In 1999, electric-pressure transducers (Druck, UK) took over operation and modified the error to type *II*, see Table B.1. Datalogger, transformer, battery, and a bag of silica gel were stored together in a waterproof equipment box with an airing tube up to just below the lid, which made operation vulnerable to a drowned airing only. The water level is measured as pressure P at the transducer level denoted c and compensated for barometric changes at the orifice of the airing denoted a, until flooding confines it to the box denoted b. Diurnal oscillation identifies when the water level h has been read erroneously to h_{error}

$$h = P_c - P_a$$
$$h_{error} = P_c - P_b$$

(B.1)

Provided that the trapped air behaves like an ideal gas, the fixed volume V_b and likewise fixed number of molecules n_b adjust P_b to follow the midday rise of the temperature T_b. The initial condition 0 refers to the midnight before oscillation begins,

$$P_b V_b = n_b R T_b \quad \Rightarrow \quad \frac{n_b R}{V_b} = \frac{P_b}{T_b} = \frac{P_{b0}}{T_{b0}} \quad \Rightarrow \quad P_b = \frac{P_{b0}}{T_{b0}} T_b$$

(B.2)

where R is the gas constant. On top of this diurnal oscillation denoted IIa, the drifting barometric pressure P_a opens a gap denoted IIb. The unknown state of the box necessitates a calibration,

$$\begin{aligned}
h - h_{error} &= (P_a - P_b)_{IIa} + (P_a - P_b)_{IIb} \\
&= -(P_b - P_a)_{IIa} - (P_b - P_a)_{IIb} \\
&= -c_{IIa}[P_i(t-j) - P_{a0}] - c_{IIb}[P_a - P_{a0}]
\end{aligned}$$

(B.3)

where the sign changes from water level to depth, and $P_{b0} = P_{a0}$ has been inserted. Omø provides barometric pressure; Flakkebjerg provides hourly temperature at the surface and at four depths in the topsoil characterized by decreasing amplitude and increasing delay with depth. Diurnal oscillation is minimized by replacing the unknown box temperature with temperature record i, calculate pressure from Equation B.2, and attune the depth difference with a lag phase j and the weights c_{IIa} and c_{IIb}. Figure B.2b shows an example of a calibration against a well at a distance of 400 m.
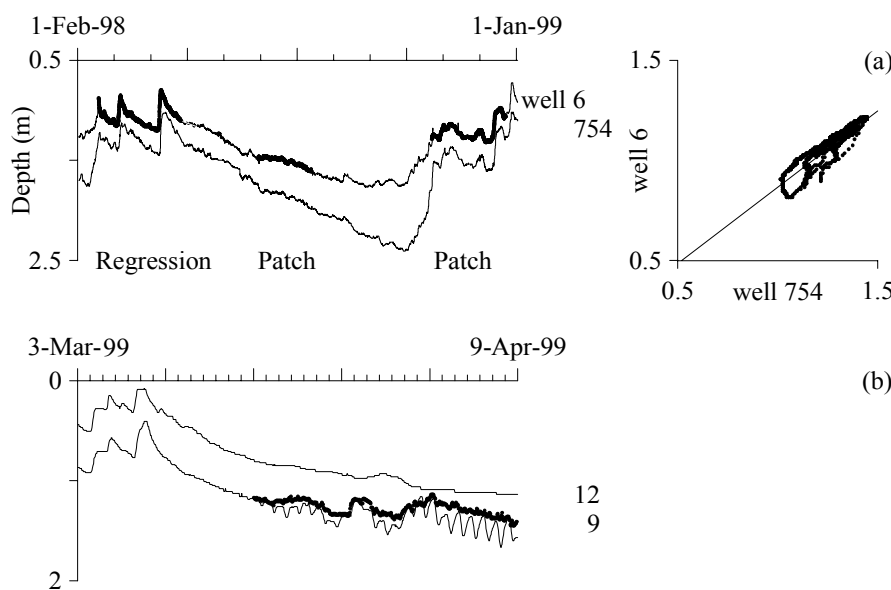

Figure B.2. (a) Well 6's error I during humid stages or flooding filled by linear regression against 754, (b) well 9's error II during submersion of the airing calibrated against 12.